POLITECNICO DI MILANO

Scuola di Ingegneria Industriale e dell'Informazione

Corso di Laurea Magistrale in
Ingegneria Nucleare

Experimental Study of Steam Chugging Phenomena in Direct Contact Condensation

Relatore: Prof. Riccardo MEREU

Co-relatori: Prof. Fabio INZOLI
Prof. Minoru TAKAHASHI

Tesi di Laurea di:

Giuseppe GREGU Matr.799612

Anno Accademico 2014 - 2015

Ringraziamenti

Il primo grazie va al Prof. Mereu, a Takahashi sensei e a Marco Pellegrini per avermi supportato costantemente nella realizzazione della tesi, e a Ninokata sensei per avermi dato una grandissima opportunità.

Questa pagina, nonostante passerà inosservata ai più, e non sono sicuro riesca ad essere effettivamente una sola, la dedico per celebrare tutte le persone che hanno avuto un influenza enorme nella mia crescita in questi pochi ma intensi anni della mia vita. Scrivo senza una logica, con le virgole a caso, lasciando che i miei pensieri riempiano spontaneamente queste righe

Per iniziare vorrei ricordare una persona che non c'è più ormai da qualche anno, mio omonimo, mancato centenario di questo duemilaquindici, che tanto avrebbe gioito nel vedermi raggiungere un traguardo così importante, pur continuando a ribadire, non a torto, la sua superiorità in matematica, così come in tutte le altre discipline, non fosse altro per il fatto che io, in questa Terra, rappresenterò sempre e solo la copia della sua persona.
Volgendo lo sguardo al passato non posso non rievocare Antonio Marras, vero padre la cui morte è ancora uno strazio per il mio cuore, Alberto Atzeni, padre-amico dall'animo buono e onesto e Salvatore Gregu, zio, padrino, babbai, padrone, educatore, esempio di una vita intera. Nel citare questi nomi mi riferisco per sinnedoche alle famiglie intere a cui vanno i miei grazie per avermi sempre trattato come figlio e fratello.
Continuando nella scia della famiglia, menzione speciale meritano Caterina, Mario, Gianluca, Maria Giovanna e i bellissimi Annarosa, Claudia, Salvatore, Ilaria e Francesca. Non dimentico zia Pietrina, zia Caterina, Giovanni, nonna, zio Giovanni, zio Raffaele, zia Nicoletta e i cugini Jacopo, Roberto e Gabriele. Ricordo anche gli altri due nonni, uno morto lasciandomi il rimorso di non averlo potuto godere di più ma di cui possiedo delle bellissime memorie e l'altra, di cui ho sempre sentito parlare solo per racconti, vere e proprie leggende di una persona che doveva essere veramente speciale come il marito.
E per quanto il termine famiglia non sia quello logicamente corretto, i miei sentimenti di stima verso queste persone colmano ampiamente i legami di sangue: Ale, Gianni e Rina, Bruno, Franco e Tonina, Carlo e Azi, Eraldo e Tina, Antonello e Valeria, Giulio, Anna e Paolo, Dania, Marcello e Chiara, Michele e Carmela.

Un grazie di cuore ai miei più grandi amici, veri sopportatori delle mie noiosissime lagne. Vi nominerò in ordine sparso: Matti, Vio, Lorentz, Genio, Lore, Giuli, Enri, Nick, Carli, Gallo, Checco, Jack, Chicco, Rasmus, Luca, Guì, Fra, Giag, Tommi, Fatto, Salar, Anna, Pasqu, Matte, Tonio, Gao san, Dan, Buccio, Camma, Ale, Papa Dongala, Emmanuel.

E ora, la parte più ardua in assoluto, scusarmi con i miei genitori, dopo 24 anni abbondanti, per non essere mai riuscito a dirvi veramente grazie. Ma proprio per questo motivo, il grazie che scrivo ora vorrei rimanesse per sempre scolpito nelle nostre menti. Potrei ringraziarvi per avermi messo al mondo, per avermi dato sempre cibo e iscrapporu , acqua, predas de errivu marrande patatas e murghende a manos tottu sa die, libri, per avermi negato le cose inutili, allevato, dato amore e botte, po tottu sas vortas i agges nau a ahiavaes su ohu ma soe mortu e vrittu, po hando agges istudau s'aria condizionada hando udi ascente, per avermi dato le opportunità di studiare, viaggiare, lavorare e divertirmi in giro per il mondo.
Però questo non è ciò che sento, non è ciò che voglio.
Ringrazio per prima cosa mio padre per aver sempre avuto da ridire su qualunque cosa e aver sempre taciuto non appena notava fermezza d'animo nelle mie decisioni. Grazie a te sono tutto quel che sono. L'altra cosa per cui non credo mi basti tutta la vita che ho davanti per poterti ringraziare è l'avermi portato in Africa che ero ancora ragazzino e avermi supportato anima e corpo nei miei tentativi folli di ritornarci, sapendo perfettamente quanto quel giorno la mia vita sia irrimediabilmente cambiata.
Dulcis in fundo mi rivolgo a mia madre, silenziosa traghettatrice della nostra famiglia. Martoriata come nell'inferno dantesco da una vita intera con due persone pesanti come me e mio padre, hai sempre mostrato il tuo lato buono e gentile, solo nel nostro interesse. Non hai mai avuto un secondo di respiro, sei la persona più viva che abbia mai visto in questo mondo. La tua umiltà e il tuo amore sono per prima cosa il motivo per cui ogni giorno voglio avere il sorriso sulle labbra e poi la ragione per cui trovare moglie mi costerà tanta fatica.

Abstract

The focus of the study is chugging phenomenon occurring during direct contact condensation (DCC) of steam in the wetwell of BWRs. Chugging is a depressurization induced by the bubble implosion at the pipe outlet that causes a cyclic suction of water inside the pipe. The presence of high pressure peaks is characteristic of this regime. The purpose of this study is to investigate the mechanisms of every phase composing a chugging cycle and to provide experimental results useful for the validation and development of CFD approaches. In order to achieve these objectives, an experimental campaign was performed. The steam mass flux range was 5.5-19.5 kg/(m^2s) while the pool temperature one was 19-46.5 °C. Two different pipe materials were used, stainless steel and transparent polycarbonate, with 27 mm as the inner diameter. Pressure pulses were measured with two semiconductor pressure transducers located inside the pipe at 3 cm and 50 cm from the outlet and a high speed video camera was used for supporting the investigation of the phenomena. From the analysis of collected data a chugging condensation regime map was created. Different bubble collapse behaviours were noticed. A qualitative interpretation of this observation, might be the different effects of the interfacial area and turbulences on the condensation process. Moreover it was found out that internal condensations generate pressure spikes higher than 1.2 MPa because of the condensation induced water hammer (CIWH) phenomena. Formation of small encapsulating bubbles and occurrence of pressure peaks happens for the same conditions of low steam mass flux and low pool temperature. Such a link between the size of the bubbles and the frequency of the pressure peaks gives an effective method for easily predicting chugging characteristic in small scale tests where the adoption of stainless steel pipes do not allow visualizing the phenomena.

Keywords

Direct Contact Condensation, Chugging, BWR, Pressure-suppression pool.

Estratto in lingua italiana

Introduzione

In data 11 Marzo 2011 è avvenuto un incidente nel complesso nucleare di Fukushima Daiichi causato da un terremoto di magnitudo 9 e dal successivo maremoto. Tra le lezioni che questo evento ha insegnato al mondo della produzione di energia da fonte nucleare ci sono sicuramente il bisogno di implentare sistemi di sicurezzi passivi e la necessità di valutare le prestazioni degli attuali reattori durante lunghi transitori. Nel presente lavoro di tesi il capitolo 1 fa riferimento ad uno degli scenari incidentali maggiormente studiato in ambito nucleare, ossia la perdita di refrigerante dal circuito primario detta LOCA. Tra tutte le funzioni che devono essere espletate durante un LOCA, limitare l'incremento di pressione nel drywell e ridurre velocemente la pressione è di primaria importanza. Nei reattori presenti a Fukushima, questo era conseguito attraverso l'iniezione passiva di vapore all'interno di piscine a soppressione di pressione in cui avviene il fenomeno della condensazione diretta. Infatti, come spiegato nel capitolo 2, il contatto e il mescolamento delle due fasi garantisce un maggiore coefficiente di scambio termico rispetto alle tecniche convenzionali. Nonostante ciò, a seconda di 3 parametri fondamentali – sottoraffreddamento della piscina, flusso di massa del vapore e diametro interno del tubo di iniezione – questa soluzione può portare ad un regime di condensazione instabile denominato chugging. Il chugging consiste nella diminuzione di pressione all'uscita del tubo, dovuta all'implosione di bolla, che causa un ciclico rientro di acqua all'interno del tubo di iniezione. Questo regime è caraterizzato da forti picchi di pressione. Gli obiettivi di questo studio sono lo studio di ogni fase componente il ciclo del chugging e fornire dei risultati sperimentali utili per la validazione di modelli CFD. Al fine di raggiungere gli scopi preposti, è stato costruito un apparato sperimentale in scala (3.1, 3.2, 3.3) ed è stata portata avanti una campagna di misure sperimentali (3.4, 3.5). Diversi valori di flusso di vapore e temperatura della piscina sono stati investigati durante gli esperimenti con intervalli pari rispettivamente a 5.5-19.5 kg/(m^2s) e 19-46.5 °C, mentre il diametro interno del tubo è stato mantenuto costante e pari a 27 mm. Le misure di maggiore interesse sono state la valutazione dei picchi di pressione attraverso due trasduttori a semiconduttore posizionati all'interno del tubo a 3 e 50 cm dall'uscita del vapore e l'utilizzo di una videocamera ad altà velocità, sincronizzata col segnale proveniente dai trasduttori, in modo da riprendere il fenomeno e dare un supporto all'analisi dei dati.

Capitolo 1 Reattore ad acqua bollente BWR e sistemi di sicurezza nelle piscine a soppressione di pressione

Attualmente, prendendo in considerazione i reattori in funzione, 78 fanno parte della tecnologia dei BWR e la maggior parte di questi presenta dei contenitori di tipo Mark I o Mark II, stesso design rispettivamente utilizzato nelle unità da 1 a 5 e nell'unità 6 dei reattori presenti a Fukushima. Nello schema dei BWR, la condensazione del vapore a seguito di LOCA è ottenuta attraverso le piscine a soppressione di pressione. In tali sistemi, il vapore è iniettato attraverso dei grossi condotti, i venting pipes, all'interno di piscine contenenti acqua fredda e la conseguente condensazione diretta consente una riduzione considerevole della pressione del contenitore. I venting pipes dei contenitori di tipo Mark I e Mark II si inseriscono verticalmente all'interno delle piscine mentre, nei design più moderni, l'introduzione di vapore può avvenire in maniera orizzontale. A parte i venting pipes, altri sistemi di sicurezza fanno largo uso delle piscine come pozzo freddo e prevedono sempre lo scarico di vapore e lo sfruttamento della condensazione diretta. Tra i più importanti si cita il sistema di depressurizzazione del nocciolo, ADS, e il suo sistema di raffreddamento, RCIC. Tuttavia, le geometrie dei tubi di scarico di vapore nelle

piscine relativi a tali sistemi sono parecchio complesse e non sono state analizzate nel presente studio. Figura 1 illustra uno schema delle piscine a soppressione di pressione dei BWR e dei relativi sistemi di sicurezza.

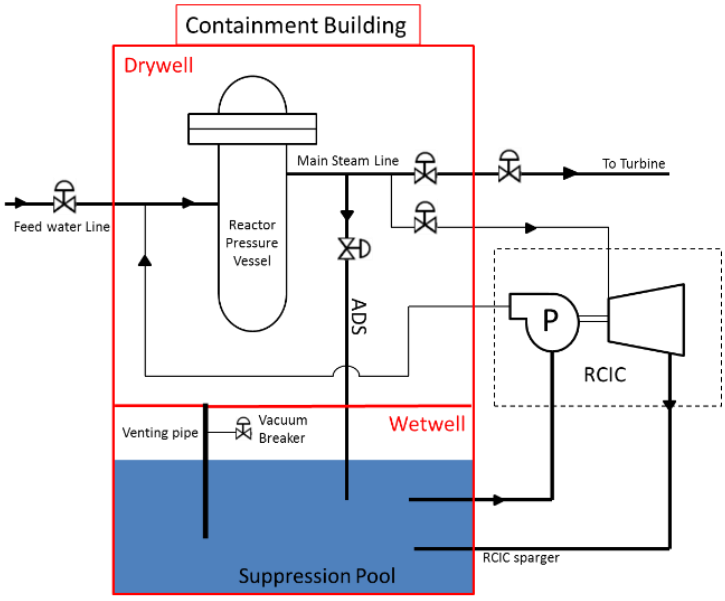

Figura 1 Schema delle piscine a soppressione di pressione.

Capitolo 2 La condensazione diretta e il regime di chugging

2.1 La condensazione diretta

La condensazione diretta è una modalità efficace di condensazione del vapore. A differenza degli usuali metodi di condensazione negli scambiatori di calore, la condensazione diretta prevede l'iniezione di vapore all'interno di acqua sottoraffreddata. Diversi regimi di condensazione possono instaurarsi a seconda di tre parametri fondamentali, rappresentati in Figura 2:

- Flusso di massa di vapore, G [kg/(m^{2}s)]
- Sottoraffreddamento dell'acqua, $\Delta T = Ts - Tw$ [°C]
- Diametro interno del tubo, D [m]

I regimi di condensazione, evidenziati in Figura 2b, possono essere classificati in tre grosse categorie:

1. Jetting
2. Bubbling
3. Chugging

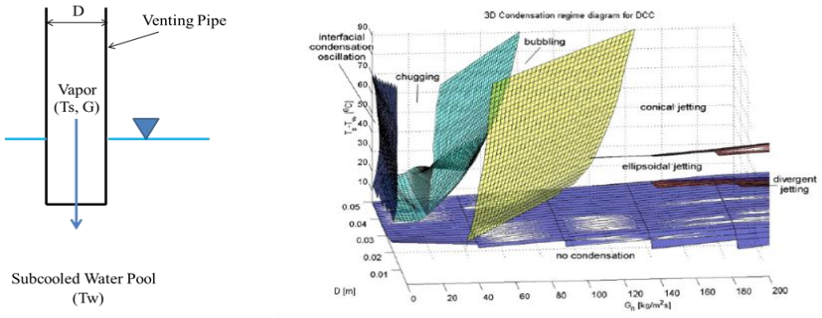

a b

Figura 2 a) Parametri e b) regimi della condensazione diretta.

Il regime di chugging è sicuramente il più critico nelle piscine di soppressione dei BWR. Tale fenomeno ciclico avviene a basse portate di vapore ed è caratterizzato da forti picchi di pressione. Ogni ciclo di chugging può essere suddiviso in cinque diversi momenti: crescita della bolla, collasso della bolla, rientro di acqua, condensazioni interne ed espulsione di vapore.

2.2 Il chugging nelle piscine a soppressione di pressione dei BWR.

Come introdotto nel capitolo 1, in caso di LOCA è prodotta una ingente quantità di vapore che pressurizza il contenitore di sicurezza. Durante le prime fasi di iniezione di tale vapore all'interno delle piscine, a seguito delle completa rimozione dell'aria dai venting pipes, si instaura con buona probabilità il regime di jetting o bubbling per via delle elevate portate. Tuttavia, nelle ultime fasi di espulsione del vapore, una volta che le portate si sono considerevolmente ridotte e l'aria incondensabile è quasi totalmente rimossa, può instaurarsi il regime di condensazione del chugging. Inoltre, a seconda delle condizioni dei tre parametri citati nella sezione 2.1, possono avvenire multiple condensazioni interne. Sia le condensazioni interne sia le implosioni di bolla all'uscita del tubo sono fenomeni rapidi e violenti, caratterizzati da forti rumori e picchi di pressione

2.3 Revisione degli studi precedenti

La condensazione diretta e il regime di chugging sono stati ampiamente studiati. La maggior parte dei ricarcatori si è focalizzata sulla creazione di mappe di condensazione come [1], [2], [3], [4]. Questi lavori sono stati sintetizzati da Petrovich de With et al. [5], i quali furono i primi a proporre l'adozione dei tre parametri fondamentali descritti nella sezione 2.1. Tuttavia, tale lavoro ha rimosso completamente le distinzioni all'interno dello stesso regime di chugging per cui è stato necessario ricreare una mappa che dettagli maggiormente tale modalità di condensazione. Altri studi si sono orientati maggiormente su un approccio sperimentale, intuendo le difficoltà nel modellare analiticamente questo tipo di fenomeno. Tra i maggiori lavori si segnalano [6], [7], [8], [9], [10], [11], [12], [13], [14], [15], [16], [17]. Molti di questi studi possiedono punti in comune con la presente analisi sebbene raramente vi sia stata una suddivisione riguardo l'origine dei picchi di pressione e la fenomenologia di tali picchi non è stata quasi mai affrontata. Inoltre i livelli di picchi di pressione registrati sperimentalmente nel presente lavoro sono risultati ben al di sopra di quelli citati nella maggior parte dei lavori e nessuno dei precedenti progetti ha mostrato un tentativo di descrivere tutte le fasi che compongono un ciclo di chugging. Un altro approccio ampiamente utilizzato nel campo della condensazione diretta è stato quello analitico in cui si è tentato di riprodurre i risultati sperimentali in modo da prevedere le caratteristiche del chugging relative a zone inesplorate delle mappe di condensazione. Tra questi lavori si segnala [18], [19], [20], [21], [22]. Nonostante ciò, sopratutto per via della complessità del tema trattato, grossi passi sono ancora necessari affinchè si arrivi ad un modello che riesca a spiegare compiutamente il regime del chugging.

2.4 Obiettivi del presente studio

Questo studio si è concentrato sulla comprensione del fenomeno del chugging che si verifica durante la condensazione diretta del vapore all'interno di piscine di acqua fredda. A differenza degli studi precedenti, l'intero ciclo descritto nella sezione 2.1 è stato analizzato. Inoltre, sono state valutate le condizioni di insorgenza dei picchi di pressione e la loro intensità è stata quantitativamente esaminata. Gli obiettivi di questo lavoro sono:

1. Investigare il meccanismo di ogni fase del ciclo del chugging

a. Classificare il fenomeno del chugging a seconda della forma delle bolle
b. Fornire un'interpretazione qualitativa sul collasso delle bolle
c. Analizzare i tipici picchi di pressione che avvengono durante un ciclo di chugging che causano problemi riguardo il rischio di danni alle strutture
d. Fornire un semplice metodo per predire le caratteristiche del chugging creando una connessione tra la forma della bolla e i picchi di pressione
e. Illustrare la scala temporale delle fasi del chugging e le sue variazioni in funzione dei parametri caratteristici della condensazione diretta

2. Fornire risultati sperimentali per la futura validazione di codici CFD

Capitolo 3 Apparato sperimentale, sistemi di misura e procedure sperimentali

3.1 Apparato sperimentale

L'apparato sperimentale, riprodotto in Figura 3, è costituito da: main tank, stam line, due linee di evacuazione e la test section. All'interno del main tank, un contenitore cilindirco di acciaio inossidabile, viene generato il vapore. In totale possiede un'altezza di 120 cm e il suo diametro interno è pari a 40 cm. Sul fondo del main tank sono stati inseriti sei riscaldatori elettrici in una configurazione non simmetrica per una potenza complessiva pari a 36kW. Il vapore prodotto è inviato verso la piscina tramite una steam line termicamente isolata, così come il main tank. Nella steam line è inoltre presente un flussometro e valvole di regolazione. Le due linee di evacuazione, denominate A e B, hanno il compito di espellere il vapore all'esterno dell'edificio. Queste linee sono state create per rimuovere l'aria dal flusso di vapore e per prevenire incidenti.

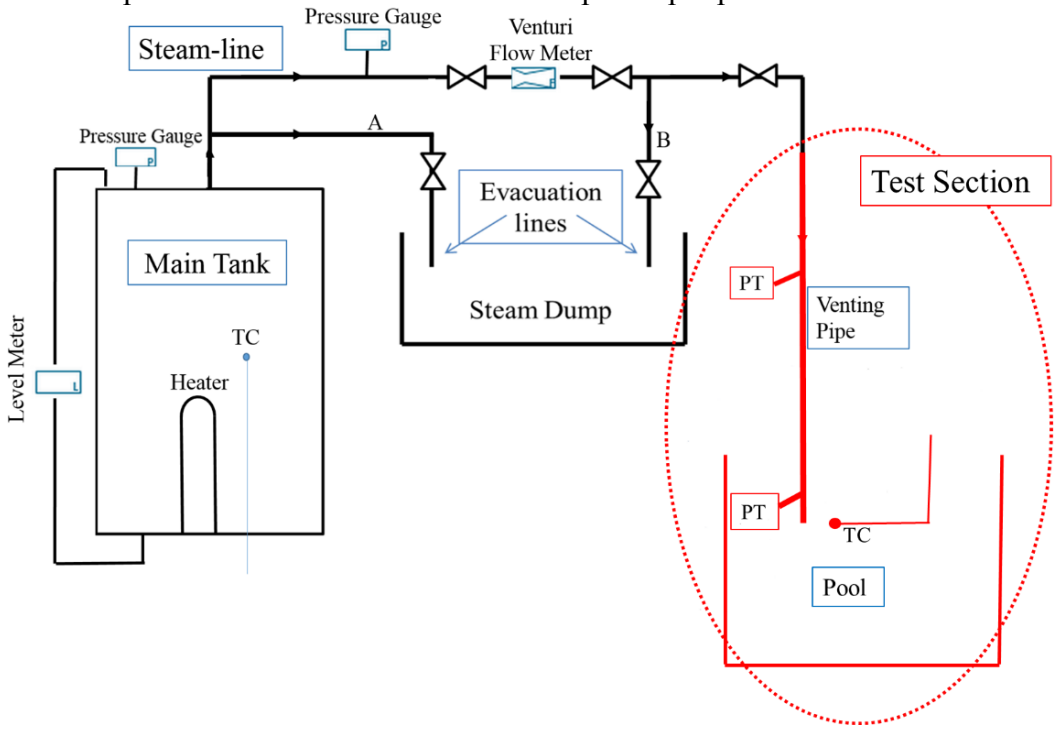

Figura 3 Apparato sperimentale.

3.2 Test section

La test section è composta da un tubo di immissione del vapore dall'alto verso il basso che si inserisce per 7.5 cm all'interno di una piscina. Diverse tipologie di tubo sono state utilizzate a

seconda dell'esperimento compiuto. Tuttavia, il diametro interno di tutti i tubi è stato mantenuto pari a 27 mm. Due trasduttori di pressione (PT) sono stati installati a 50 cm e 3 cm dall'uscita del tubo. La riproduzione dei venting pipes è stata costruita con due materiali differenti: acciaio inossidabile e policarbonato. La piscina cubica di 50 cm di lato e 0.5 cm di spessore è stata costruita utilizzando l'acrilico. La scelta di questo materiale non ha consentito il raggiungimento di temperature dell'acqua superiori ai 70 °C.
Una termocoppia (TC) del tipo K 1 mm, è stata introdotta all'interno della piscina, allo stesso livello dell'uscita del tubo, 3 cm distante dal suo asse. In questo modo, il fenomeno della stratificazione termica creata dalla differenza di densità nell'acqua è stato trascurato. La presenza di questa termocoppia è stata fondamentale per la valutazione del sottoraffreddamento, uno dei parametri che governano la condensazione diretta

3.3 Strumenti di misura

Gli strumenti di misura adoperati negli esperimenti sono stati due trasduttori di pressione a semiconduttore e una videocamera veloce. Questi strumenti sono stati collegati al medesimo sistema di acquisizione dati, TEAC es8, che è stato adoperato con una frequenza di campionamento pari a 5 kHz. Le elevate prestazioni della videocamera hanno consentito di sincronizzare alla perfezione i segnali dei diversi strumenti. Infatti è stato possibile ottenere un segnale TTL al momento dell'attivazione del trigger start della videocamera il quale ha costituito lo zero temporale degli esperimenti. L'utilizzo della videocamera è stato particolarmente proficuo quando accoppiato con l'adozione di tubi trasparenti in policarbonato per cui è stato possibile studiare il comportamento dell'interfaccia all'interno del tubo. Per fare in modo che le immagini fossero sufficientemente chiare, una lampada alogena è stata installata dalla parte opposta della videocamera rispetto al tubo.

3.4 Condizioni sperimentali

Le condizioni sperimentali sono riassunte in Tabella 1.

Temperatura della piscina	[19 – 46.5] °C
Flusso di massa del vapore	[5.5 – 19.5] kg/(m^2s)
Diametro interno del tubo	27 mm
Materiali del tubo	Policarbonato / Acciaio inossidabile
Sommersione del tubo	75 mm
Pressione della piscina	atmosferica
Frequenza di campionamento	5000 Hz
Pressione del vapore	[0.1 – 0.13] MPa
Frame al secondo della videocamera	1000, 2000, 3000 and 5000 fps

Tabella 1 Condizioni sperimentali.

3.5 Procedure sperimentali

Prima di avviare l'acquisizione dei dati, diverse operazioni sono state compiute. Inizialmente si è riempito il main tank di acqua e sono stati accesi i riscaldatori elettrici a bassa potenza. Questa fase di riscaldamento è durata circa tre ore. Nel frattempo è stata inserita dell'acqua nei tubi del flussometro e dei trasduttori di pressione facendo attenzione che l'aria sia stata completamente rimossa ed è stata fatta la regolazione dello zero strumentale. Una volta generato il vapore, è stato iniettato per 15 minuti circa all'esterno dell' edificio attraverso le linee di evacuazione in modo da rimuovere completamente l'aria dal flusso. A questo punto, la linea B è stata completamente

chiusa, il flusso stabilizzato con le valvole sulla steam line e il vapore è stato inviato all'interno della piscina in modo da ottenere il regime del chugging. Due diversi tipi di esperimenti sono stati effettuati:

1. Nel primo tipo di esperimento il segnale proveniente dai trasduttori di pressione è stato registrato simultaneamente alle riprese video. In questo caso, la durata dell'esperimento è stata pari a circa un minuto per via delle ridotte dimensioni di memoria della videocamera ai fps indicati nella sezione 3.4. La temperature della piscina è aumentata di meno di 1 °C, il che ha consentito di considerare tale valore come costante. Lo stesso discorso è avvenuto per il flusso di massa, soggetto a variazioni contenute a ±0.1 kg/(m^{2}s).
2. La seconda tipologia di esperimento è stata attuata senza il supporto della videocamera veloce. In questo caso è stato rimosso il vincolo della durata per cui sono state raccolte misure di pressione in un tempo compreso tra i 15 e i 30 minuti consecutivi. Il flusso di vapore è stato tenuto costante nei limiti esposti nella prima tipologia di esperimento mentre la temperatura della piscina è stata fatta incrementare naturalmente dai 21 °C ai 41°C. Tale valore è stato monitorato a video, ma non registrato.

Capitolo 4 Risulati sperimentali

In questo capitolo sono mostrati i risultati sperimentali seguendo il medesimo oridine della sequenza di eventi che compone un ciclo di chugging: crescita della bolla, collasso della bolla , rientro di acqua, condensazioni interne e espulsione di vapore.

4.1 Classificazione delle bolle

Nel capitolo 2 è già stata sottolineata l'influenza dei tre parametri sull'instauramento di diversi regimi di condensazione diretta. Al fine di dettagliare gli effetti del flusso di vapore e del sottoraffreddamento sul chugging, è stata creata una mappa di condensazione ad hoc, Figura 4.

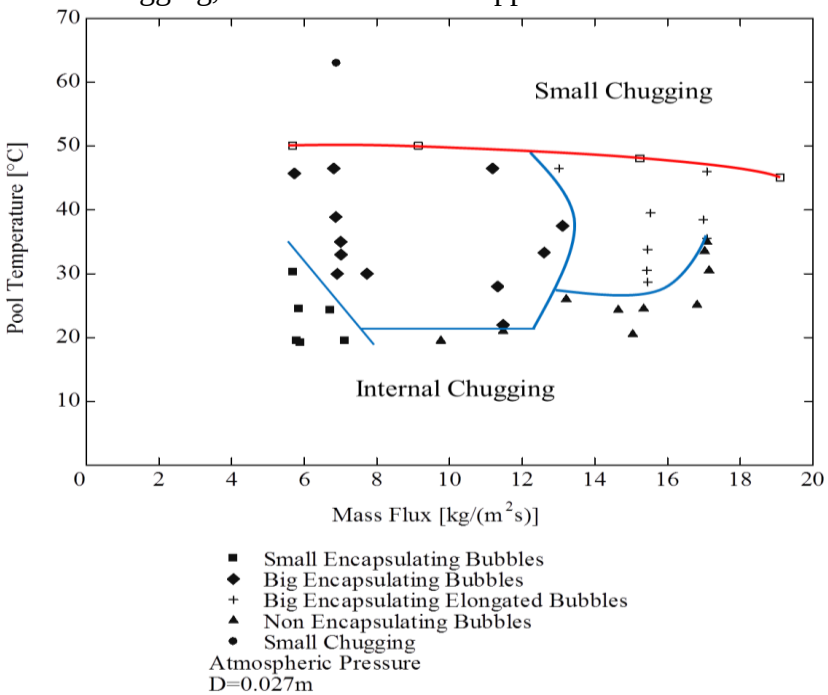

Figura 4 Mappa di condensazione.

Tale mappa è stata divisa in due grosse aree, internal e small chugging, riprendendo il lavoro svolto da Nariai et al. [8]. La regione dell'internal chugging si trova a basse temperature ed è

caratterizzata da alte elevazioni di acqua all'interno del tubo e forti picchi di pressione associati, mentre la zona del small chugging identifica un moto dell'interfaccia liquido-vapore circoscritto all'uscita del tubo con elevazioni contenute. In questo studio la transizione tra i due regime è stata imposta come le condizioni per cui l'elevazione non è mai superiore alla sommersione del tubo. La regione del small chugging è una zona di transizione e ciò spiega il motivo per cui quasi tutti gli esperimenti sono stati effettuati in regime di internal chugging, vero interesse di questa tesi.
All'interno della regione dell'internal chugging sono state evidenziate quattro aree che si differenziano per la forma della bolla in uscita dal tubo di eiezione:

- *Small Encapsulating Bubbles*
- *Big Encapsulating Bubbles*
- *Big Encapsulating Elongated Bubbles*
- *Non Encapsulating Bubbles*

Il termine *encapsulation* è stato adottato riferendosi a Chan et al. [2] e si riferisce al grado di avvoglimento della bolla attorno al tubo ed è principalmente legato alla forza di galleggiamento. La Figura 5 mostra degli esempi di bolla per ogni categoria. La divisione delle bolle a seconda della forma riguarda la principale modalità di condensazione per ogni esperimento. Raramente è accaduto che diverse condizioni si sono verificate all'interno dello stesso esperimento.

Small Encapsulating Bubble | *Big Encapsulating Bubble* | *Big Encapsulating Elongated Bubble* | *Non Encapsulating Bubble*

Figura 5 Immagini relative alle quattro categorie di bolle.

Le *small encapsulating bubbles* occupano la regione a basse portate e temperature. In queste condizioni, il tasso di condensazione è elevato ma, allo stesso tempo, la quantità di vapore iniettata nella bolla è bassa per cui le dimensioni sono parecchio ridotte. Così come avviene per tutte le bolle che ricoprono completamente o parzialmente il tubo, il galleggiamento è dominante o paragonabile all'inerzia del vapore per via delle non eccessive velocità. La seconda zona è occupata dalle *big encapsulating bubbles* e copre la maggior parte della mappa. Le dimensioni sono nettamente superiori rispetto alla precedente categoria. A pari flusso di vapore, le dimensioni delle bolle crescono a causa del minor tasso di condensazione mentre, a pari temperatura della piscina, le bolle diventano più grandi per via del maggior apporto di vapore. Le *big encapsulating elongated bubbles* si trovano nella zona ad alte portate. Galleggiamento e inerzia hanno lo stesso ordine di grandezza e la superficie delle bolle è elevata. A causa delle alte velocità del vapore è facile osservare getti di vapore prima della formazione della vera e propria bolla. L'ultima regione appartiene alle *non encapsulating bubbles*. Questo regime, presente alle basse temperature, è altamente rapido e instabile. Difatti il vapore non ha il tempo di riscaldare

gradualmente il liquido circostante e formare una bolla. Le analisi di questa porzione di mappa richiedono considerazioni a parte rispetto alle altre categorie.

4.2 Tempo di crescita delle bolle

L'interesse principale nello studio dei tempi di crescita delle bolle è legato alla possibilità di stimare quali fasi del chugging occupano un ruolo principale nella durata del ciclo. La Figura 6a mostra l'effetto della temperatura dell'acqua sulla crescita delle bolle con portata costante e pari a 7 [kg/(m^{2}s)]. Al crescere della temperature si ha la transizione tra *small* e *big encapsulating bubbles* evidenziata da uno step nel *growing time*. Infatti, mentre le prime hanno un tempo medio di circa 65 ms, per le ultime è pari a circa 80 ms. Questo poichè, se le bolle sono più piccole, è più veloce arrivare alle massime dimensioni. Inoltre, al crescere della temperatura si nota una maggiore dispersione dei dati. La Figura 6b rappresenta il *growing time* al variare del flusso di massa di vapore, con temperatura del liquido pari a 30 °C.In questo caso la variazione di forma di bolla e portata non sembra avere alcun effetto sul tempo di crescita. La regione delle *non encapsulating bubbles* presenta dei tempi di crescita e collasso dominati da fenomeni di turbolenza per cui non è possibile fare alcuna comparazione. In questo caso, infatti, il growing time è sempre inferiore a 30 ms, limite inferiore per il resto delle bolle.

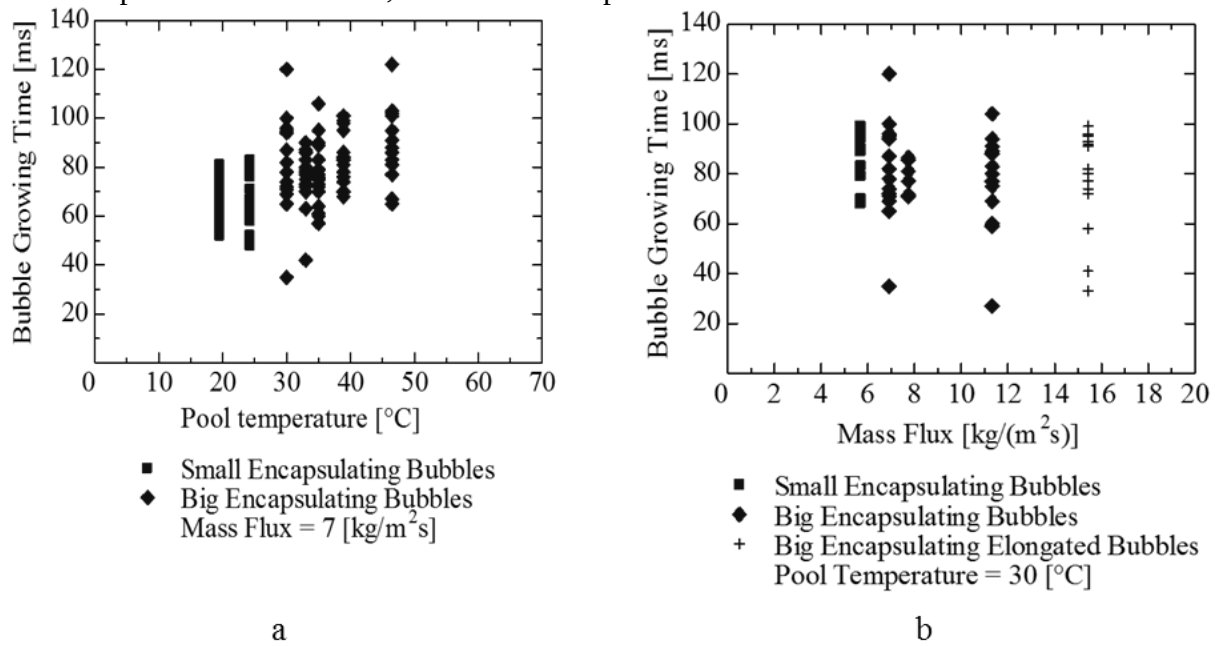

a b

Figura 6 Tempo di crescita delle bolle in funzione di a) temperatura dell'acqua e b) portata di vapore.

4.3 Implosione delle bolle

Lo studio del meccanismo di implosione delle bolle è di fondamentale importanza per incrementare la comprensione del fenomeno in modo da migliorare i modelli analitici e computazionali. Le modalità di collasso sono dipendenti dal tipo di bolla considerata. Le bolle che ricoprono il tubo implodono molto più lentamente rispetto alle *non encapsulating* e la posizione in cui avviene inizialmente il collasso è sempre diversa. Una possibile interpretazione qualitativa può essere dovuta al diverso effetto che la superfice di scambio della bolla e le turbolenza hanno sul regime. Entrambe le interpretazioni mostrate hano comunque bisogno di studi ulteriori analitici e computazionali e di setup sperimentali con array di termocoppie nella piscina. La Figura 7 mostra il collasso di una *encapsulating bubble* con il relativo segnale di

pressione. Quando la bolla è circa al massimo delle sue dimensioni si ritiene che si instaurino delle instabilità che rendono increspata la superficie esterna. Questo causerebbe un incremento dell'area di scambio e un conseguente aumento del tasso di condensazione che provocherebbe il collasso. La perdita di massa di vapore induce una riduzione di pressione, meglio rivelata dal trasduttore posizionato a 3 cm dall'uscita perchè più vicino al fenomeno. Questa repentina depressurizzazione porta all'aspirazione di acqua all'interno del tubo e l'inizio della terza fase del chugging. Quando l'acqua entra nel tubo si ha la competizione di due fattori contrastanti: da un lato il movimento dell'acqua pressurizza localmente il vapore mentre dall'altro l'ingresso di acqua fredda dal bulk causa un aumento della condensazione. A seconda della forza di questi due fenomeni, la risalita della pressione può essere più o meno brusca.

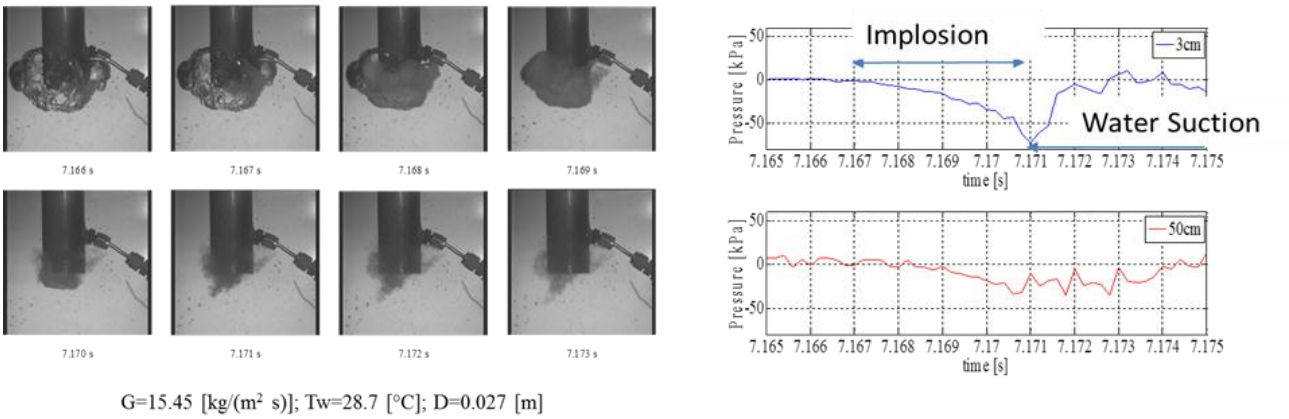

Figura 7 Collasso di una *encapsulating bubble* e relativi segnali di pressione sincroni.

Figura 8 mostra il collasso e i segnali di pressione inerenti una *non encapsulating bubble.*

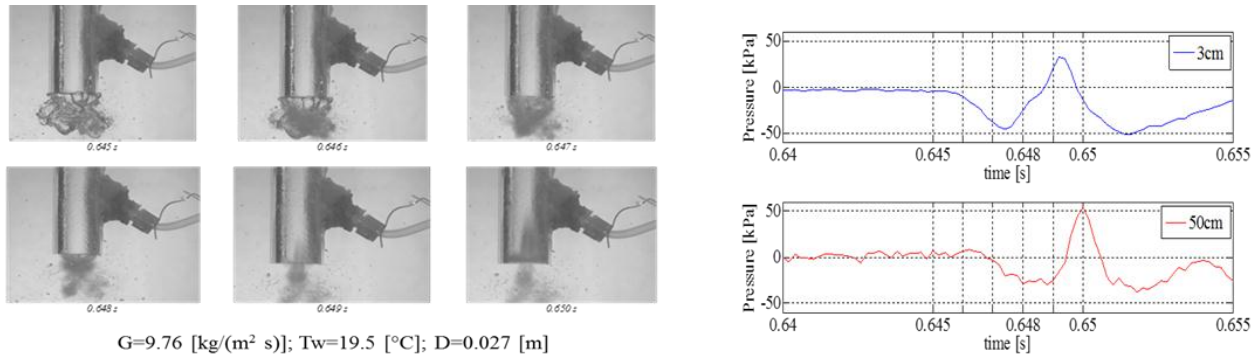

Figura 8 Collasso di una *non encapsulating bubble* e relativi segnali di pressione sincroni.

La spiegazione del collasso delle *non encapsulating bubbles*, per quanto grossolana per via di un'analisi solo visiva delle bolle, può essere'improvviso contatto con acqua fredda che causa un rapido incremento del tasso di condensazione e quindi il collasso della bolla. Così come accadeva per il tempo di crescita delle bolle, anche il collasso delle *non encapsulating bubbles* è più rapido. Non appena avviene l'implosione di bolla, si ha una riduzione di pressione, evidenziata dal trasduttore a 3 cm, che causa il rientro di acqua nel tubo. Ancora una volta, a causa dell'accelerazione del liquido verso il vapore circostante, la pressione risale nonostante la continua condensazione. Lavori come quelli di Ueno et al. [16] e Pellegrini et al. [23] sono alla base di uno studio più dettagliato del collasso di bolla.

Le differenti modalità di implosione di bolla descritte, giustificano ulteriormente la suddivisione della mappa nelle diverse regioni.

4.4 Condensazioni interne

In Figura 9a è mostrato un tipico picco di pressione causato da condensazioni interne al tubo. Per via della posizione in cui avvengono questi fenomeni, il trasduttore a 50 cm risulta essere più adatto alla loro rivelazione. Il picco di pressione massimo registato, attorno a 1.2 MPa, è più di due ordini di grandezza superiore rispetto a quelli relativi all'implosione di bolla pari circa a 40 kPa.

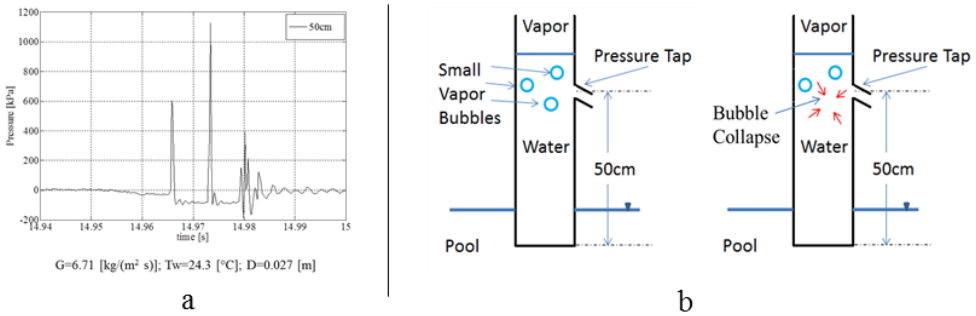

Figura 9 a) Picchi di pressione e b) fenomenologia delle condensazioni interne.

La pressione è inizialmente costante e pari a quella del vapore. Per via del mescolamento all'interno del tubo è possibile che piccole bolle di vapore si trovino intrappolate attorno a liquido freddo e avvengono fenomeni di condensazione, Figura 9 b. La riduzione della pressione che ne consegue causa accelerazioni del liquido che, per via della sua inerzia, comprime il vapore provocandone il collasso. Quando la bolla scompare, lo spazio vuoto è colmato dal liquido che, urtando su se stesso, genera delle deformazioni elastiche e la successiva formazione di un'onda di pressione. Bisogna sottolineare che in questo caso, il trasduttore a 50 cm misura la pressione nella fase liquida. Questo fenomeno appena spiegato prende il nome di *condensation induced water hammer*, CIWH o colpo d'ariete in italiano [24].

Una serie di esperimenti lunghi, esposti nella sezione 3.5, sono stati effettuati al fine di studiare questi picchi di pressione legati alle condensazioni interne al tubo. La Figura 10 mostra i risultati di tali esperimenti. La scala delle pressioni in ascissa è stata divisa in diverse classi di ampiezza pari a 100 kPa mentre la temperatura della piscina ha un intervallo pari a 5°C. Per ogni classe di temperatura, e quindi per ogni intervallo temporale per via della linearità tra queste due grandezze, i picchi di pressione sono stati contati e collocati nel rispettivo range di appartenza. Da Figura 10 appare evidente come i picchi di pressione siano più frequenti e intensi alle basse temperature e basse portate. Infatti, se l'acqua che rientra nel tubo è molto fredda è più semplice che causi l'implosione delle piccole bolle isolate mentre, le basse portate di vapore causano sia una maggiore risalita di liquido all'interno del tubo sia una maggiore difficoltà nel riscaldare il liquido e quindi il tempo per cui l'interfaccia si trova all'interno del tubo è notevolmente maggiore, agevolando in questo modo la formazione di picchi di pressione. Le due condizioni di basse temperature e portata corrispondono esattamente a quelle individuate per la formazione delle *small encapsulating bubbles*. Questo significa che, ogni volta che le bolle in uscita sono prevalentemente appartenenti a tale categoria, bisogna aspettarsi dei forti picchi di pressione all'interno del tubo. Questo metodo semplice ma efficace è di fondamentale importanza se si considera che, nella maggior parte dei small scale test, sono utilizzati tubi di acciaio che non consentono di vedere ciò che sta avvenendo all'interno.

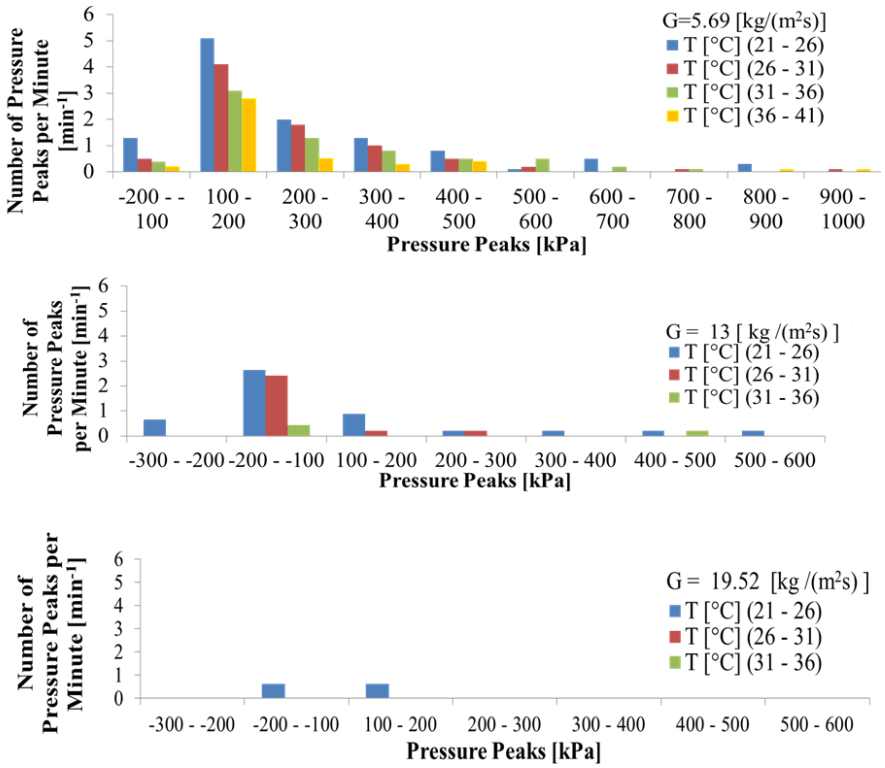

Figura 10 Numero di picchi di pressione al minuto al variare della temperatura e della portata.

4.5 Frequenza del chugging

Questa sezione si focalizza sulla frequenza di ripetizione di un ciclo di chugging ossia sul tempo medio che intercorre tra due formazioni di bolla. In Figura 11 appare il grafico dell'effetto della portata di vapore sulla frequenza del chugging a temperatura costante e pari 33 °C.

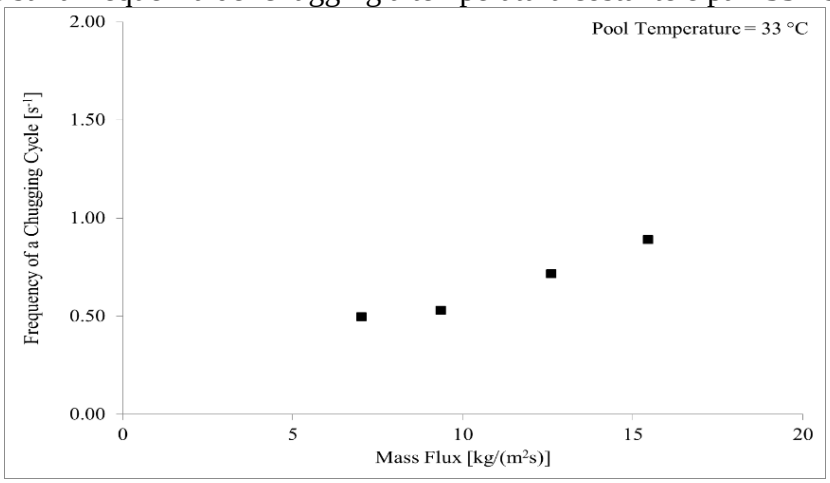

Figura 11 Effetto della portata di vapore sulla frequenza del chugging.

A basse portate, condizione di massima occorrenza dei picchi di pressione, la durata del chugging è strettamente legata alla fase delle condensazioni interne per cui ogni ciclo ha una durata molto lunga e la frequenza è bassa. Al crescere della portata, il vapore riscalda l'acqua molto più rapidamente e la frequenza aumenta. Infatti, come visto nella sezione 4.2, il tempo di crescita delle bolle non varia considerevolmente. In maniera duale, la Figura 12 riporta l'influenza della temperatura del liquido per due valori di portata pari a 6.9 kg/(m^2s) e 15.4 kg/(m^2s).

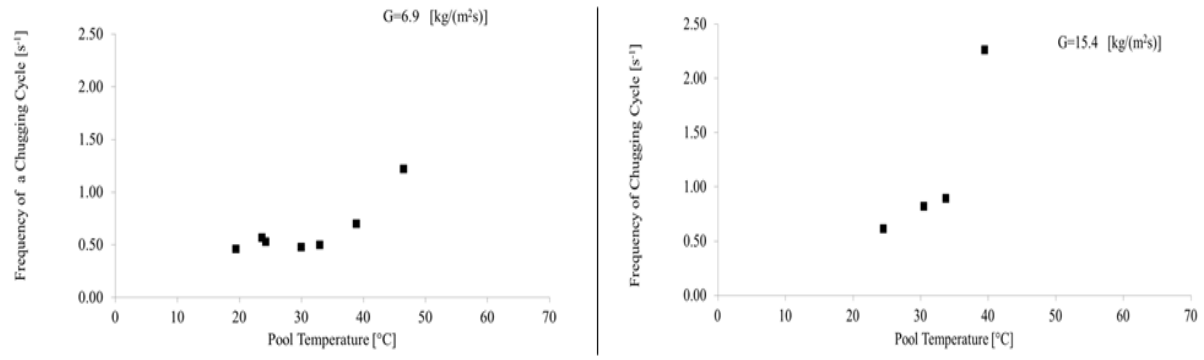

Figura 12 Effetto della temperatura della piscina sulla frequenza del chugging.

Quando la temperatura è attorno ai 20°C, nel caso di basse portate la formazione di bolla è rara a causa delle condensazioni interne mentre, per elevate portate, si ha la formazione di *non encapsulating bubbles* per cui la frequenza del chugging non è paragonabile rispetto agli altri casi. Al crescere della temperatura della piscina, esattamente come avveniva per la portata, le condensazioni interne diventano meno dominanti e la frequenza aumenta.

Capitolo 5 Sviluppi, miglioramenti futuri e conclusioni

A parte lo studio già previsto del chugging sfruttando tecniche CFD, diverse modifiche possono essere apportate all'apparato sperimentale in modo da perfezionarne le prestazioni. Tra la più importanti si segnala l'adozione di un ciclo di controllo della temperatura della piscina oppure la riiniezione dell'acqua calda della pool all'interno del main tank. Inoltre, è consigliabile la misura del flusso di massa più vicina al tubo di immissione, l'inserimento di un array di termocoppie sia nella piscina sia nel tubo, un miglioramento delle connessioni dei riscaldatori elettrici e la costruzione di una piscina di materiale diverso dall'acrilico. Nuovi spunti di studio possono essere trovati inserendo riscaldatori sulla steam line per ottenere vapore surriscaldato o posizionando la videocamera a 50 cm in modo da visualizzare le bolle isolate durante le condensazioni interne. Inoltre, sono necessari diversi passi in avanti dal punto di vista analitico. La migliore base di partenza è sicuramente seguire gli studi di Sargis et al [20] ed i miglioramenti introdotti da Ali et al [21]. Nonostante ciò il presente studio ha consentito di:

1. Investigare il meccanismo di ogni fase del ciclo del chugging
   a. Classifica il fenomeno del chugging a seconda della forma della bolla grazie alla creazione di una mappa di condensazione.
   b. Fornire due possibili interpretazioni che spieghino il diverso tipo di collasso riscontrato nelle bolle. Ulteriori analisi sono fondamentali per la validazione.
   c. Analizzare i tipici picchi di pressione che avvengono durante un ciclo di chugging che causano problemi riguardo il rischio di danni alle strutture. Si è evidenziato come questi picchi siano dovuti a condensazioni interne, abbiano ampiezze massime di 1.2 MPa e avvengano con maggiore frequenza a basse temperature e basse portate di vapore.
   d. Fornire un semplice metodo per predire le caratteristiche del chugging creando una connessione tra la forma della bolla e i picchi di pressione. Infatti, la formazione di *small encapsulating bubbles* e l'insorgenza di picchi di pressione avvengono entrambe per basse temperature della piscina e portate di vapore.
   e. Illustrare la scala temporale delle fasi del chugging e le sue variazioni in funzione dei parametri caratteristici della condensazione diretta.
2. Fornire risultati sperimentali per la futura validazione di codici CFD. Le immagini provenienti dalla videocamera di alta qualità saranno un tool unico e fondamentale a tal proposito.

English Version

Contents

List of Figures

List of Tables

List of Acronyms and Symbols

LOCA	Loss Of Coolant Accident
CFD	Computational Fluid Dynamics
LWR	Light Water Reactor
BWR	Boiling Water Reactor
PWR	Pressurized Water Reactor
ADS	Automatic Depressurization System
RCIC	Reactor Core Isolation Cooling
RHR	Residual Heat Removal
DCC	Direct Contact Condensation
CIWH	Condensation Induced Water Hammer
PT	Pressure Transducer
TC	Thermocouple
TTL	Transistor-Transistor Logic
DC	Direct Current
BNC	Bayonet Neill–Concelman
PTFE	Polytetrafluoroethylene
P	Pump
G [kg/(m^2s)]	Steam Mass Flux
ΔT [°C]	Water Subcooling
Ts [°C]	Steam Temperature
Tw [°C]	Pool Temperature
D [m]	Pipe Inner Diameter

m_v [kg/s]	Steam Mass Flow Rate
m_C [kg/s]	Condensation Rate
Q [W]	Heat Exchange Rate
S [m^2]	Interfacial Area
h_{fg}[kJ/kg]	Vaporization Enthalpy
h [W/(m^2°C)]	Convective Heat Transfer Coefficient
R [Ω]	Electrical Resistance
I_L [A]	Line Current
I_{ph} [A]	Phase Current
V_L [V]	Line Voltage
V_{ph} [V]	Phase Voltage
P [W]	Power
Δp [kPa]	Pressure Difference
fps	Frame per Second
M_s [kg]	Steam Mass
m_{in} [kg/(m^2s)]	Steam Mass Flux at Inlet
A_{in} [m^2]	Inlet Area
m_{out} [kg/(m^2s)]	Steam Mass Flux at outlet
A_{out} [m^2]	Outlet Area
m_{wall} [kg/(m^2s)]	Steam Mass Flux on walls of downcomer
A_{wall} [m^2]	Surface Area of downcomer wall
C_D [kg/(m^2s $Pa^{0.5}$)]]	Mass Inflow coefficient
p_D [Pa]	Drywell Pressure above orifice

p_s [Pa]	Steam Pressure in the downcomer
$p_{Sat}(T)$ [Pa]	Steam Pressure at Saturation temperature T
α	Accommodation coefficient for condensation
T_i [°C]	Interface Temperature
R_s[J/(kg°C)]	Gas constant for Steam
ChuGSA	Chugging Suppression Analysis

Introduction

On the 11th of March 2011 an accident occurred in Fukushima Daiichi Nuclear Power Plant caused by a magnitude 9 earthquake and the consequent tsunami wave. Among the lessons that this severe event taught to the nuclear world there are for sure the need to implement passive safety systems and evaluate the performance of current reactors during long transients. The loss of coolant from the primary loop (LOCA) is one of the postulated accident evaluated during the design of a nuclear reactor. Two different kind of reactor containment concepts can be installed in order to provide a barrier that prevents fission product release to the atmosphere subsequent a LOCA. The first type is a large dry containment, the second one, which was the solution used in Fukushima units, is a pressure suppression containment. The latter allows to limit the maximum drywell pressure and to obtain a rapid pressure reduction through the passive injection of steam, generated by the flashing of water during a LOCA, inside a pool [4]. Indeed, the direct contact condensation (DCC) of steam assures a higher heat transfer coefficient than usual condensation techniques. However, depending on 3 main parameters - water subcooling, steam mass flux and pipe inner diameter - an unstable flow condition called chugging may occur. Chapter 1 focuses on the definition of LOCA and on the explanation of the pressure suppression safety systems in BWRs, whereas chapter 2 highlights the DCC features and specifically chugging phenomenon. Chugging can be defined as a depressurization induced by the bubble implosion at the pipe outlet that causes a cyclic suction of water inside the pipe. The presence of high pressure peaks is characteristic of this regime. The purpose of this study is to investigate the mechanisms of every phase composing a chugging cycle and to provide

experimental results useful for the validation and development of CFD approaches. In order to achieve these objectives, a small scale facility was constructed (3.1, 3.2, 3.3) and an experimental campaign was performed (3.4 and 3.5). The steam mass flux range was 5.5-19.5 kg/(m^2s) while the pool temperature one was 19-46.5 °C. Two different pipe materials were used, stainless steel and transparent polycarbonate, but the inner diameter was kept constant and equal to 27 mm. Pressure pulses were measured with two semiconductor pressure transducers located inside the pipe at 3 cm and 50 cm from the outlet and a high speed video camera was used for supporting the investigation of the phenomena.

Chapter 1

Boiling Water Reactors and Safety Systems in the Pressure Suppression Pool

Nowadays nearly one fourth of the electric energy used in Western Europe countries is produced using nuclear reactors even if this number is expected to decrease due to high concerns among the public about the exploitation of this source, especially following the mentioned accident [25]. Among all nuclear reactors, Light Water Reactors (LWRs) are by far the most used technology [26]. This category of reactors can be divided into two parts depending on the state of the water in the core. When the water is boiling inside the vessel and the steam produced is sent with a direct cycle to the turbines, the reactor is called Boiling Water Reactor (BWR) whereas, on the other hand, when the water is pressurized in order to have it always in the liquid phase and another cycle is added to produce the steam for the turbines, the reactor is called Pressurized Water Reactor (PWR).

An example of a typical BWR configuration is shown in Fig. 1.1.

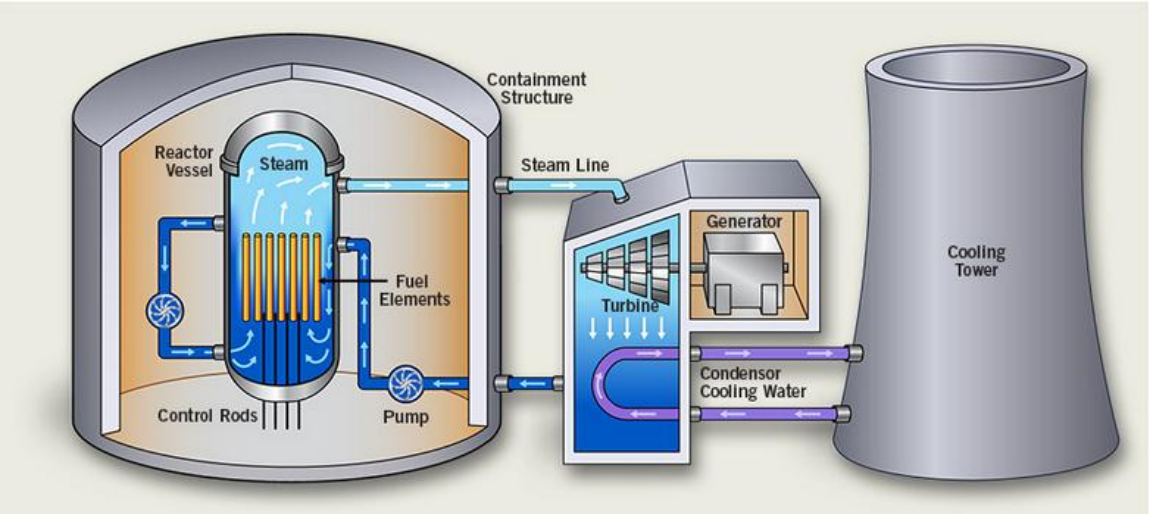

Fig. 1.1 BWR simplified scheme **[27]**.

The reactors used in Fukushima power plant were all BWR type; units 1 to 5 were built with Mark I type containment building while unit 6 had a Mark II containment.

Fig. 1.2 and Fig. 1.3 show these two kinds of pressure suppression containment. It must be highlighted that Fig. 1.2 b and Fig. 1.3 b do not represent exactly the design of Fukushima Daiichi Nuclear Power Plant.

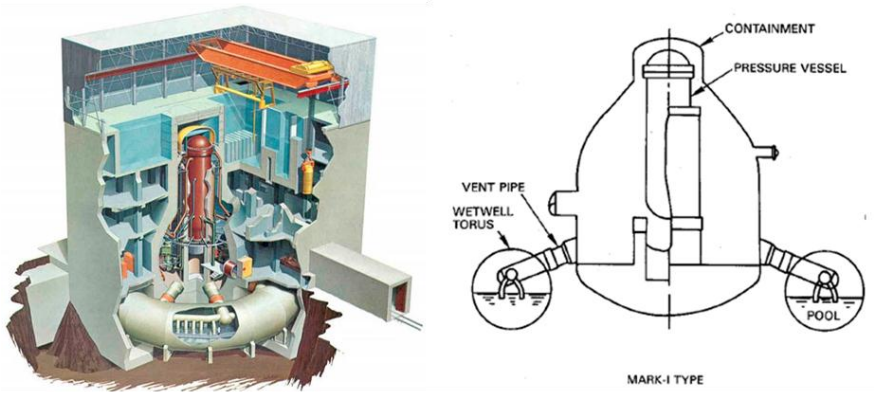

a b

Fig. 1.2 Mark I Containment.

(a) General Electric Design **[28]**, **(b)** Modified Japanese Mark I **[4]**.

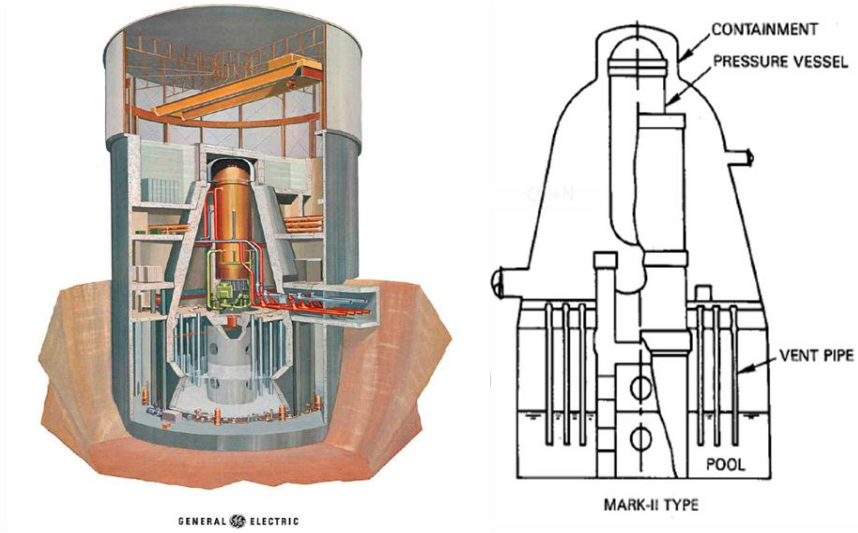

a b

Fig. 1.3 Mark II Containment.

(a) General Electric Design **[28]**, **(b)** Modified Japanese Mark II **[4]**.

At this moment, there are 78 operational BWRs in the world with a total net electrical capacity of 74686 MW. Most of these reactors are in the US with a total of 35 BWRs and Japan with 24 BWRs [29]. However, none of the Japanese nuclear power plants is currently producing electric energy. Among the 35 BWRs located in US, 23 are operating with a Mark I containment design [30].

Even if the technology of BWRs was employed since the beginning of nuclear energy production era, huge progresses were made during the years to improve the performances of this kind of systems from every point of view: exploitation of the fuel, minimization of wastes, safety, economics, etc. Safety assessment on nuclear reactor performances always begins with the identification of initiating events and the definition of design basis accidents which the reactor must withstand. Amidst these postulated accidents there is the LOCA from the primary loop due to a guillotine cut of the main steam line or recirculation line. When this circumferential pipe rupture and double-ended blowdown of reactor coolant begins, drywell pressure increases. Thanks to a series of venting pipes that connect the drywell, where the vessel is located, to the wetwell, which is approximately half filled with water, it is possible to remove the steam from the drywell and later condense it. Indeed, in this way the pool of a pressure suppression containment provides a heat sink for the DCC of steam produced during a LOCA or the continuous quantity generated by the core decay heat. Once the venting pipes inserted in the pool are completely cleared from the water, this expulsion of air and steam allows to obtain a pressure reduction assuring that working conditions are below the designed drywell pressure. It must be guaranteed that the suppression pool is able to absorb energy for at

least 6 hours if the Residual Heat Removal (RHR) system is unavailable for the cooling of the water pool [4].

Another passive feature of the pressure suppression system is the retention of the radioactive fission products inside the water pool. Moreover, apart from withstanding LOCA, pressure suppression pool is fundamental in at least other two safety system. The first one is the Automatic Depressurization System (ADS) which allows the reduction of pressure inside the vessel. This operation is important both in operational condition and during an accident if the level of water inside the core cannot be maintained at high pressure. It basically involves the DCC of steam produced in the core onto the pool in the suppression chamber. The other safety system that involves the use of the suppression pool as a heat sink is the Reactor Core Isolation Cooling (RCIC) system which assures a cooling of the reactor exploiting the steam produced by the fission product decay heat. This steam is expanded in a turbine which drives a pump that injects coolant, which might be taken from the suppression pool itself, inside the core. The exhausted steam is then injected inside the pressure suppression pool and DCC occurs. Fig. 1.4 shows a schematic drawing of a BWR containment building and its safety systems related to the pressure suppression pool.

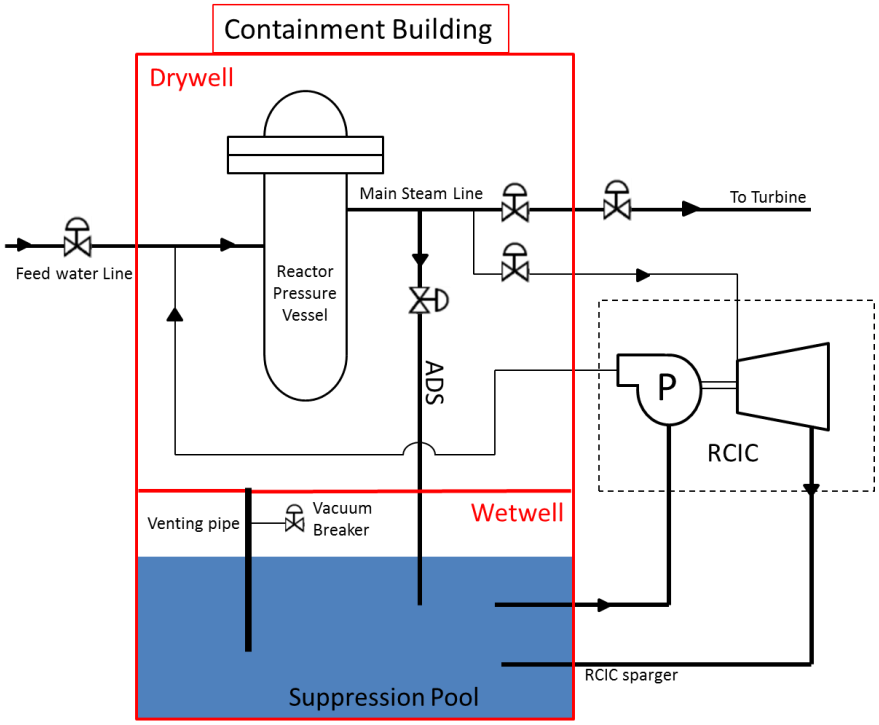

Fig. 1.4 General scheme of the pressure suppression pool.

The venting pipes in Mark I and Mark II containment building are vertically inserted inside the water pool while, on the other hand, Mark III, shown in Fig. 1.5, have horizontal venting pipes. Beside this, steam quenchers on the ADS and RCIC spargers might have really complicated shapes [31] [32].

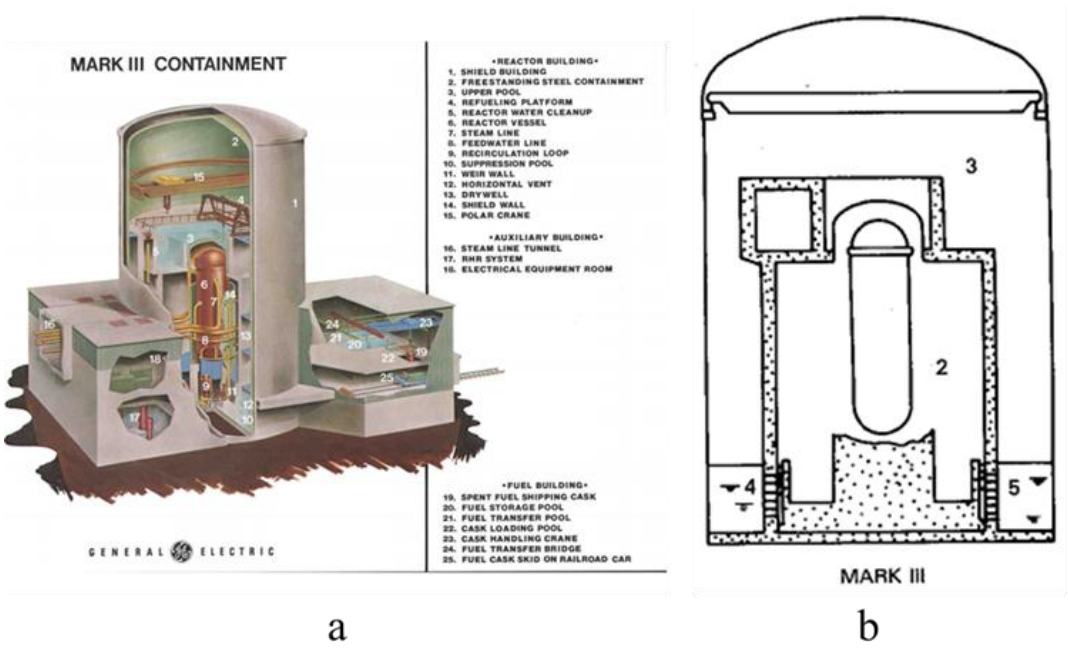

Fig. 1.5 Mark III Containment.

(a) General Electric Design **[28]**, **(b)** General Electric scheme **[4]**.

Chapter 2

Direct Contact Condensation and Chugging Phenomena

2.1. Direct Contact Condensation (DCC)

The direct contact condensation is an effective way to condense steam. Despite the way of condensing in heat exchanger, DCC involves simply the ejection of the steam inside a subcooled water pool. The contact and mixing of the two phases assure a higher heat transfer coefficient and thus a higher condensation capability than usual techniques where the two fluids are separated.

Different condensation regime may develop depending on three main parameters [5] :

- Inlet steam mass flux , G [kg/(m^2s)]
- Water Subcooling, $\Delta T = Ts - Tw$ [°C]
- Pipe inner Diameter, D [m]

The three parameters can be visualized in Fig. 2.1.

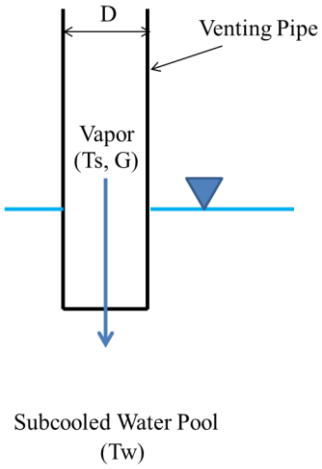

Fig. 2.1 DCC Fundamental Parameters.

The steam mass flux is a measure of the driving mechanism, the water subcooling takes into account the magnitude of the condensation rate and the pipe inner diameter is a

characteristic dimension of the test section. Depending on the steam mass flux, the water subcooling and the pipe inner diameter, different regimes can be identified observing visually DCC. In this way, the three mentioned quantities become the three axes for the construction of condensation regime diagram which allow cataloguing the phenomena peculiar of DCC. In Fig. 2.2 a regime diagram is shown.

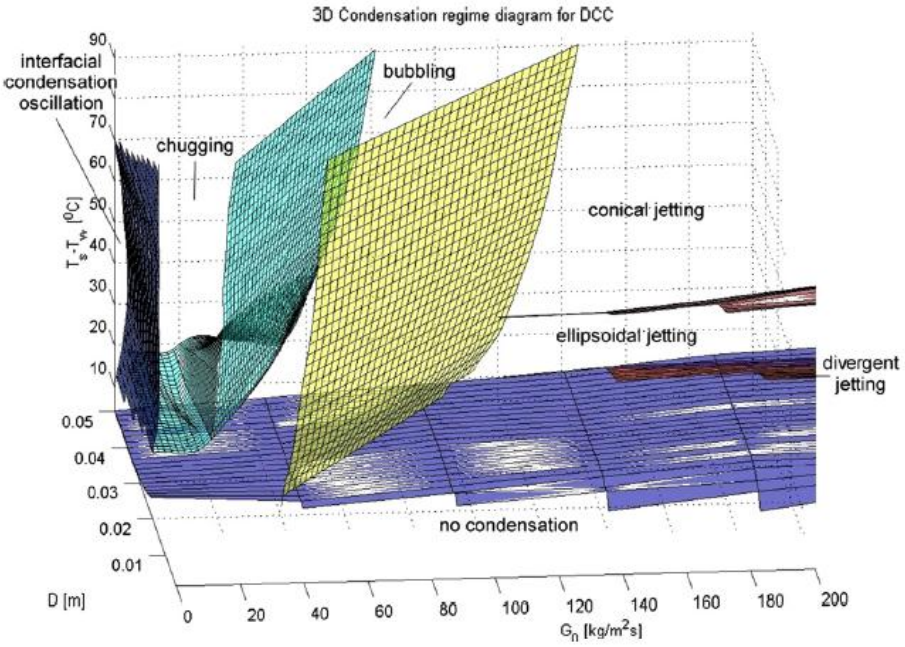

Fig. 2.2 DCC 3D regime diagram **[5]**.

Three main regimes can establish:

1. Jetting
2. Bubbling
3. Chugging

Jetting occurs at high steam mass flux and it is characterized by a constant shape of the steam plum at the outlet of the pipe. Depending on the conditions of the three parameters previously mentioned, the steam region can have different aspects (conical, ellipsoidal and divergent). Fig. 2.3 shows a representation and a picture of the jetting regime.

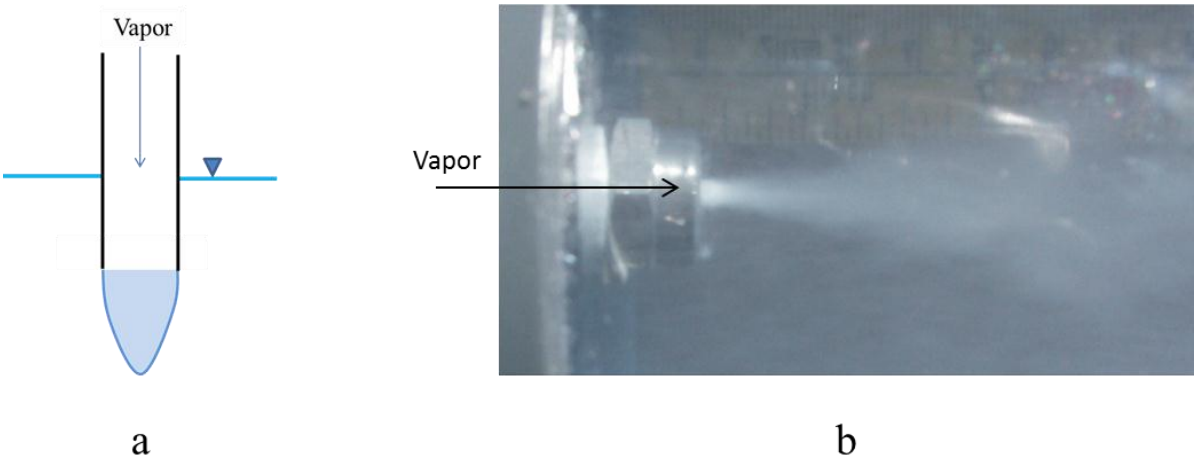

Fig. 2.3 Jetting steam plume.

(a) Scheme of jetting regime, **(b)** picture of jetting regime [5].

Bubbling regime, which occurs mostly at intermediate mass flux of the steam, is the periodical generation of bubbles that detach from the pipe outlet. Fig. 2.4 shows a typical bubbling cycle.

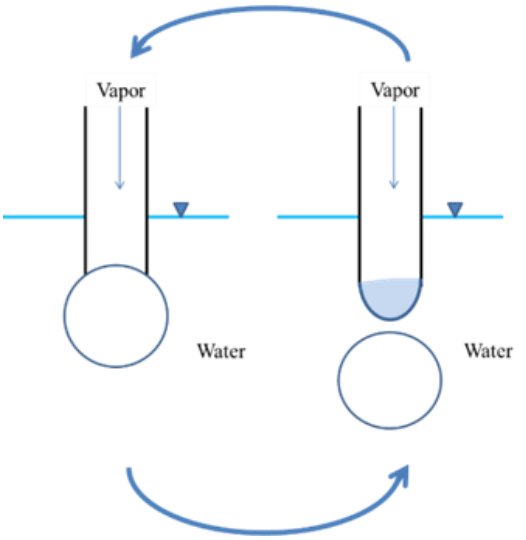

Fig. 2.4 Bubbling cycle.

Chugging occurs at very low steam mass flux. It is characterized by the collapse of the bubble at the outlet of the pipe and the suction of water inside the pipe. Chugging is a cyclic repetition of sequences of events, shown in Fig. 2.5, but its nature is more chaotic and unstable. This phenomena is always associated to pressure pulses that cause dynamic loads to the pipe and the pool.

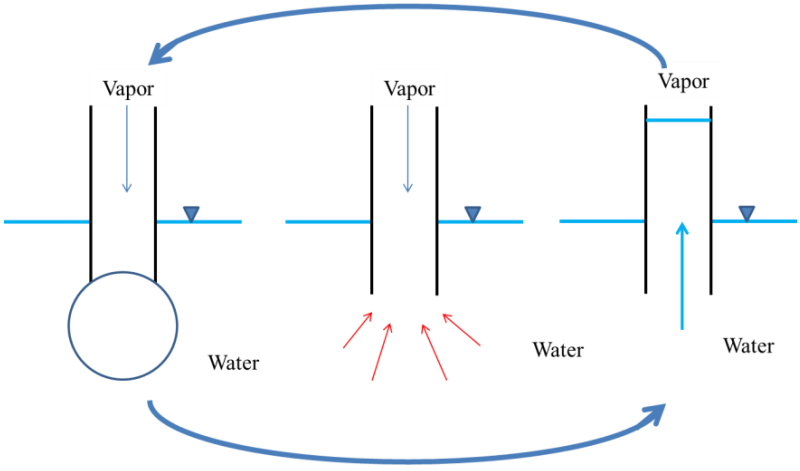

Fig. 2.5 Chugging scheme.

Every chugging cycle can be divided into five different moments:

1. Bubble Growth
2. Bubble Collapse
3. Water Suction
4. Internal Condensations
5. Steam Ejection

Fig. 2.6 shows the five sequences previously mentioned. For every event a representative picture with the correspondent number is inserted. An idea of the time scale is also added.

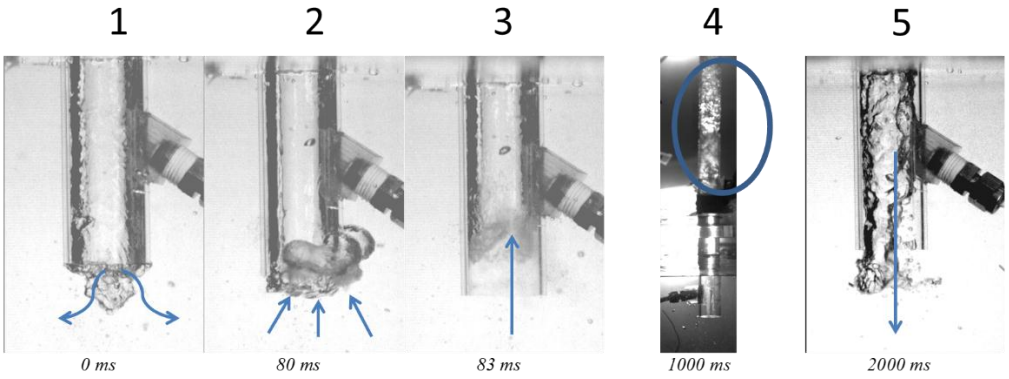

Fig. 2.6 Chugging cycle.

The whole chugging cycle depends strongly on the continuous unbalance between the inlet steam mass flow rate m_v and the condensation rate m_c. The interface moves in different directions depending on the inequation 2-1:

$$\boldsymbol{m_v \gtreqless m_c} \qquad (2\text{-}1)$$

When the inlet steam mass flow rate m_v is higher than the condensation rate m_c a bubble is formed at the outlet of the pipe. Then the bubble increases its size due to the continuous

supply of steam coming from the steam line leading to an enhancement of the condensation due to the bigger interfacial area. There will be a condition in which m_c equals m_v and the bubble reaches its maximum dimension. At this point, both instabilities of the bubble surface that increase abruptly the interfacial area S and the mixing of the steam with cold water coming from the bulk of the pool, increase the heat exchange rate Q and the condensation rate m_c and the bubble finally collapses. A general energy balance at the bubble surface is expressed by equation 2-2.

$$\boldsymbol{Q = h * S * (T_S - T_W) = m_c * h_{fg}} \qquad (2\text{-}2)$$

Where h is the convective heat transfer coefficient and h_{fg} is the vaporization enthalpy of the steam inside the bubble.

The collapse of the bubble and the subsequent loss of steam mass induces a pressure reduction at the pipe outlet. Then water can flow inside the pipe reaching high elevations. When the interface is inside the pipe, the condensation rate is higher than the inlet steam mass flow rate and the temperature of the liquid is cold enough to cause quick internal condensations inside the pipe. Only when m_c decreases due to the heating of the liquid at the interface, the steam flows back outside the pipe. Before a new bubble starts growing, is necessary to wait until the steam heats up enough the surrounding liquid. At the time that this condition is achieved a new chugging cycle takes place.

2.2. Chugging Phenomena in BWRs' Pressure Suppression Pool

As introduced in chapter 1, in case of a LOCA steam is produced and pressurizes the drywell. In order to reduce the drywell pressure, the steam is injected in the wetwell where

it condenses because of the direct contact with subcooled water. In this way, the water of the pool represents a passive heat sink which is normally used also in operation condition to depressurize the core through safety relief valves. A typical pressure history in the drywell and in the wetwell after a LOCA accident is shown in Fig. 2.7. Pressure initially increases in the drywell because of the steam production but, when the water is completely removed from the pipe, pressure decreases again to level a little higher than the wetwell.

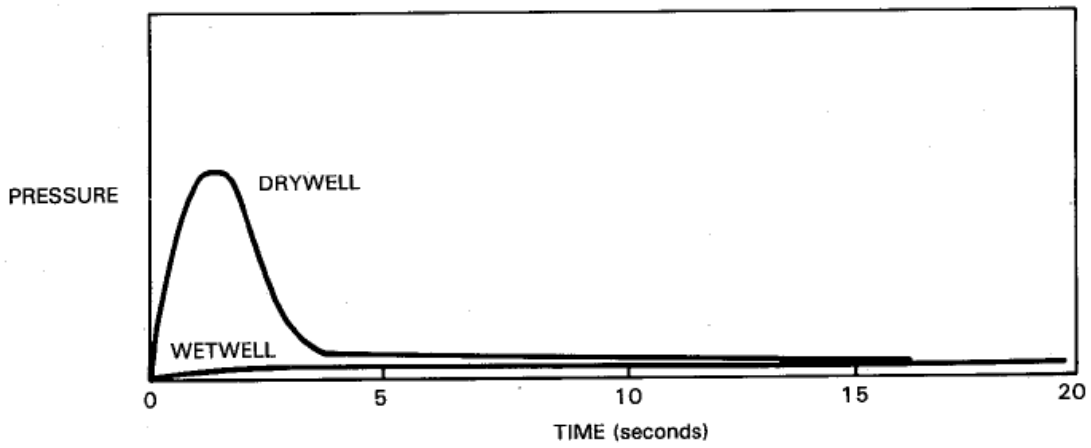

Fig. 2.7 Pressure history after a LOCA accident in the drywell and in the wetwell **[4]**.

During the initial phase of a LOCA, the water is expelled from the venting pipe and it is replaced by air. After the clearing of air from the venting pipe, DCC of steam occurs. Initially the steam flow rate is high and jetting or bubbling are expected to develop so that no dynamical loads should occur in this condensation regimes. However, in the latest phase of steam expulsion, when the flow rate decreases considerably and non-condensable air is almost totally removed from the flow, the unstable condensation regime called chugging may take place. Aya et al. [1], Pitts [17] and Kukita et al. [33] wrote about the possibility of insurgence of chugging phenomena in pressure suppression pool during a LOCA.

Moreover, as it will be more detailed in section 4.3.1, depending on the conditions of the steam and of the water in the pool, multiple internal condensations when the interface between steam and water is inside the pipe might happen. Both internal condensations and bubble implosion are very violent phenomena characterized by pressure peaks which cause dynamical loads to the structure. This unstable flow condition with hydrodynamic loads related to both air expulsion and chugging were not predicted by analytical methods in use at the time when pressure suppression systems were initially studied. For this reason, the design was based only on experimental tests with well-accepted design factors that could not employ current technologies [4].

2.3. Reviews of Previous Studies

DCC and chugging phenomena had been deeply investigated. This review is divided into three parts depending on the main objective of the study: DCC map creation, experimental approach and analytical work.

Condensation regime map were the main purpose of some researchers like Aya et al. [1] who created a DCC regime map depending on the pressure pulses characteristics and Chan et al. [2] who added also a rough explanation of the bubble shapes including the term ‘’encapsulation’’ widely used in this study. Cho et al. [3] developed a DCC regime map injecting steam horizontally inside a subcooled pool but the steam mass flux range is higher than the one considered in the present study and pressure pulses are relative to the pool walls. Lahey et al. [4] created a qualitative regime map of DCC and analysed bubble

behavior based on Rayleigh equation and on an energy balance. Petrovic de With et al. [5] presented a three dimensional regime map, adding the injector size diameter as a fundamental parameter. He was the first one proposing the use of the three main parameters (steam mass flux, water subcooling and pipe inner diameter) and he was able to summarize the previous works but distinctions among chugging regimes were not considered.

An experimental approach was mostly used by other scientists, understanding the difficulties in modelling this kind of phenomena with analytical studies. Youn et al. [6] investigated the frequency of generation of the pressure pulses characteristics of chugging phenomena by counting the number of peaks observed in the signal. The injector nozzle is horizontal and with a diameter similar to the one used in the present study. However, no distinction among the origin of the pressure peaks and their amplitude was made. Marks [7] investigated the characteristics of the pressure signals during chugging and condensation oscillation phase and proposed an interpretation that account simultaneously for both regimes. Both phenomena were accurately described, and the presence of internal chugs was highlighted. Nariai et al. [8] evaluated the oscillation frequency of chugging phenomena. Purhonen et al [9] and Laine et al. [10] detected high pressure peaks related to internal condensations. Water hammer was also highlighted to be the cause of the pressure pulses inside the pipe. However, the frequency of occurrence of the pressure peaks and the effect of the mass flux, bubble shape and pool temperature was not analysed. Also Class et al. [11] performed experiments on chugging phenomena placing thermocouples and strain gauges along the pipe and the pool. The entrainment of steam pockets, exactly like what

happened in horizontal pipes in the condensation induced water hammer phenomena, was believed to be the cause of the revealed chugging pressure peaks. However those peaks are not comparable to the level obtained in the present study. Liang et al. [12] investigated the effect of air addition to the steam flow in suppressing chugging occurrence and gave a method for evaluating the transition criteria between the different regimes. Araneo et al. [15] investigated the effect of air on bubble growth and implosion and the necessary air mass flow rate that suppresses chugging phenomena. Effect of pool mixing cause by the air was also considered. Solom et al. [13] and Song et al. [14] focused on the effect of the pool stratification on a suppression pool simulated system. Different experiments were performed varying the pressure of the wet well but, in every conditions, chugging regime occurred for low pool temperatures. The strong mixing induced by chugging maintained the temperature uniform suppressing the thermal stratification. Other experimental studies were mostly focusing on the bubble implosion with different applications from the one proposed in this thesis. Ueno et al. [16] investigated the bubble collapse at low steam velocities in order to take into account only the effect of the condensation and showed that the collapse occurs only when small disturbances on the bubble surface arises. However, in contrast with Pellegrini et al. [23] work, they insist that the interfacial instability that causes the collapse is not the Rayleigh-Taylor.

Analytical models, supported by experimental results, were also developed. Bankoff [18] studied condensation phenomena related to safety issues in LWRs. Water hammer subsequent bubble collapse is included in one of the potential problems, even if the main concern is not focused on pressure suppression pool but on PWR's steam

generators. Pitts [17] analysed chugging phenomena on physical principles without the addition of any free parameters. Block [19] studied common features related to different DCC regimes summarizing the state of art dated back to the time the paper was written. Sargis et al. [20] proposed an extensive chugging model facing different problems related to the phenomena. Mostly, pressure signals in different location where considered. The formulation is relatively free from empiricism and good agreement with experimental results is achieved. The model proposed by Sargis was then completed and expanded by Ali et al [21] who introduced in their study the effect of non-condensable gases and the effect of the condensation on the vent pipe inner surface on chugging phenomena. Sursock et al. [22] proposed a dynamic model in order to capture the main feature on chugging. He mostly focuses on the bubble behaviour and on the condensation heat flux evaluation.

The creation of 3D map made no distinction among chugging phenomena regime. This causes the need to construct a new diagram map which considers the different ways of behavior of the interface in chugging regime. Moreover, as it might be clear, most of the experimental studies have some point in common with the present analysis. However, it was rarely studied the origin of the pressure peaks and their mechanism. In addition to this, the pulses revealed during the present experiments were considerably higher than most of the previous study and none of them tried to explain deeply all the phases composing a chugging cycle.

Table 2.1 gives a summary of the previous study that focused mostly on DCC map creation and approached chugging experimentally [34], [35], [36].

Table 2.1 Summary of the previous experimental studies related to chugging phenomena and bubble collapse.

Reference	Pipe Inner Diameter [mm]	Pool Temperature [°C]	Mass Flux kg/(m^{2}s)	Pipe Orientation	Measuring Instruments and their location	Notes
Aya et al. [1]	18.29	10 - 85	0 - 40	Vertical	Pool temperature 5cm from the pipe outlet.	
Chan et al. [2]	50.8	40 - 90	0 - 175	Vertical	Movie camera. Thermocouple at the pipe outlet. Pressure transducers inside the pipe and in the pool walls.	Superheated steam. Steam dump for degassing. Control of the pool temperature.
Petrovich de With et al. [5]	10 - 50	10 - 100	0 - 200			Collection of experiments performed by other authors.
Cho et al. [3]	5-20	20 - 95	24 - 1190	Horizontal	Pressure sensor at the pool wall, 75 cm from the pipe outlet. Video camera with halogen lamps. Thermocouples in the pool.	Calibration of the flow meter with the constant volume method.
Youn et al. [6]	15.9 and 19	20 – 70	10 - 80	Horizontal	High speed camera synchronized with a pressure sensor located in the pool. Resistance temperature detector far from the outlet.	High pressure steam. Direct loop to control the pool temperature. No effect of the pipe material and the drywell.
Marks et al. [7]	25.4, 4.5, 101.6 and 304.8	20 – 90	10, 20 and 30	Vertical	Piezoelectric pressure transducers in the pool. Strain gages in the pipes. Thermocouples in the pool. Measure the air flow rate.	No effect of the drywell. Installation of a steam dump. Development of an analytical model.
Nariai et al. [8]	18.29	20 – 80	0 – 200	Vertical		Linear frequency analysis.
Purhonen et al [9]	85, 110, 214	11 – 76	4 - 13	Vertical	Pressure transducers inside the pipe. Thermocouples inside the pool and inside the pipe. High speed camera.	Detection of high pressure peaks inside the pipe. Low fps of the camera. High pressure steam.
Class et al. [11]		25	20	Vertical	High speed camera. Thermocouples in the pipe and in the pool. Strain gauges inside the pipe.	Steam pressure equal to 117 kPa. Only 4 chugging cycles per experiment.
Liang et al. [12]	19	60 – 90	0 – 50	Vertical, upward		Investigation of the effect of air in suppressing chugging.
Solom et al. [13]	38	40 – 100	34 (steam + water)	Vertical	Arrays of thermocouples distributed in the pool. Thermocouple inside the pipe, near the outlet.	Deionized water pool. Hot water from the pool is sent inside the steam generators.
Song et al. [14]	4.2	40 – 88	3.06 - 19	Vertical	High speed camera/ halogen lamp system. Arrays of thermocouples.	Heaters in the steam line to prevent condensation. Experiments under sub-atmospheric pressure.
Araneo et al. [15]	200	10 - 100	1 and 3	Vertical	Thermocouples inside the pool. High speed camera	Investigated the effect of air on chugging. Nearly constant water level during experiments.
Ueno et al. [16]		30 – 100		Vertical, upward	High speed camera. Control of the pool temperature with a cooling loop. Generator of single bubbles. Thermocouple in the pool.	Bubble implosion analysis related to a different field from chugging
Sargis et al. [20]	22.25	20		Vertical	Pressure measurements inside the pool and inside the pipe. High speed films.	Analytical model compared with experimental results.

2.4. Purpose of this Study

This study focuses on chugging phenomena occurring during DCC of steam inside a water pool. Despite the previous studies, the entire chugging cycle described in the section 2.1 is investigated, using transparent pipes and pool, pressure transducers and a high speed video camera. Because Youn et al. [6] observed no noticeable effect of the downcomer material and of the presence of a drywell, these aspects were chosen freely. Moreover Pitts [17] showed that there is no effect of pipe submergence in chugging which allowed having fewer restrictions in the design of the facility. The purposes of this study are:

1. Investigate the mechanisms of every phase of the chugging cycle:
    a. Classify chugging phenomena depending on the bubble shapes
    b. Give a qualitative interpretation of bubble collapse phase
    c. Inspect the typical pressure peaks occurring during chugging cycle which arise concern on damages to the structure.
    d. Give a simple method for predicting chugging characteristics creating a link between bubble shapes and pressure peaks
    e. Illustrate time scale of chugging phases and its variation as a function of DCC parameters.
2. Provide experimental results for the validation and development of CFD approaches.

Experimental results are shown following the same sequence of the chugging cycle. At first is evaluated the bubble growing time in order to consider what are the main components that affect chugging duration. Then bubble implosion dynamics is analysed in order to assure an improvement on the understanding of the phenomenon that might lead to an

improvement of the analytical and numerical models. After this, the phase when the interface is inside the pipe is studied focusing mostly on the intensity of the pressure peaks and chugging frequency. All these physical quantities characteristics of chugging phenomena are analysed as a function of the steam mass flux, the pool temperature and the bubble shape.

Chapter 3

Experimental Apparatus, Measuring Instruments and Experimental Procedures

ChuGSA Facility has been built to study chugging phenomena in the laboratories of Tokyo Institute of Technology. Its construction started in early October 2014 and it was completely finished in December 2014. Every component had been carefully selected in order to reach the desired working condition and operate in safety. It is mainly composed by a main tank, a steam line, two evacuation lines and the test section. The test section consists of a venting pipe and a pool. Inside the main tank, boiling occurs thanks to six electrical heaters and steam is produced. Through the steam line and the venting pipe, steam is transferred and injected inside a transparent, acrylic pool where it rapidly condenses.

3.1. Experimental Apparatus

The experimental apparatus, shown in Fig. 3.1, is constituted by:

- Main tank
- Steam line
- Two Evacuation lines, A and B
- Test section.

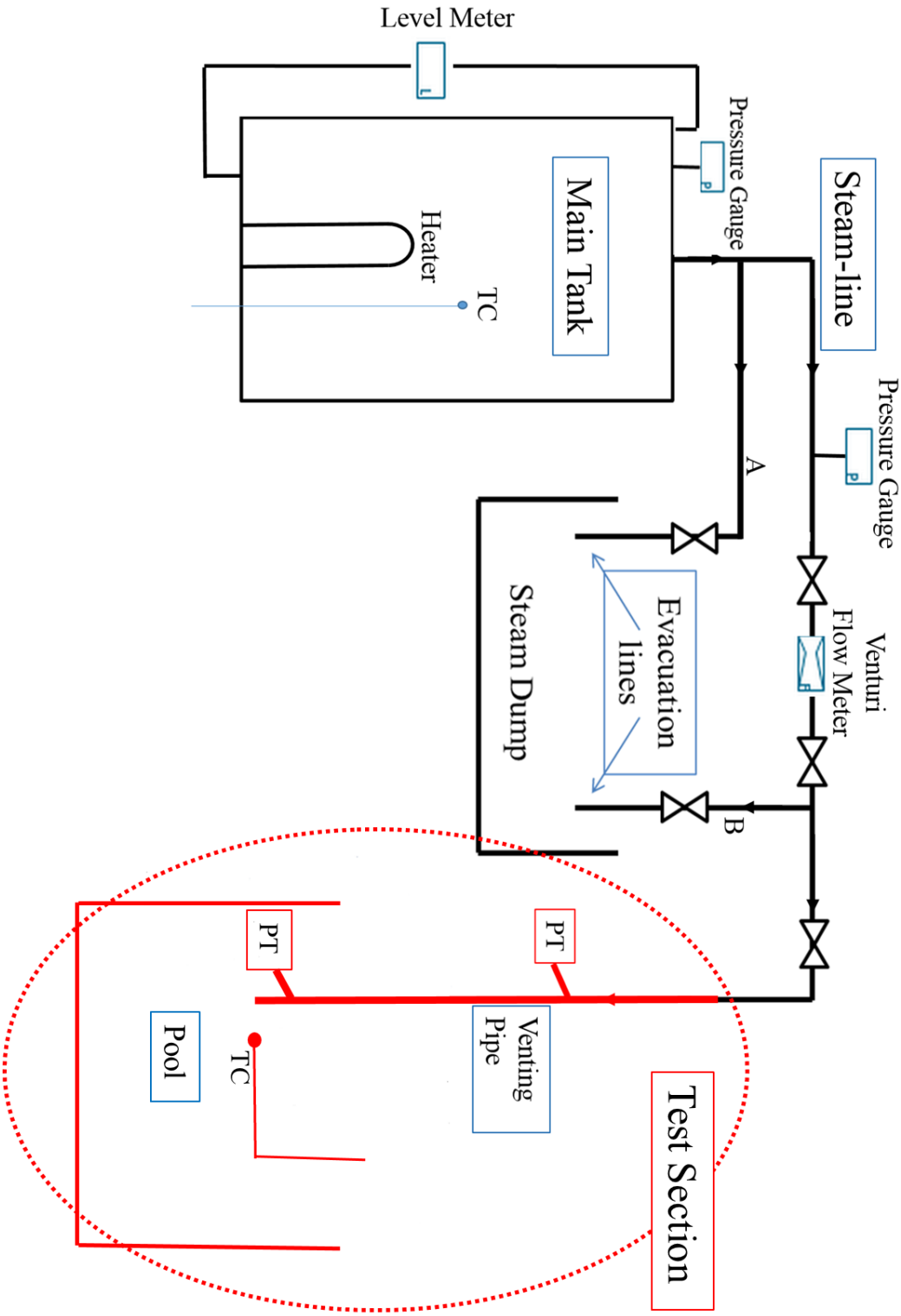

Fig. 3.1 Experimental apparatus scheme.

3.1.1. Main Tank

The boiling occurs in a stainless steel cylindrical shape main tank. It is totally 120 cm height and its inner diameter is equal to 40 cm.

The design of the main tank is reported in Fig. 3.2, whereas Fig. 3.3 shows two pictures of the main tank.

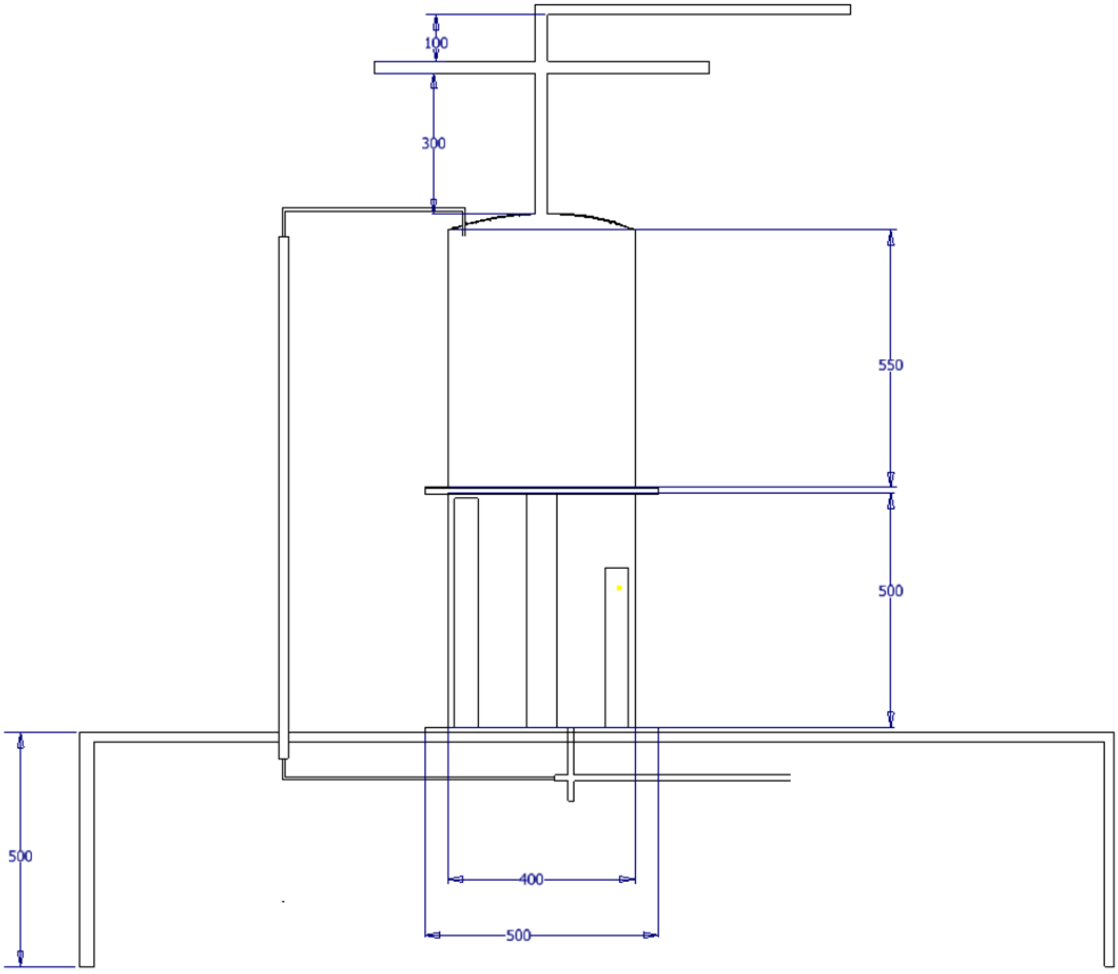

Fig. 3.2 Design of the main tank.

a **b**

Fig. 3.3 Pictures of the main tank **(a)** with and **(b)** without insulator.

The whole tank is composed by two stainless steel parts flanged together. In Fig. 3.3 b is possible to distinguish easily these two parts because of the different colour. The lower part, shown in Fig. 3.4, is 50 cm high, while the upper part is 55 cm high. The inner diameter of both the components of the main tank is 40 cm and the thickness is only 0.4 cm. The lower part is flanged at the bottom with a stainless steel plate through which are inserted six electrical heaters. The dimensions of this two flanges, one connecting the plate to the lower part and the other connecting the lower part to the upper part, are exactly the same with an inner diameter equals to 40 cm, an outer diameter of 50 cm and a thickness of 1 cm. Both flanged connections are kept together with 16 bolts and the use of a silicon packing that prevents water leakages. The upper part is equipped with two handle to facilitate the lift up

and is curved toward the centre of the tank where it ends with a 2 inch (roughly 5.1 cm) diameter hole that connects the main tank to the steam line. In order to limit the heat losses due to heat exchange from the main tank to the environment, a thick insulator covered the entire tank as it is possible to see in Fig. 3.3.

The main tank is 50 cm elevated from the ground thanks to a supporting stainless steel structure. This elevation was made in order to better handle the connections of the electrical heaters, inserted from the bottom, and to facilitate the access to the main tank.

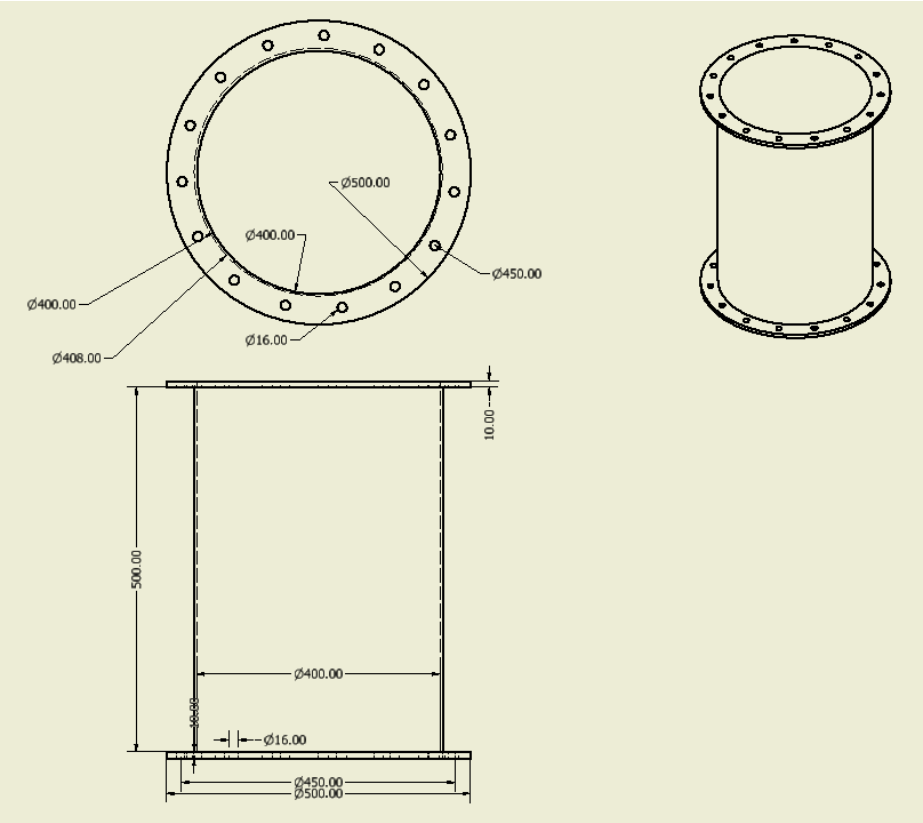

Fig. 3.4 Lower Part of the main tank.

In Table 3.1 are summarized the fundamental dimensions and characteristics of the main tank.

Table 3.1 Summary of the dimensions and the characteristics of the main tank.

Total Height of The Main Tank	1200 mm
Inner Diameter of the Main Tank	400 mm
Thickness of the Main Tank	4 mm
Elevation of the Main Tank from the Ground	500 mm
Outlet Diameter	50.8 mm
Number of Parts Composing the Main Tank	2
Connection between the two Parts and the Plate	16 Bolts Flanges with Silicon Packing
Inner Diameter of the Flange	400 mm
Outer Diameter of the Flange	500 mm

At the bottom of the tank six electrical heaters have been installed in a non-symmetrical disposition. The connection of the electrical heaters to the plate is made with a thread and the addition of different rubber O-rings to avoid water leakages. The heaters should not be tightened excessively to the plate to prevent high deformations or ruptures of the O-rings. Fig. 3.5 shows the connection of the heaters to the lower plate. From Fig. 3.5 is also possible to notice the non-symmetrical disposition and the presence of the sixteen small holes in the outer part of the plate that enables the connection with the lower part of the main tank.

Fig. 3.5 Picture of the electrical heaters connected to the lower plate of the main tank.

Four of the six heaters have a power of 6 kW while the other two remaining have a power of 4kW and 8 kW respectively. They provide a total 36 kW power for the boiling of the water. The 8 kW heater is also the tallest one with a height of 50 cm. This dimension is particularly important because it must be always assured that the water level is higher than this value in order to avoid the heaters burnout. The fact that the height of the tallest heater is equal to the height of the lower part of the main tank allows easily understanding the location of 50 cm from the bottom and being sure to be working always with the minimum quantity of water that is needed during the experiments. This is possible even if the tank is insulated because the flange connecting the two parts of the tank has an outer diameter which is bigger than the one of the tank and the location of 50 cm from the bottom can still be easily located. The positions of the heaters and general dimensions are reported in Fig. 3.6

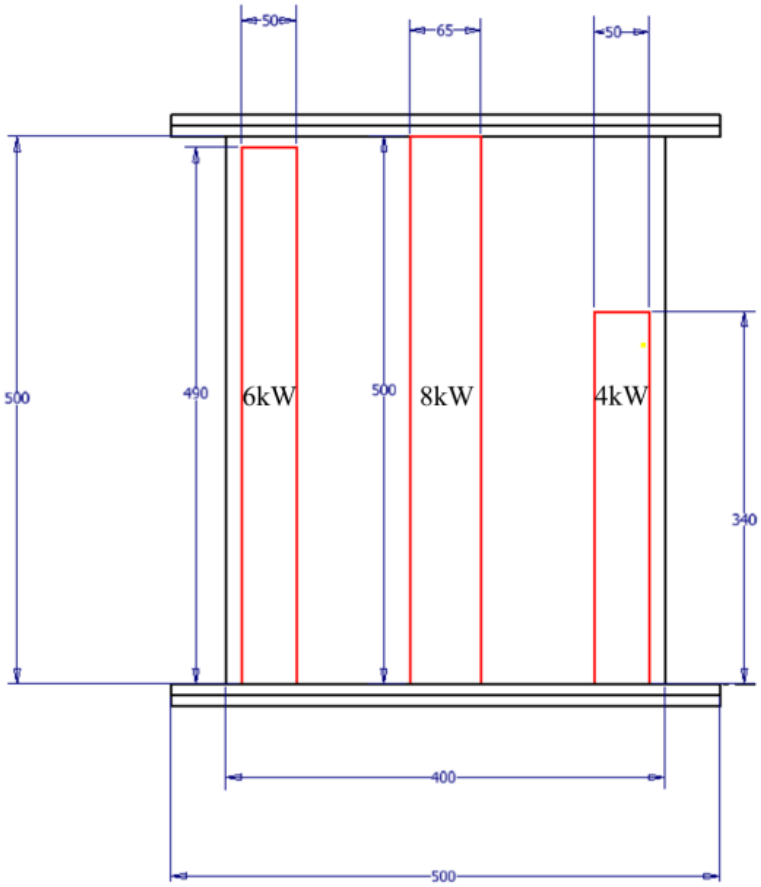

Fig. 3.6 Position of the electrical heaters in the main tank.

The generation of steam is determined through the power of the heaters. To establish the exact power associated to each heater, they are connected to three Yamabishi Electric volt sliders: one for the 4 kW heater, one for the 8 kW heater and the other one is used in parallel for the 6 kW heaters. Volt sliders receive in input the current coming from the electricity grid and allow deciding the output voltage which will constitute the input for the heaters. By choosing the voltage of the volt sliders is possible to modify the power of the

heaters, as it is possible to see from equation 3-3. All the heaters can be analysed with a delta circuit configuration, shown in Fig. 3.7.

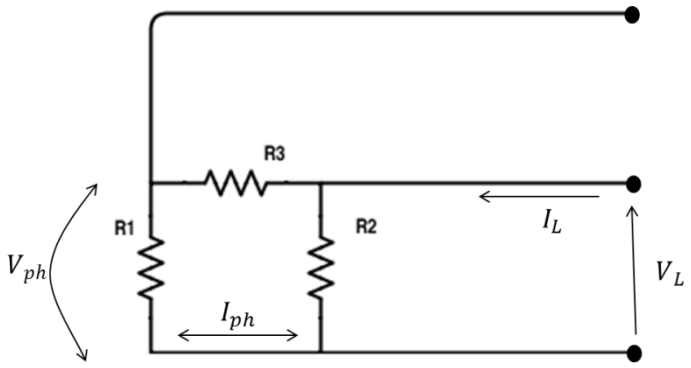

Fig. 3.7 3-phase delta configuration for heaters' analysis.

Equations for 3-phase delta configuration for balanced load:

$$\boldsymbol{I_L = \sqrt{3} * I_{ph}} \quad (3\text{-}1)$$

$$\boldsymbol{V_{ph} = V_L} \quad (3\text{-}2)$$

$$\boldsymbol{P = \sqrt{3} * I_L * V_{ph}} \quad (3\text{-}3)$$

Because of the well-known quadratic relation of power-current, the selection of the cables must be done carefully, in order to be sure to work below the maximum capacity of the volt sliders which correspond to 45 A for the volt slider connected to the 6 kW heaters and 30 A for the other two. The current capacity of the volt slider connected with the four heaters of 6 kW is lower than the total current that will circulate if the volt slider is operated with the maximum voltage, V_{ph} , which is equal to 200 V. Indeed, the line current I_L can be calculated by:

$$\boldsymbol{I_L = 4 * \frac{P_{1H}}{\sqrt{3} * V_{ph}} \cong 69} \text{ A} \quad \boldsymbol{(3\text{-}4)}$$

Where P_{1H} is the power of one heater and equal to 6 kW in this case.

In order to avoid the burning of the considered volt slider and operate with a current which is lower than the capacity, the maximum voltage that can be set in this volt slider is equal to roughly 120 V. This condition limits the total power that it is possible to obtain from the electrical heaters to only 22 kW. The other two volt sliders can operate in safety even using the maximum voltage which is equal to 200 V.

Because of the small thickness of the main tank, it was necessary to install a pressure gauge on the top of the main tank in order to keep the pressure under control. The maximum pressure reached in the experiment was equal to 0.13 MPa. In addition a K-type thermocouple (TC) was introduced to evaluate steam temperature and detect the moment of insurgence of the boiling. Although the boiling can be easily spotted through the production of steam, the instalment of the thermocouple allowed a better planning of the experiments and gave another tool to evaluate the pressure of the steam inside the main tank. Indeed, saturation condition of the steam inside the main tank can be assumed.

The water level is visually controlled using an external transparent teflon tube. However, this kind of measurement is not really accurate because of the voids created by the boiling. These voids cause the level inside the tank to be lower than the level read outside. To avoid the water level going below the height of the heaters causing their burnout, the facility was always operated with a large excess of water.

3.1.2. Steam line

The steam line has the function of connecting the main tank to the pool. In the steam line there are a flow meter and three operation valves that enables wide control of the flow. As in the main tank, also this line is thermally insulated from the outside. The steam line is sustained by a stainless steel structure to avoid bending and stresses during the experiments. A pressure gauge is also installed to monitor steam pressure. Every part of the steam line is connected together with the use of a Nichias PTFE tape to avoid leakages. This tape was placed over the thread in the clockwise direction at least for five times due to the dimensions of the pipes.

In the steam line the measurement of the steam flow rate is obtained with a flow meter. The evaluation of this parameter (together with the assessment of the water subcooling) is fundamental in every DCC experiment in order to estimate the driving force of the steam ejected inside the pool. This instrument consists of a Venturi tube inserted in the steam line and a differential pressure transducer, Yokogawa DPF110 4-20 mA 1-5V, which evaluates the pressure difference created in the convergent section. Fig. 3.8 shows a schematic drawing of the Venturi tube and the differential pressure transducer.

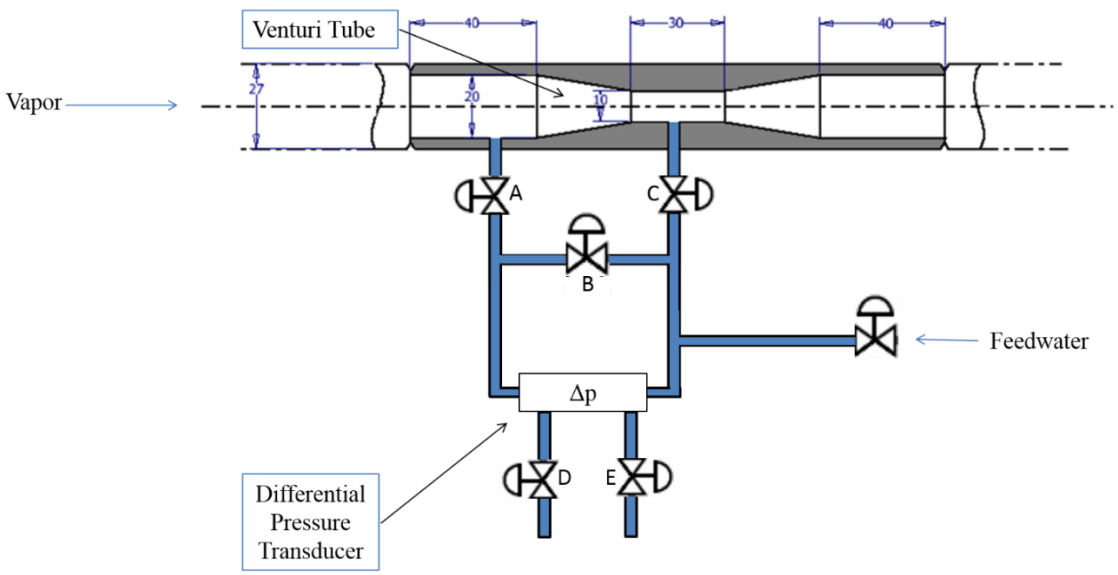

Fig. 3.8 Venturi tube in the steam line and flow rate measurement.

The tubes of the flow meter must be filled carefully with only water. Indeed, if only a small quantity of compressible air is inside the system, the output of the flow meter is not reliable. In order to assure this condition, this simple procedure is performed:

1. Supply water with valves A, C, E closed and B and D open
2. Close valve D and then open valve A
3. Close valve B and then open valve E
4. Close valve E and then open valve C
5. Open valve B.

After this operation is completed, the supply of the feed water is shut. Every step lasts roughly one minute. This procedure must be done not only for the calibration of the instrument but also before every experiment.

Because the presence of air in the tubes of the flow meter can strongly affect the performances, transparent vinyl pipes have been adopted. In this way, water level and presence of air bubble is easily spotted, even during the experiments with violent pulses given by the phenomena to the structure. Before starting the experimental campaign it was necessary to calibrate the flow meter in order to have a relation between the pressure difference and the steam flow rate. The calibration was obtained by condensing the steam in a copper tube condenser and, using a calibrated cylinder, the volumetric flow of condensed water in a fixed interval of time was measured. Due to the compressibility of the steam it was necessary to keep the pressure constant and equal to the experimental conditions value. In order to take into account the different values of density, the condensed water temperature was measured. The output of the flow meter, in mV, was divided in a range from 0 to 100% and the correspondent quantity of condensed liquid was recorded. Through this procedure it was possible to obtain the calibration curve of the flow meter shown in Fig. 3.9.

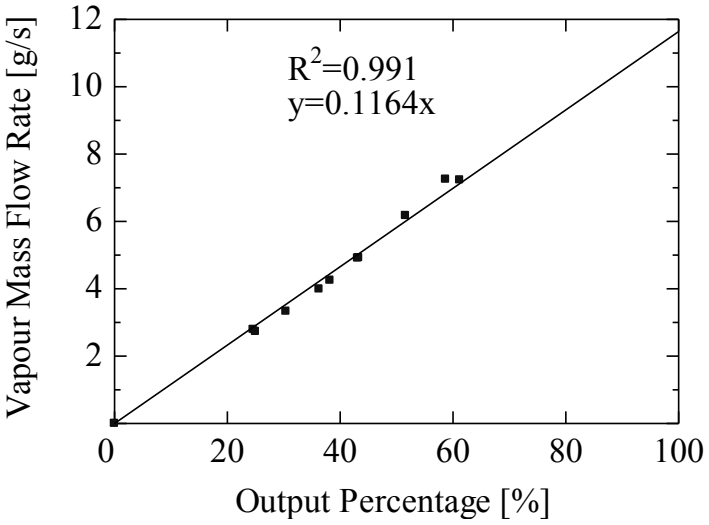

Fig. 3.9 Calibration of the Flow Meter.

3.1.3. Evacuation Lines

Beside the main steam line, there are two evacuation lines which eject the steam outside of the building having the function of a steam dump. The first line (A) departs from the upper part of the main tank while the second one (B) is installed immediately after the Venturi tube. Their position is schematically drawn in Fig. 3.1. These lines were created for three reasons:

1. The first reason is to be sure to eliminate the air in the steam flow through the boiling. Indeed, when the temperature rises, the solubility of the gases decrease and it is possible to remove them from the steam flow. Gas removal is important because the presence of non-condensable and their presence will have a large inference on chugging.
2. Another reason for discharging the steam outside of the building before doing the experiments is to avoid heating the water inside the pool unnecessarily and be able in this way to manage more easily its temperature, fundamental parameter in DCC experiments. Indeed, no cycle for controlling pool temperature was installed.
3. The other reason is mainly related to safety and to avoid high pressure inside the main tank. The evacuation lines, especially the one installed immediately at the outlet of the main thank, allowed a rapid condensation and expulsion of steam.

3.2. Test Section

The test section consists of a venting pipe and a pool. Fig. 3.10 shows two pictures of the test section while Fig. 3.11 shows a scheme of the test section.

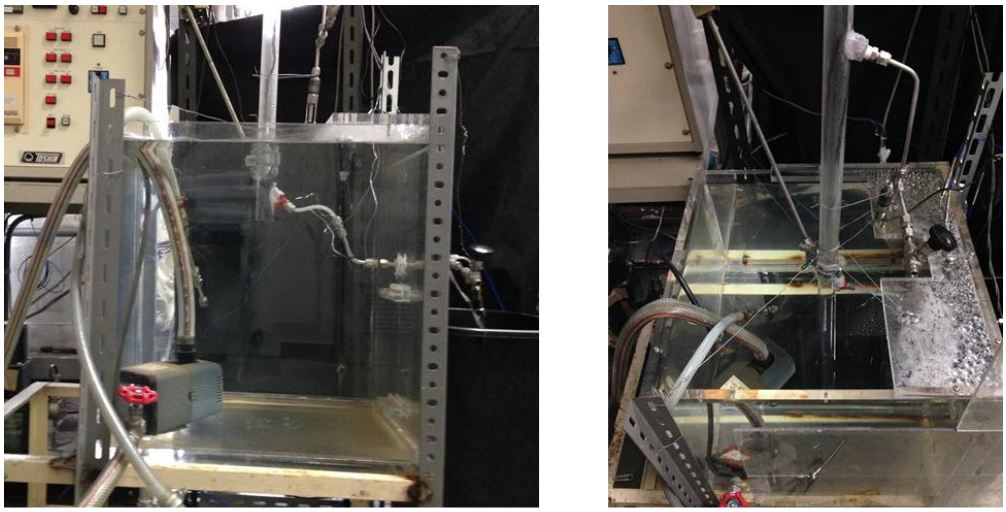

a **b**

Fig. 3.10 Pictures of the test section: **(a)** frontal and **(b)** top view.

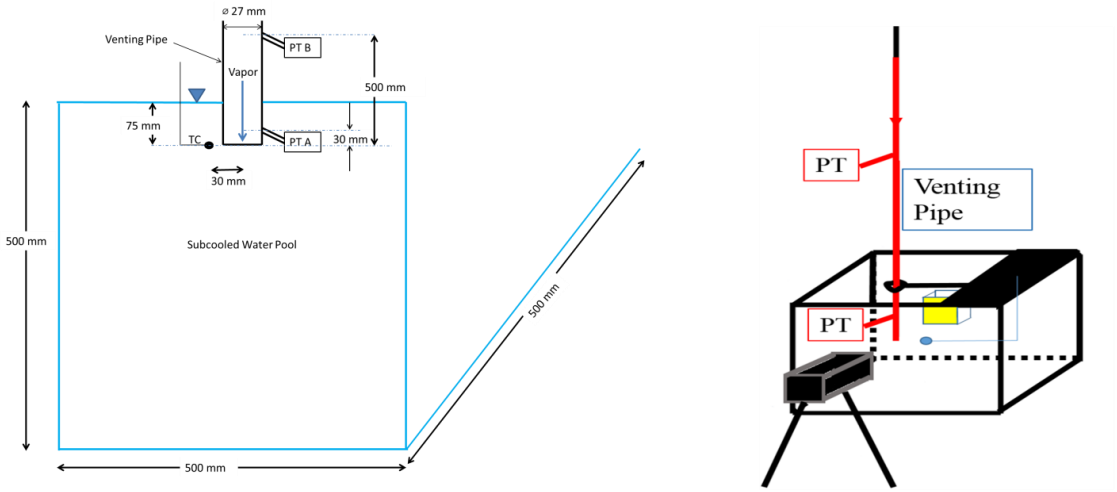

a b

Fig. 3.11 Scheme of the test section.

(a) Dimensions of the test section, **(b)** measuring instruments in the test section.

Different kind of venting pipes were used depending on which types of measures were of interest. However, they all had the same inner diameter equal to 27 mm. Two pressure transducers (PT) at 50 cm and 3 cm from the outlet of the pipe were installed. The pressure transducer at 3 cm from the outlet allows a better investigation of the chugging phases in which the interface is close to the outlet, while the pressure transducer at 50 cm from the outlet is more suited to analyse what happens when the interface is abundantly inside the pipe. The selected pipe materials were polycarbonate (thermoplastic polymer) and stainless steel. The polycarbonate pipes allowed visualizing the behaviour of the interface inside the pipe and assure good mechanical properties at temperature below 120 °C. Their use, supported by the high speed camera, was fundamental for a better understanding of chugging mechanism. One of the polycarbonate pipes was built with the pressure tap at only 50 cm from the outlet to be sure that the measurement system did not affect the bubble implosion. In order to create a pressure tap, a hole was made in the pipe at the selected position and a special connector of the same material of the pipe was created. The connectors were designed so that the water stays inside the pipe of the transducer during the operation and no damping of the signal occurs. In order to achieve this, the connector formed an angle ranging from 70° to 80° with the direction of the pipe axis. Fig. 3.12 shows a schematic drawing of a venting pipe and the connection to the pressure transducers.

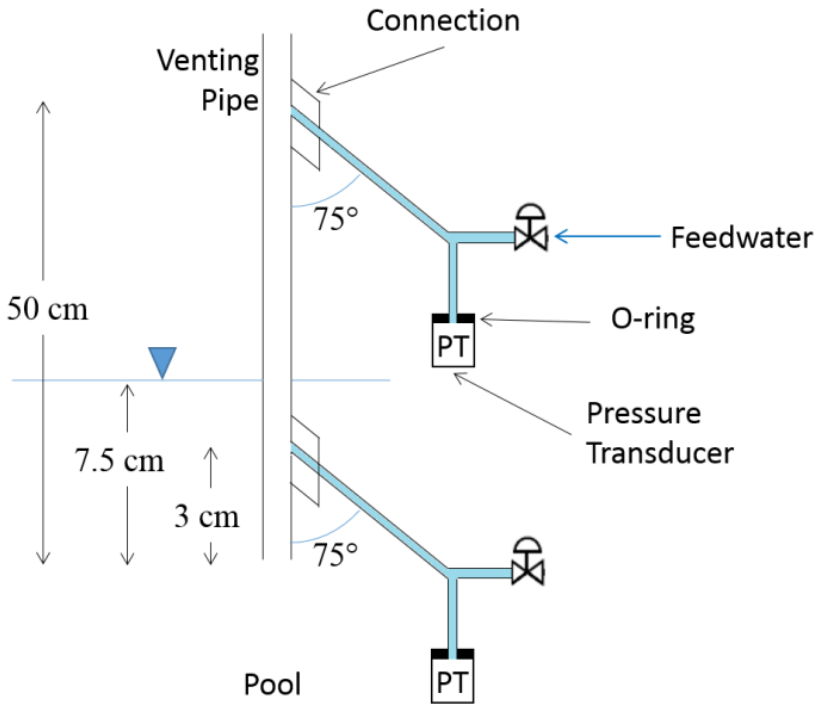

Fig. 3.12 Schematic drawing of a venting pipe and the connection to the pressure transducers.

In case of polycarbonate venting pipes, the connector and the pipe were tied using methyl chloride instilled with an injector. Moreover, glue was added to absorb the vibrations during the experiments. Because of the high pressure peaks characteristic of chugging phenomena, this connection was occasionally broken and this caused the production of different pipes. Fig. 3.13 a shows a detailed view of the polycarbonate pipes outlet and makes it possible to notice the design of the connections while Fig. 3.13 b shows a whole polycarbonate pipe with the pressure taps at 50 cm and 3 cm from the outlet.

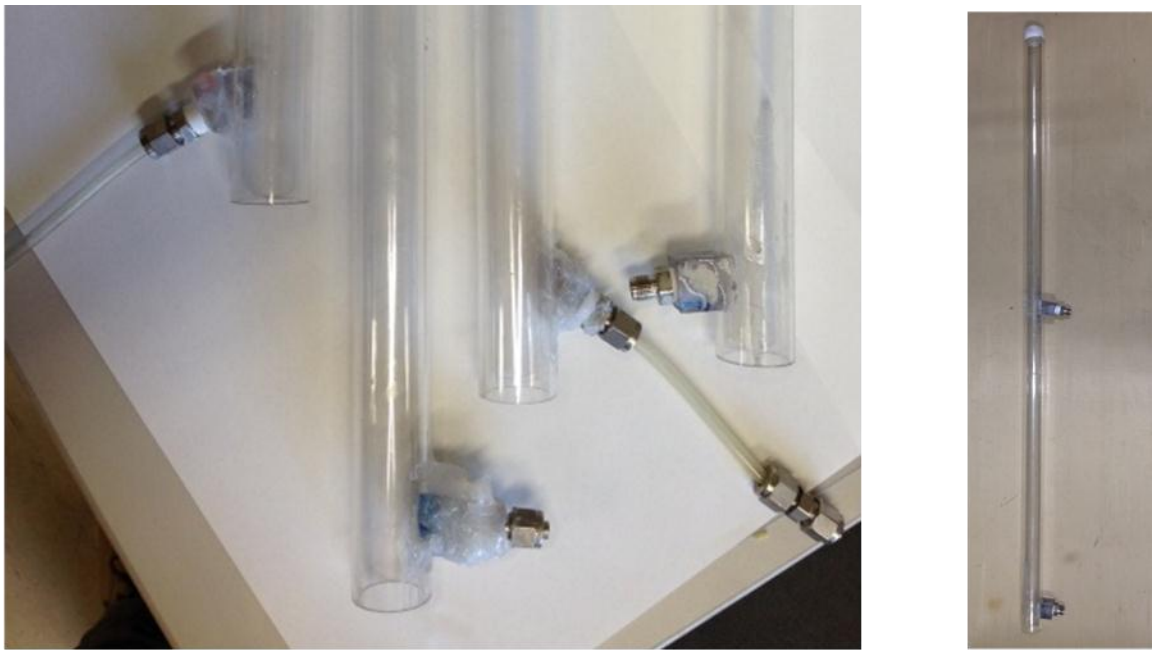

Fig. 3.13 Polycarbonate venting pipes.

(a) Detail of the pipe outlet, **(b)** whole polycarbonate venting pipe.

The stainless steel pipe, shown in Fig. 3.14, was mainly used when the goal of the experiment was improving the understanding of the bubble implosion at the outlet of the pipe. Its use allowed to remove the problem of the weak point in the connection between the pipe and the pressure transducer's tubes. Indeed the stainless steel connector was simply welded to the venting pipe.

Fig. 3.14 Stainless steel venting pipe.

The pool is an acrylic cube of 50 cm side and a thickness of 0.5 cm. The use of such a material does not allow the water temperature to be higher than 70 °C. Part of the pool has a lid on top of which was built a system to anchor the pipe and to easily insert and block a thermocouple. The construction of this support was fundamental because, without any locking, the venting pipe would be subjected to high oscillations due to the chugging. The thermocouple is a K-type, 1mm diameter and it was placed at the same level of the pipe outlet and roughly 3 cm distant from the pipe axis. Indeed, in this way, the thermal stratification effects inside the pool created by the density difference between the cold and the hot water can be neglected. The presence of this thermocouple inside the pool was fundamental to evaluate the level of water subcooling, one of the three main parameters in

DCC. Exactly like in Marks et al. experiments [7], the pool temperature is not controlled with a cooling loop in order to limit turbulences and flow in the water to the one characteristics of chugging phenomena. Inside the pool it was placed a submerged pump that allows removing rapidly the hot water.

Table 3.2 summarizes the main properties of the test section.

Table 3.2 Main properties of the test section.

	Material	**Dimension**	**Measuring Instruments**
Venting Pipe	Polycarbonate and stainless steel	D 27 mm	2 pressure transducers (PT)
Water Pool	Acrylic	500X500X500 mm	Thermocouple (TC)

3.3. Measuring Instruments and Data Acquisition System

The measuring instruments used in the present experiments are:

- Two Semiconductor Pressure Transducers, A and B
- High Speed Video Camera of maximum 1.5 million frame per second.

These instruments were connected to the same data acquisition system, TEAC es8 with 8 channels and maximum 5 kHz sampling frequency. Fig. 3.15 shows the location of the measuring instruments in the test section.

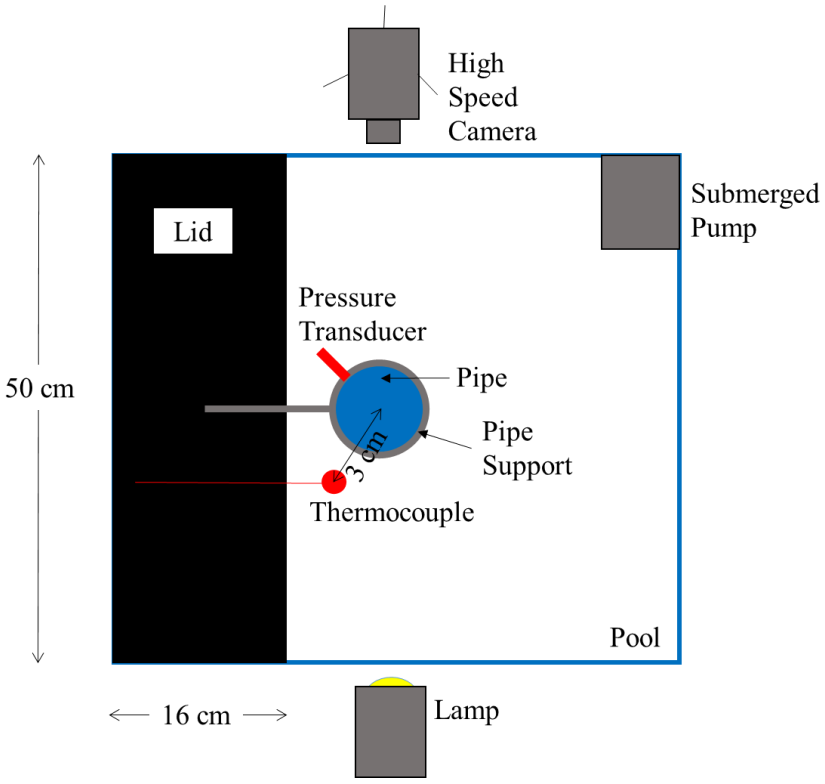

Fig. 3.15 Measuring instruments in the test section, top view.

Two different semiconductors pressure transducer, A and B, have been installed in the injection pipe. Fig. 3.16 shows a picture of these two measuring instruments.

Fig. 3.16 Semiconductor Pressure Transducers, A and B.

The pressure transducers A is a PMS-5M-2 by JTEKT Corporation while the pressure transducer B is a PMS m5 SN8006. These two sensors are based on the piezoelectric effect: due to the external pressure, a deformation is induced in a lamina and its electrical resistance change proportionally with it. In order to evaluate the variation of resistance a bridge circuit was built. A scheme of the bridge circuit is shown in Fig. 3.17 whereas Table 3.3 shows the main properties.

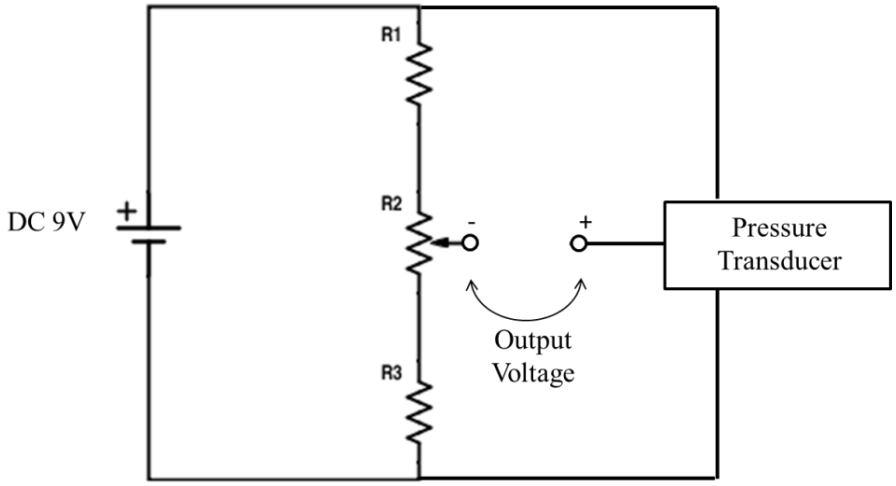

Fig. 3.17 Bridge circuit for resistance measurement in the pressure transducers.

Table 3.3 Parameters of the bridge circuit for pressure measurement.

R1	2000 Ω
R2	Variable resistor
R3	2000 Ω
Power Supply	six batteries of 1.5V each

Both transducers were calibrated using an air compressor and a precise Bourdon tube with a range of 0-500kPa. The calibration curve of pressure transducer A is shown in Fig. 3.18 a while Fig. 3.18 b shows the calibration curve of pressure transducer B.

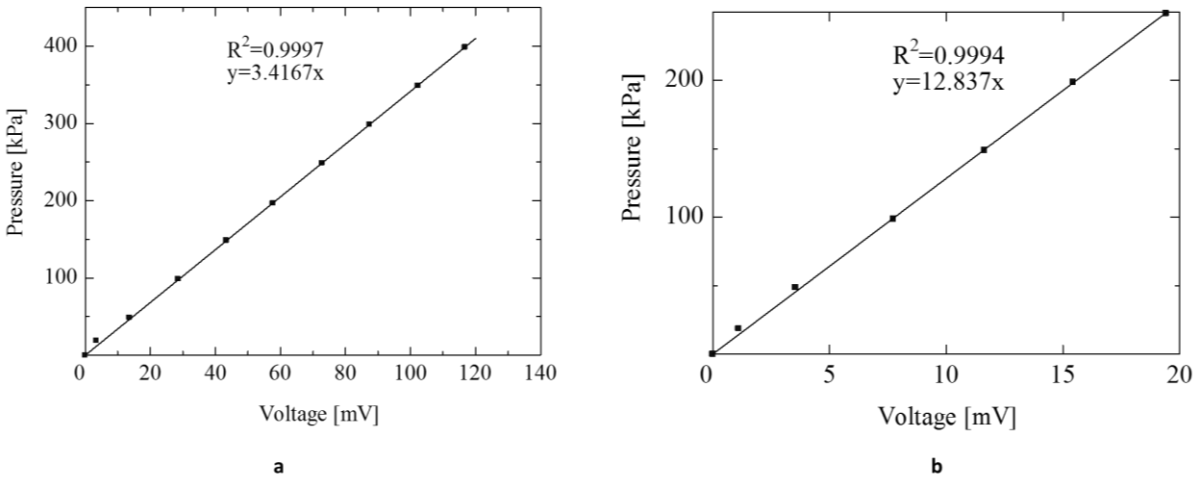

Fig. 3.18 Calibration of pressure transducers.

(a) Calibration of pressure transducer A**, (b)** calibration of pressure transducer B.

Even if the calibration was made without water, during the measurements it must be assured that only water is filled in the tubes. This is because water is incompressible and the pressure signal is immediately transferred to the transducer without any damping and without delays. For this reason, as it happened in the flow meters, transparent vinyl tubes were used. Moreover, after different calibrations it was found out that if alkaline batteries are used as the power supply for the bridge circuit of the pressure transducer, the noise is limited to ±1mV. Other calibrations were made using electricity from the grid and a Yokogawa 2554 DC Voltage standard with NI-Cd battery as the power supply for the

pressure transducers but they show a bigger noise with a signal varying around ±10mV. Every transducer was consequently supplied with 6 batteries of 1.5V connected in series.

The use of a high speed camera, especially when combined with the installation of a polycarbonate venting pipe, represented a very important tool in the understanding of chugging phenomena. Because of the speed of the phenomena itself, a really high performance camera was used. Even if Photron FASTCAM SA5, shown in Fig. 3.19 a, permits to reach more than 1.5 million frame per second (fps), most of the time 1000 fps was the selected value. 2000 fps, 3000 fps and 5000 fps were seldom used. A metal halide lamp (Photron HVC-UL, Fig. 3.19 b), positioned on the opposite side of the pipe respect of the camera, was used to illuminate the scene as shown in Fig. 3.15. Some sheets of paper were put in front of the lamp in order to diffuse the light.

a b

Fig. 3.19 Video image system.

(a) High speed video camera, **(b)** metal halide lamp.

The characteristics of the camera make it possible to have a TTL signal in output when trigger started. This TTL signal recorded by TEAC es8 data acquisition system will

constitute the time zero of the experiment. This method allowed having a perfect synchronization between the images and the pressure transducers' signal. Indeed, the delay of the signals due to the transmission is estimated to be around 5 ns per meter of cable which is abundantly below the time scale of the experiments which is around 0.1 ms. An example of synchronization with a typical output signal from TEAC es8 data acquisition system is shown in Fig. 3.20.

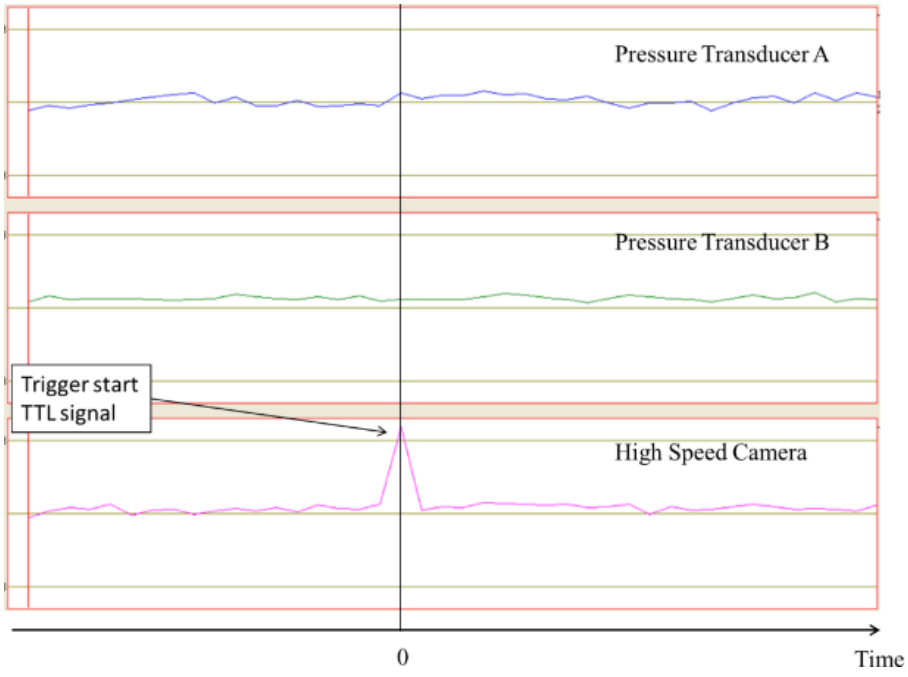

Fig. 3.20 Synchronization high speed camera-pressure transducers.

Two different data acquisition systems were used during the experiments according to the different measurements:

- Cadac data acquisition system
- TEAC es8 data acquisition system.

Cadac 2 Eto Denki, Model 9220A, coupled with the same desktop computer used for TEAC es8, shown in Fig. 3.21, was used to collect the data from the flow meter and from the thermocouple of the pool and of the main tank. TEAC es8 was used to record signals from the pressure transducers. Sampling frequency was always set to be 5000 Hz which is the maximum possible value.

Fig. 3.21 TEAC es8 data acquisition system.

Moreover the high speed camera was also connected to one of the eight total channel of this device through a BNC cable in order to get a pulse when the trigger was activated and synchronize the measuring instruments. Data was then visualized, processed and analysed using the software provided, esNavi and ExtrTAFF. Because of the high quantity of data, it was necessary to use an external 1 TB hard disk for storage.

A schematic drawing of the data transfer is shown in Fig. 3.22.

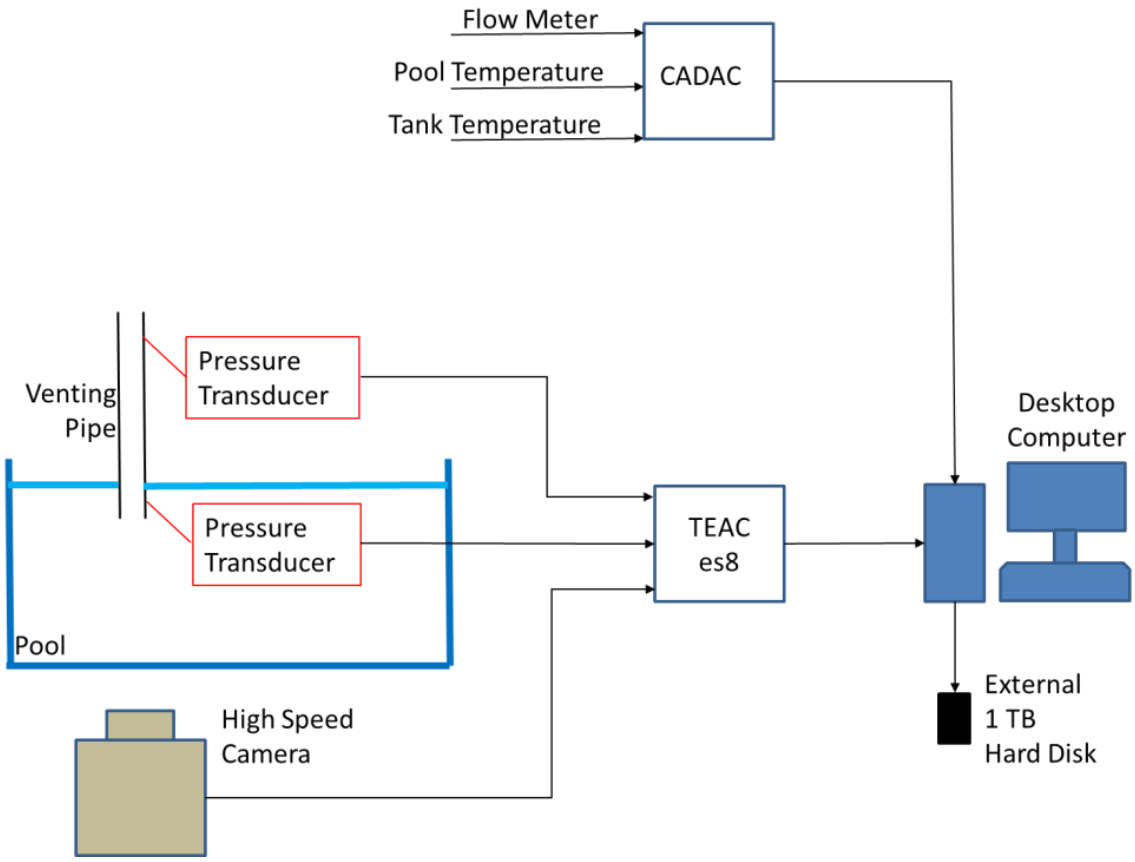

Fig. 3.22 Data Transfer.

3.4. Experimental Conditions

Experimental conditions are briefly summarized in the table 3.4.

Table 3.4 Summary of the experimental conditions.

Pool Temperature	[19 – 46.5] °C
Steam Mass Flux	[5.5 – 19.5] kg/(m^2s)
Pipe Inner Diameter	27 mm
Pipe Material	Polycarbonate / Stainless Steel
Pipe Submersion	75 mm
Pool Pressure	atmospheric
Sampling frequency	5000 Hz
Steam Pressure	[0.10 – 0.13] MPa
High Speed Camera frame per second	1000, 2000, 3000, 5000 fps

The first three parameters are fundamental in order to evaluate the established DCC regime. Another important parameter is the pressure of the steam produced in the main tank. These values had never deviated too much from the atmospheric pressure. Pressure drop in the steam line were relatively low which means that outside pressure in the pool is the one that governed the phenomena. The highest pressure of the steam registered was equal to 0.13MPa. In these range of pressure, steam density does not change considerably.

3.5. Experimental Procedures

Before doing the experiments, different operations must be completed. Initially the main tank was filled with water and the electrical heaters were switched on at low power. This phase of heating up, until the boiling started, lasted nearly three hours. In the meanwhile, water was inserted in the tubes of the flow meter, repeating the procedure illustrated in the section 3.1.2, being careful that no air was left inside. A similar procedure must be done to fill with water the tubes of the pressure transducers. In order to assure that no air was inside the pipe, it was necessary to supply water from the feed water valve, connect the pressure transducer with the O-ring to avoid water leakages and then shut the feed water. Looking at figure 3.12 is possible to better understand these simple operations. When the pipes were filled with water, the zero adjust of the instruments was performed. The zero adjust of the pressure transducers, executed by changing the resistance of the variable resistor, was done with the pool full and with the valve connecting to the steam dump completely opened. When steam started to be produced, it was ejected outside of the building through the evacuation line B, which is the one closer to the pool (see figure 3.1). This operation lasted roughly 15 minutes and allowed the removal of air from the tank and to check whether the flow meter was working. During the discharge of steam it was possible to operate with the valves in the steam line in order to have the desired steam flow rate and reach a condition of stability of the flow. This procedure was possible because the pressure drops in the evacuation line and in the venting pipe were nearly similar so that, closing the valve of the pipe leading to the steam dump and opening the one leading to the pool did not cause a strong variations on the flow conditions. To assure that the pressure inside the tank did not

increase considerably, the steam was occasionally discharged from the evacuation line A on the top of the main tank. When the air was completely removed from the stream, the steam was injected inside the pool being sure that the evacuation line B is fully closed. This is necessary in order to grant that the measurement of the flow rate was exactly the quantity of steam injected inside the pool. Before starting the experiments, it was again controlled that the flow meter was working correctly and that the flow conditions were stable. Finally, measurement of the pressure peaks and video recording were performed.

Two different kinds of experiments were implemented:

1. In the first type, the signal of the pressure transducers and the video images were recorded simultaneously. This kind of experiment lasted no more than 1 minutes because the memory of the camera could not allow longer recording at the selected frame per second and resolution. In this case, pool temperature rises of less than 1°C which allow to consider this quantity constant. Measurement of the flow rate was also subjected to variations, but deviations of ±0.1 kg/(m^2s), or ±0.5%, were considered as constant for the purposes of this study.
2. The second kind of experiment was performed without the use of the high speed camera and thus only pressure signals are recorded. In this case, the duration of the experiment was much longer than before, ranging from 15 to 30 minutes. Steam flow rate was kept constant, in the limits explained in the previous point, with careful and continuous operation of the valves in the steam line while the pool temperature increased gradually due to the steam ejection inside the pool. The pool temperature was only monitored, not measured.

Chapter 4

Experimental Results

In this chapter, experimental results will be shown following the chronological sequence of events. As introduced in chapter 3, the measures mostly focus on the visualization of the phenomena, the acquisition of the pressure signals in two different positions of the venting pipe and the evaluation of the time scale of a chugging cycle. The use of the high speed video camera permits a better understanding of the interface behavior during chugging. Indeed the analyses of the images give information about the time duration of every event composing a chugging cycle and give a high tech support to experimental data in explaining the physical mechanisms. Pressure transducers were also used in long experiments, as explained in section 3.5, without the high speed camera in order to evaluate the effect of the slow increase of the pool temperature on the development of chugging pressure peaks.

In section 2.1 it was highlighted that chugging is one of the regime of direct contact condensation. It can be defined as a depressurization induced by the bubble implosion at the pipe outlet that causes a cyclic suction of water inside the pipe. Once chugging occurs it is easily detected because of the loud sounds associated to the cyclic collapse of the steam bubbles formed at the pipe outlet and because of the high water elevation inside the pipe. Looking at the common characteristics related to the phenomenon, a chugging cycle was divided, always in section 2.1, into five different sequences of events: bubble growth, bubble collapse, water suction, internal condensations and steam ejection. In Fig. 4.1, the different phases related to a single chugging cycle and a typical time scale of the phenomenon are shown. The beginning of each phase is marked with the corresponding number, following the classification made in section 2.1.

Pressure signals at 3 cm and 50 cm from the outlet are also plotted in Fig. 4.2.

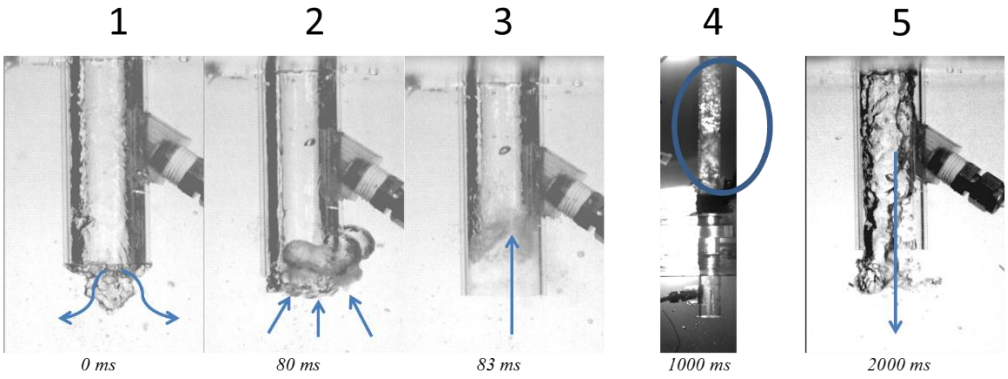

Fig. 4.1 Events characteristics of a chugging cycle.

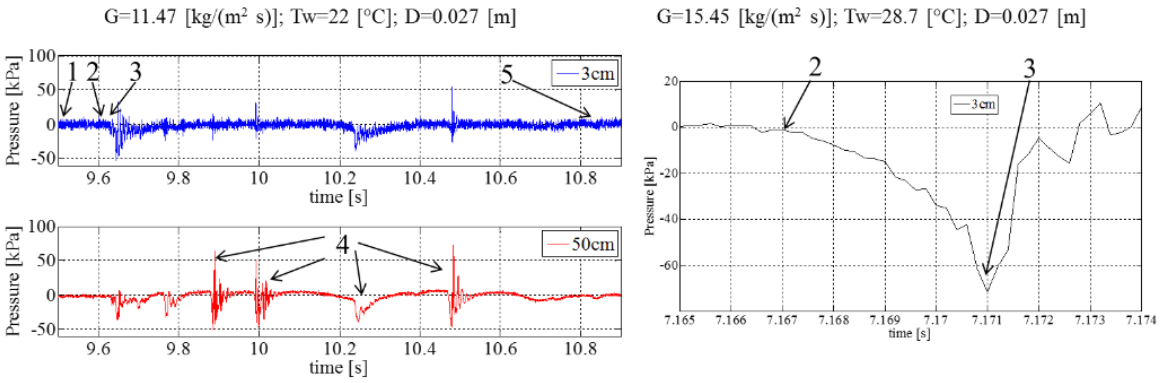

Fig. 4.2 Pressure signals during a chugging cycle.

(a) Events characteristics of a whole cycle, **(b)** detail of the bubble implosion and the water suction.

All the five events of the chugging cycle were analysed through the images and the signal of two pressure transducers located at three centimetres and fifty centimetres from the outlet. The transducer at 3 cm is mostly suited to observe the events occurring at the outlet

and the fact that it is positioned at a slightly higher position from the exit grants that any interference on the phenomenon is negligible. On the other hand, the transducer at 50 cm allows investigating mostly what happens inside the pipe. From Fig. 4.2 it is possible to observe that the two transducers are suited for analysing different parts composing chugging cycle.

The chugging cycle begins with the bubble formation at the outlet of the pipe. In this phase, denoted with the number 1 in Fig. 4.1, the condensation rate is low so that the bubble can start growing. In addition to this, the constant supply of steam coming from the tank allows a continuous bubble growth. With the increase of the dimension of the bubble, the condensation rate increases and the growth is slowed down until the condensation rate equals the inlet steam mass flow rate and the bubble arrives at its maximum dimension. During this time, the pressure signals are both constant and equal to the steam inlet pressure which is nearly atmospheric. At this point the phase number 2 takes place and the bubble suddenly implodes due to an abrupt increase of the condensation rate. During the bubble collapse it is always possible to see the production of microbubbles that aggregate forming a black cloud. The bubble collapse at the outlet of the pipe causes a steep reduction of pressure as it is possible to see in Fig. 4.2 b. The implosion of the bubble and the interrelated loss of steam mass and pressure reduction are responsible for the water suction inside the pipe and the beginning of the third phase. Even if the bubble collapse is the trigger of the water suction, the reason why the water might reach elevation of nearly one meter inside the pipe is the continuous condensation of steam in contact with cold water coming from the pool. Moreover few milliseconds after the bubble implosion is

common to observe quick and violent condensations inside the pipe but close to the outlet which enhance the altitude of the water column. Because of the turbulences and mixings, different small bubble collapses may occur inside the pipe leading to the phenomenon called condensation induced water hammer (CIWH). This fourth phase is highly unstable and dependent on the local values of temperature. Although it is really difficult to predict when and in which position of the pipe this internal condensation are going to take place, this aspect of the chugging cycle is definitely the one that mostly arises concerns from the practical point of view. Indeed, how it is possible to notice looking at the pressure signal at fifty centimetres from the outlet, Fig. 4.2 a, the internal condensations are connected with really high pressure peaks which can damage the structures. Because of this threat, this part of the chugging cycle needs to be evaluated with extreme attention.

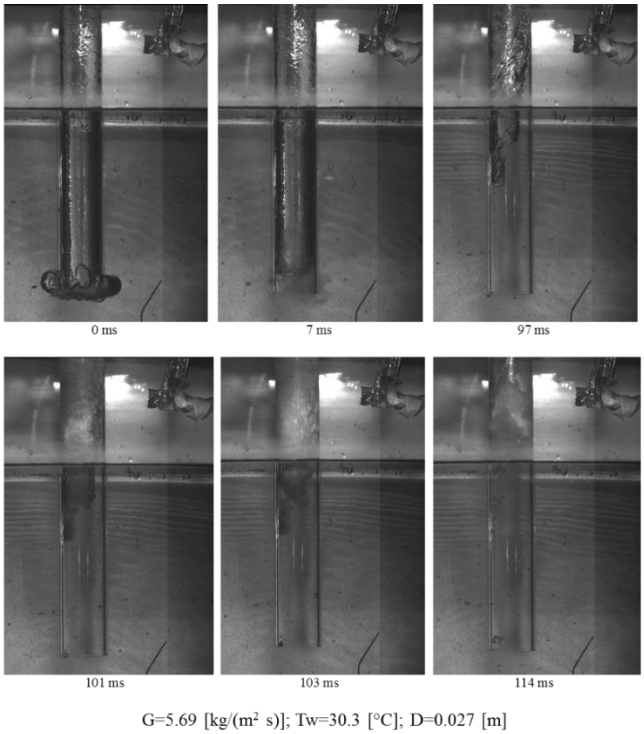

Fig. 4.3 Typical condensation inside the pipe.

Fig. 4.3 shows a typical condensation inside the pipe. It generally begins when the interface velocity is low. This can happen when the steam starts flowing down the pipe and the interfacial area is not flat anymore. Indeed steam tends to flow downward at the centre of the pipe much faster than the water which has an annular flow. Another typical condition when the internal condensation may start is when the interface reaches the maximum elevation inside the pipe and, again, the interfacial area is not flat anymore. The latter is the situation illustrated in Fig. 4.3 in which the maximum elevation, in this case similar to the level of submergence of the pipe, is reached 97 ms after a bubble implosion at the outlet. The starting point of the internal condensation is always localized at a specific position of the pipe close to the interface as it is possible to see after 101 ms. Then a collapse of the whole steam column is observed at 103 ms and water elevation inside the pipe increases at 114 ms. Only when the water temperature is high enough and the condensation rate is significantly reduced, steam can again reach the outlet of the pipe and phase number five takes place. Normally the interface slows down significantly before reaching the outlet.

If the pool water temperature is sufficiently high a new bubble is formed, otherwise the steam is ejected without bubble formation and increases locally the water temperature until the point that the new bubble formation is possible again.

4.1. Outline of Chugging Phenomena in This Study

4.1.1. Bubble Shapes

In chapter 2, it was already highlighted the influence of three main parameters – steam mass flux, water subcooling and pipe inner diameter - in the Direct Contact Condensation of steam with cold water and the different regimes that can be obtained.

In order to investigate the effects of the mass flux and the pool temperature on chugging mechanism, it was necessary to create a regime map ad hoc. Different regions on the map where identified cataloguing the bubbles depending on their shape and on the encapsulation. This partition of the bubbles depending on their appearance has the goal of giving a tool to predict the features of the chugging cycle – pressure peaks, frequency, etc – only looking at the outlet of the pipe. The effectiveness of such a method can be easily understood if it is considered that most of the venting pipes in industrial applications are made of stainless steel, in order to have a higher stability of the structure, that does not allow seeing what is happening inside the pipe. Fig. 4.4 shows the regime map obtained through the experiment of this study. The classification of the bubbles regards the main way of condensation for every experiment. It happens rarely that different regimes are observed in the same experiment. Moreover, every point on the map denotes a different experiment but the boundaries should not be considered rigid because what happens in the limits of every region was not of interests in this study. Only where there are two different experiments close to the limits of a region, the boundary is accurately drawn.

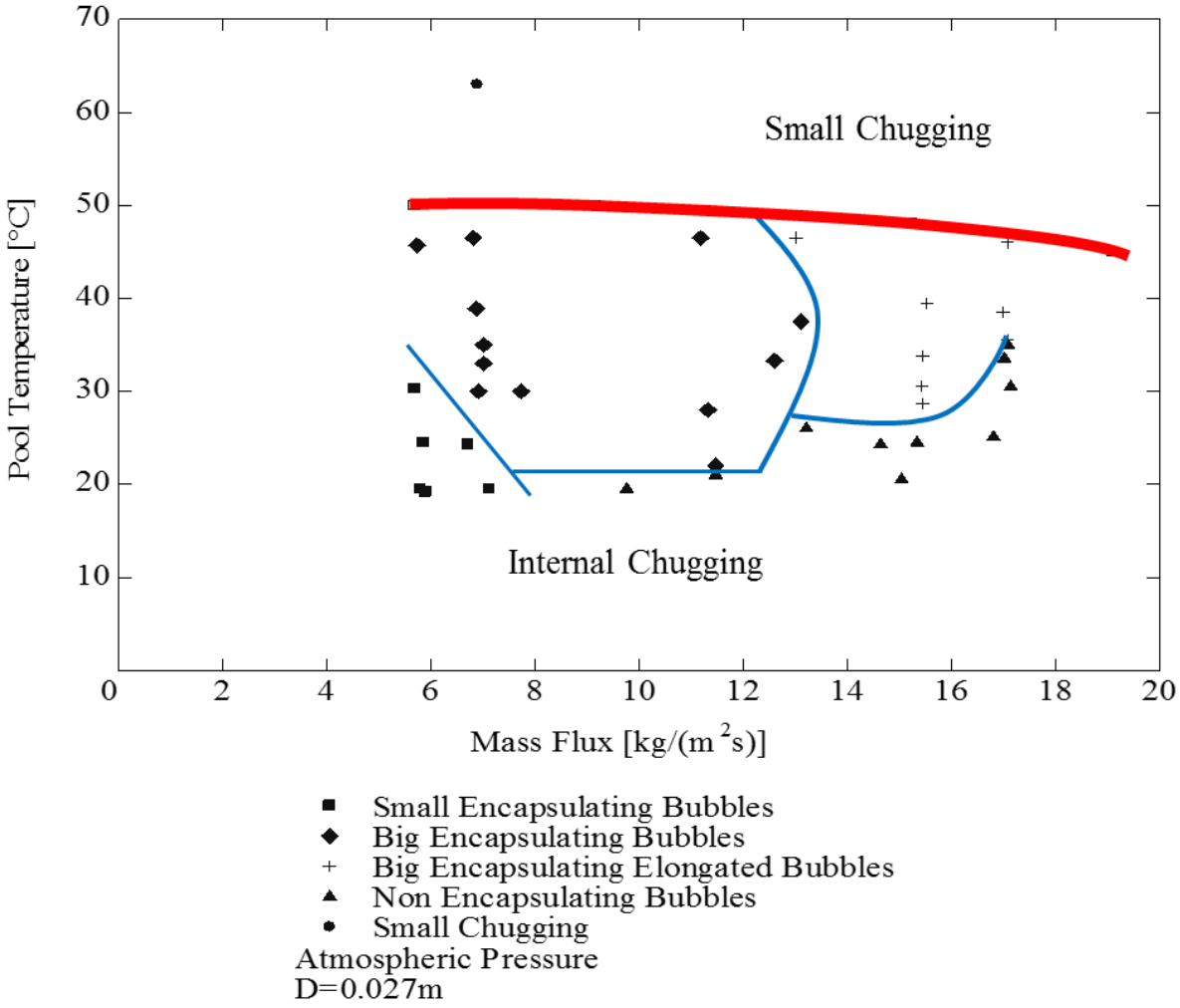

Fig. 4.4 Condensation map in chugging regime.

The map is mainly divided in two parts, small chugging and internal chugging, using the terminology from Nariai et al [8]. Internal chugging occurs at low pool temperature and is characterized by high elevation of water inside the pipe following the bubble collapse. High pressure peaks are associated to this kind of chugging.

Small chugging is characterized by the movement of the interface close to the pipe outlet. The elevations of the water are much smaller than the previous case. In this work, the boundary was set to be the condition for which the elevation is never higher than the pipe submergence, equal to 7.5 cm. As explained in [8], this is only a transition regime. This clarify why, in the presented map, most of the points are located in the internal chugging area which is the one that primarily is of interested because of the high pressure peaks and high elevations.

The four regions in which the internal chugging area was divided are:

- Small Encapsulating Bubbles
- Big Encapsulating Bubbles
- Big Encapsulating Elongated Bubbles
- Non encapsulating Bubbles

The term encapsulation was taken from Chan et al. [2] and stands for the bubble covering and wrapping the pipe and it is linked to the buoyancy force exerted on the bubble.

Small encapsulating bubbles occupy the region of low pool water temperature and low steam mass flux. In these conditions the condensation rate is really high due to the cold water but, on the other hand, the inlet steam inside the bubble is small. This causes the formation of small bubbles that encapsulate the pipe because of the dominance of the buoyancy force respect the inertia of the steam. Indeed, steam velocity is low and every time the steam is able to reach the outlet of the pipe a bubble is formed. In this region it is not possible to observe any steam jetting in the fifth phase.

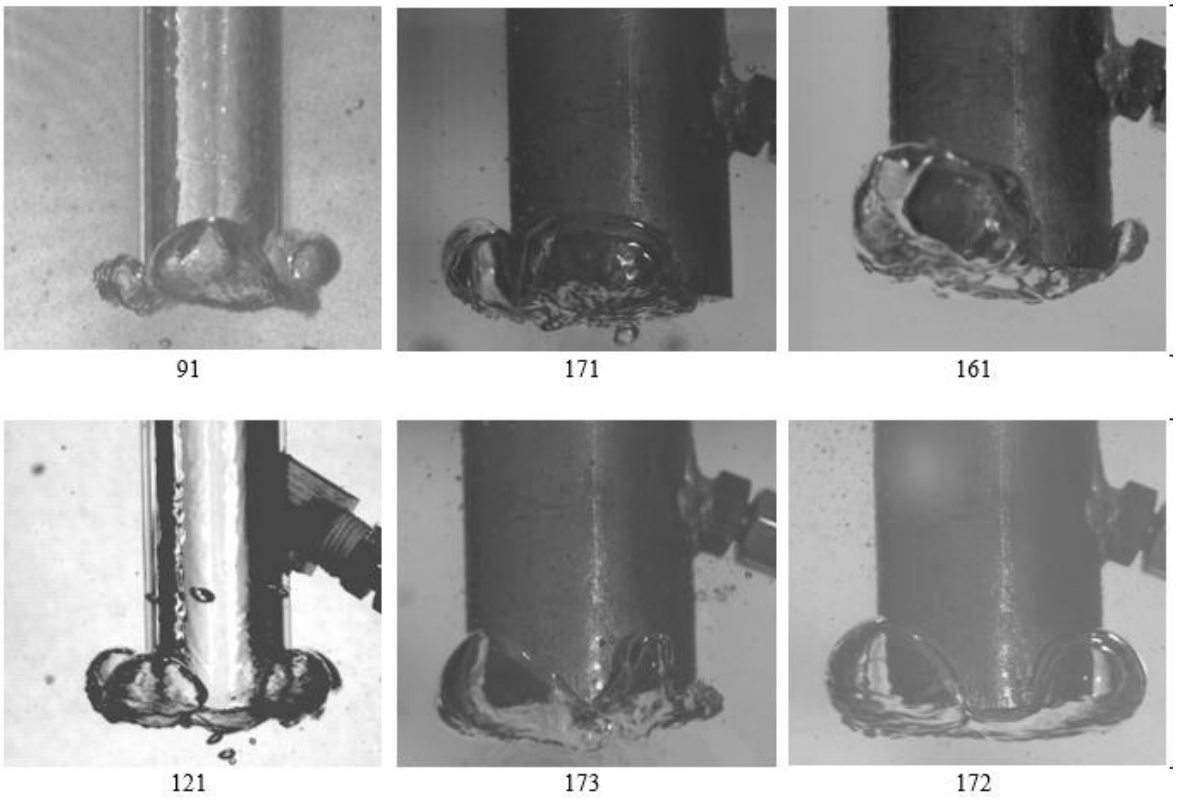

Fig. 4.5 Small encapsulating bubbles.

The Fig. 4.5 shows six small encapsulating bubbles representative of the six experiments conducted in this region. The number at the bottom of every picture represents the experiment label. Experiments 91 and 121 were conducted with a polycarbonate pipe but the first one had only one pressure tap at 50 cm from the outlet. The other four experiments were performed with the use of a stainless steel pipe. More detail information about every experiment can be seen in Appendix. Clearly bubble shapes cannot be exactly identical but the main features seem to be respected with enough coherence.

The second area is occupied by the big encapsulating bubbles and it covers most of the map. Unlike the bubble analysed before, the dimensions are considerably bigger, especially considering the level of encapsulation of the bubble around the pipe.

With the same mass flux of the small encapsulating bubbles, the sizes of the bubbles increase due to a smaller condensation rate. However, with the same pool temperature the size become bigger with an increase of the mass flux because of a higher supply of steam. As in the case of the small encapsulating bubbles, the encapsulation is due to the dominance of the buoyancy force. Big Encapsulating Bubbles characteristic of every experiments are shown in Fig. 4.6. Also in this case every bubble relates to a different experiment marked with the corresponding label. Moving from bubble 112 to 124 (apart 143), the mass flux is nearly constant and equal to 7 kg/(m^2s); the only difference is an increase of the pool temperature. The same logic is used to classify the bubbles from 71 to 83. In this case, the mass flux is roughly equal to 12 kg/(m^2s). As it is possible to see from Fig. 4.6, this increase of temperature or mass flux does not lead to a modification on the bubble shapes and dimensions so that, this bubbles can be considered as belonging to the same category.

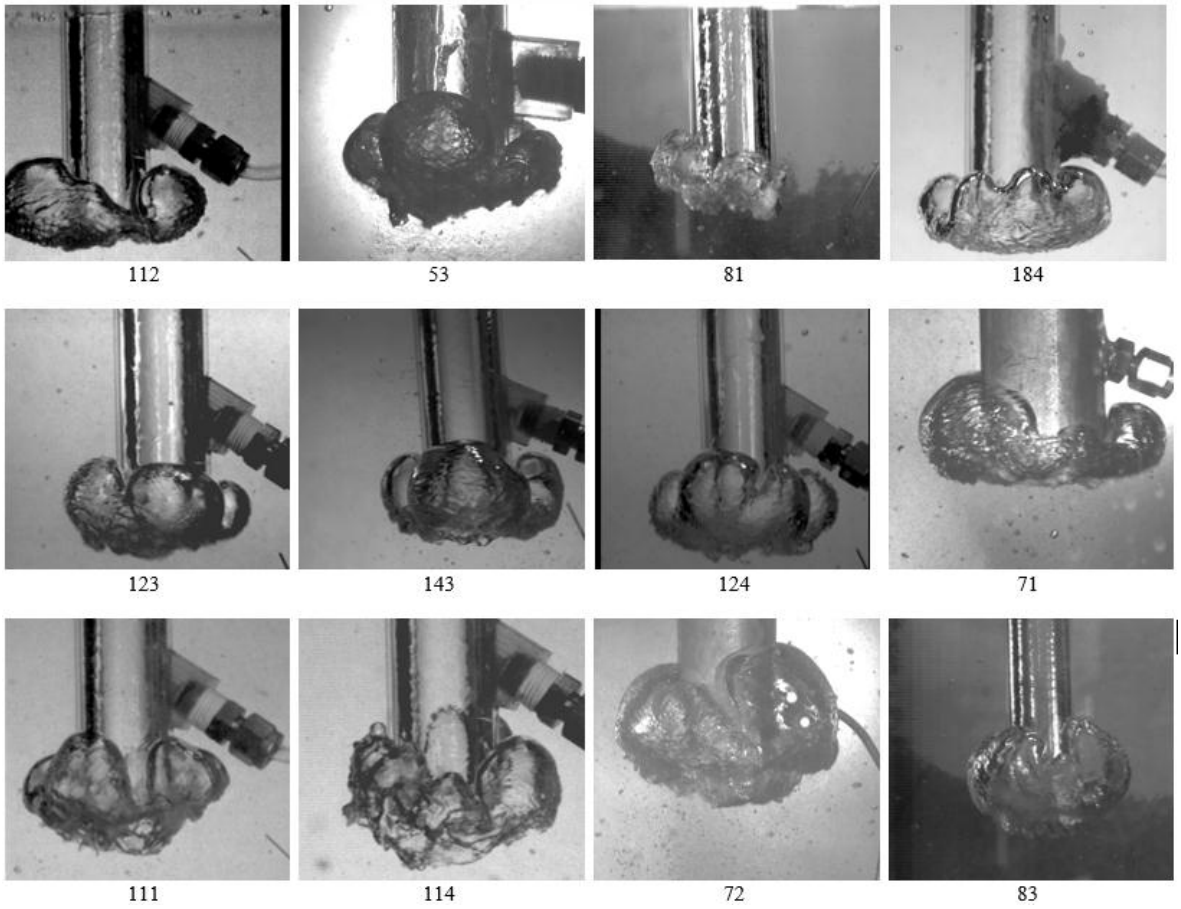

Fig. 4.6 Big encapsulating bubbles.

The third region is the one of the big encapsulating elongated bubbles. In this region the inertia of the steam can contrast the buoyancy, giving an elongated form to the bubble. The creation of bubbles with this characteristic is mostly dependent on the increase of the mass flux while the pool temperature has a smaller effect. Because of the high steam velocity, in this region it is possible to observe different steam jets before the new bubble is actually formed. In Fig. 4.7 the big encapsulating elongated bubbles are shown. In the first line, from 152 to 74, the mass flux is constant and equal to 15.5 kg/(m^2s), whereas the

temperature gradually increases. Also in this case, the shape of the bubble does not change considerably.

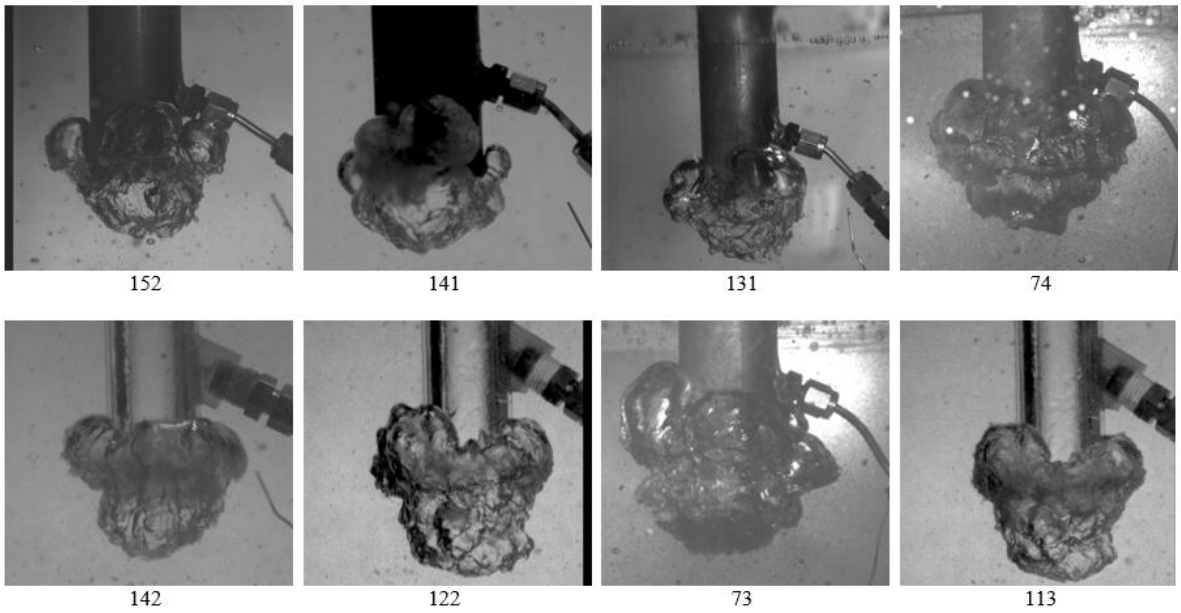

Fig. 4.7 Big encapsulating elongated bubbles.

The last region is the one of the non encapsulating bubbles. In this region the bubbles do not encapsulate the pipe due to the inertia and due to the high condensation rate because of the low temperatures. The creation of these unstable bubbles can be explained with a very fast phenomenon. Steam has no time to gradually heat up the surrounding water and form the bubble. Both the growing and the collapse appear to be significantly different from the rest of the map and is not possible to make any comparison. The fact that the bubbles do not encapsulate the pipe reduces extremely the sound associated to the implosion but this region was still considered as chugging in this study because of the

subsequent depressurization and water suction inside the pipe. Examples of these bubbles and the related experiment label are shown in Fig. 4.8.

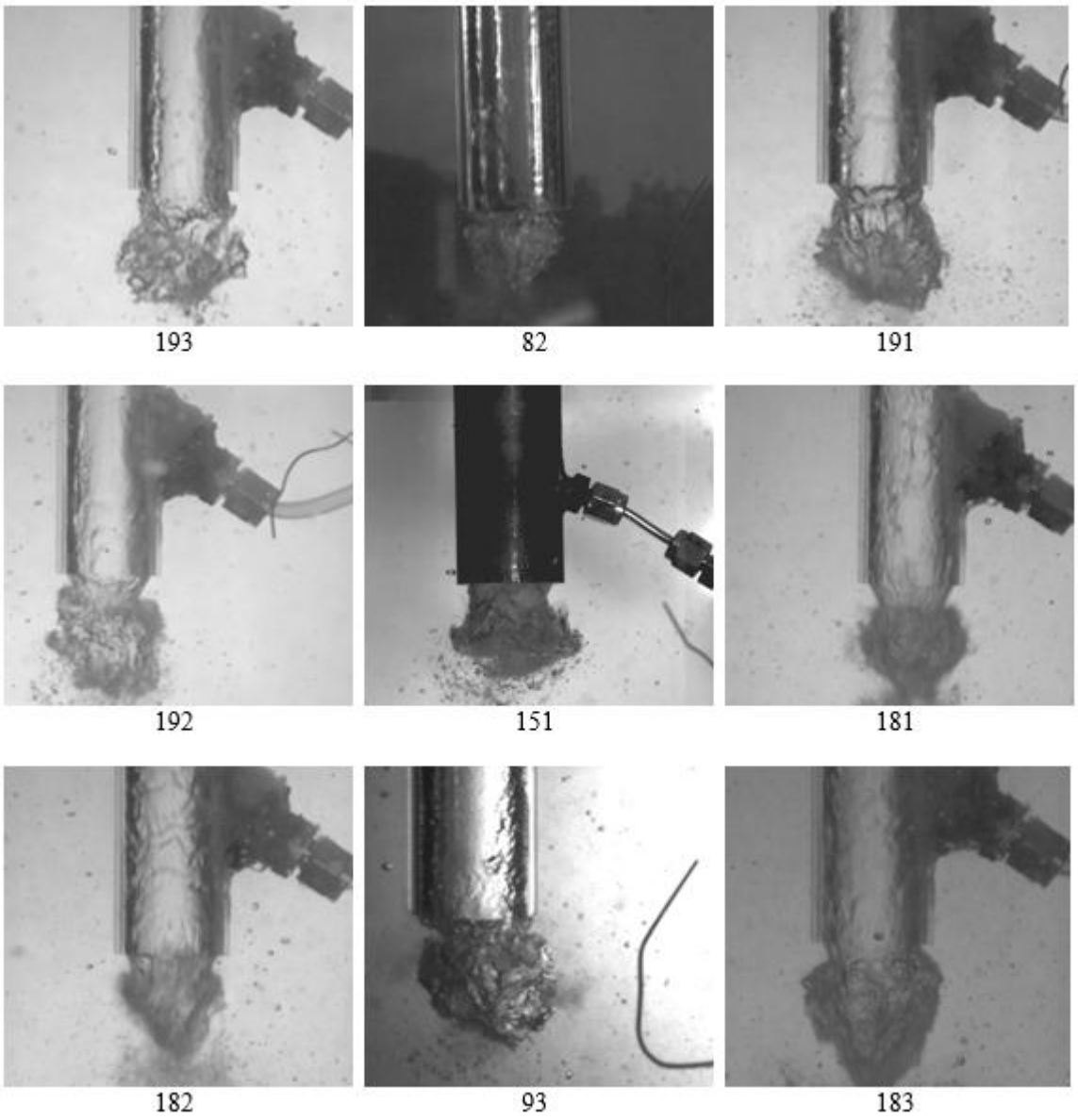

Fig. 4.8 Non encapsulating bubbles.

Moreover, for every bubble shape in Fig. 4.5, Fig. 4.6, Fig. 4.7, Fig. 4.8, when the polycarbonate pipe is used, it is possible to note the annular flow of droplets entering the bubble from the pipe during the growth. This appear as a black layer next to the pipe wall.

In order to make quick analysis on bubble behavior and give an idea on bubble dimension, a drawing of the different kind of bubble presented is shown in Fig. 4.9.

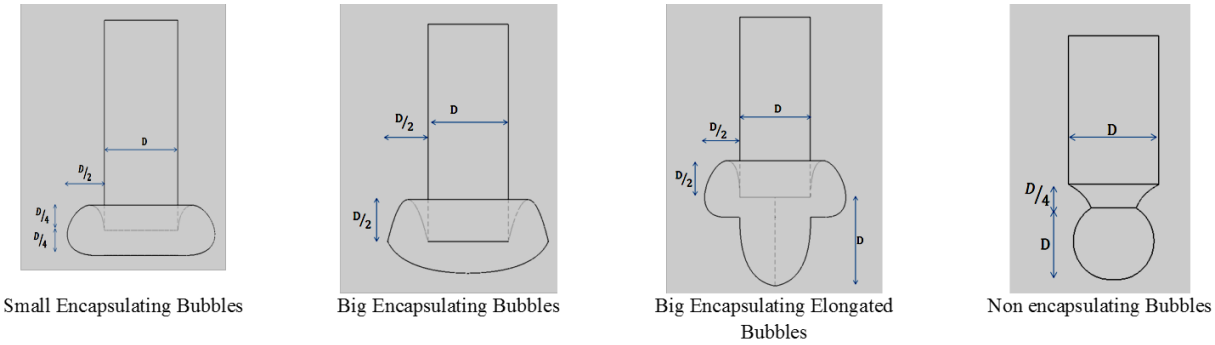

Fig. 4.9 General drawing of the bubble shapes.

4.1.2. Bubble Growing Time

In the introduction of this chapter the phases peculiar of chugging phenomenon were highlighted. The main interest on the first phase, bubble growth, is to estimate the time scale of this process and to evaluate if there is any dependency on the parameters characteristic of the DCC. In addition to this, it would be possible to evaluate if chugging duration is affected by the growing time or other components play a major role in the cycle extent. Bubble growing time was considered to start when the bubble dimension perpendicular to the pipe axis becomes bigger than the pipe radius. Besides this, bubble

growing time was considered to terminate when the pressure signal at three centimetres from the outlet decreases that is to say when the bubble collapse begins.

Fig. 4.10 shows the moments when the growing time starts and finishes.

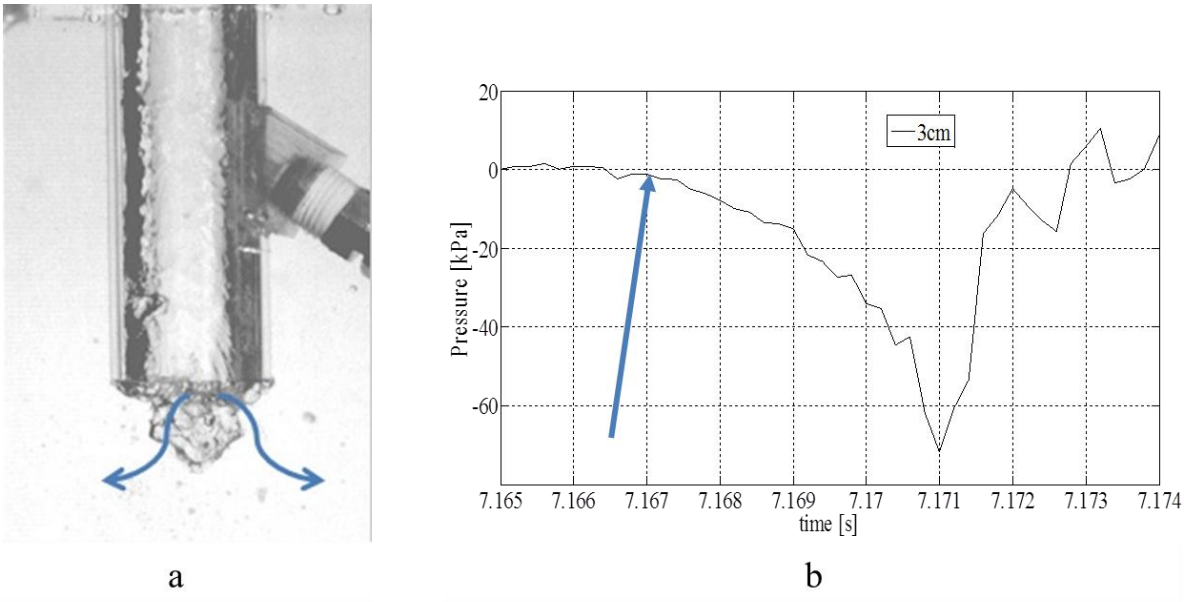

Fig. 4.10 Growing time analysis.

(a) Bubble growth begins, **(b)** bubble growth stops.

Fig. 4.11 a shows the bubble growing time as a function of the pool temperature. Moreover bubbles were distinguished depending on their shape. Mass flux was kept constant and equal to 7 [kg/(m^2s)] as shown with the green line in Fig. 4.11 b.

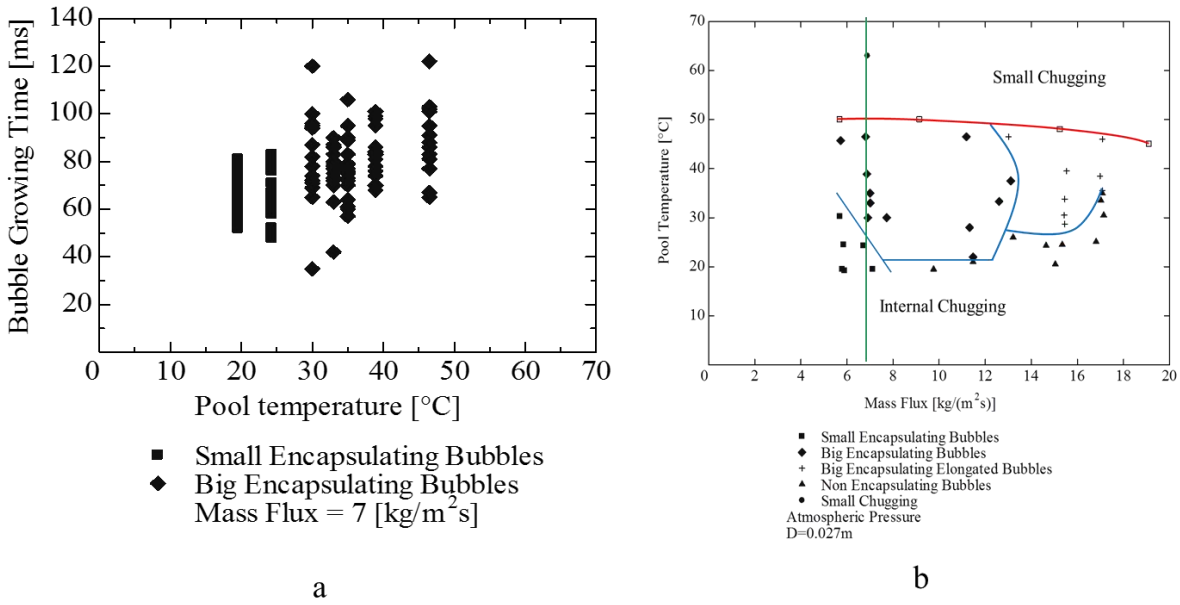

a b

Fig. 4.11 Bubble growing time as a function of the pool temperature.

Increasing the pool temperature there is the transition between the small encapsulating bubbles and the big encapsulating bubbles. The bubble growing time shows a step when this transition occurs: small encapsulating bubbles have an average growing time equal to 65 ms, while big encapsulating bubble have an average growing time of 80 ms. Indeed, if the bubbles are smaller, it is easier to reach the maximum dimension and the growing time is shorter. Moreover it is possible to highlight that there is a high variability on the growing time if big encapsulating bubble are considered whereas this variability is much lower if the small ones are taken into account.

Fig. 4.12 a shows the effect of the mass flux, keeping constant the pool water temperature. In this case, the growing time seems to be not affected by the mass flux. Indeed, the increase of the mass flux causes an increase of the interfacial area and thus an increase of the condensation rate.

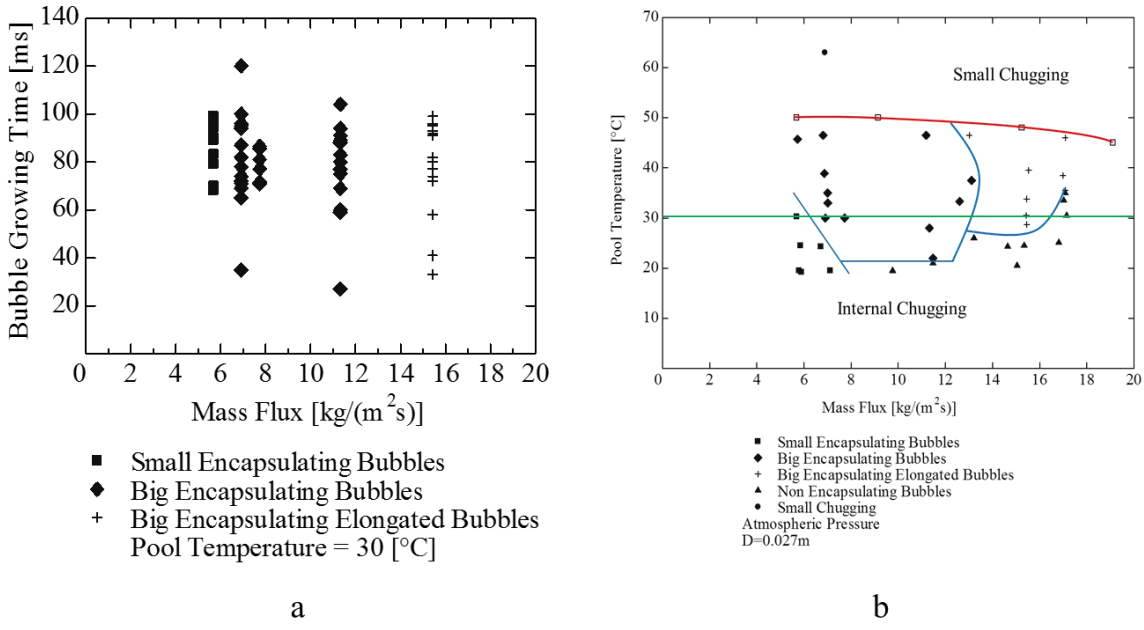

Fig. 4.12 Bubble growing time as a function of the mass flux.

In the region of the non encapsulating bubbles, located at low pool temperature and high mass flux, both the growing and the collapse time are dominated by turbulences and the phenomenon is unstable. In this case, growing time never exceed 30 ms which corresponds to the lowest value registered for the other kind of bubbles. For this reason and because the bubble sizes vary extremely among each other, it is impossible to make any comparison with the other regimes.

4.2. Bubble Collapse

In this section, an interpretation for the second phase of the chugging cycle, the collapse of the bubbles, is presented. This study is fundamental in order to assure a better

understanding of the phenomenon that might lead to an improvement of the analytical and numerical models. To the knowledge of the author few experimental or analytical studies concentrates on the bubble collapse mechanism. Pellegrini et al [23] described the collapse of the bubble using a Rayleigh-Taylor instability model whereas Ueno et al. [16], whose application is different from the nuclear field, assert that some interfacial instabilities different from the Rayleigh-Taylor is the cause of the implosion.

Bubble collapse analyses were made possible thanks to the capability of having a perfect synchronization between the camera and the pressure transducers' signals. Bubble implosion characteristics are considered to be highly dependent on what kind of bubble is formed. Apart from the dimensions, on a first approximation bubbles can be divided into encapsulating, marked with an A in Fig. 4.13, or non encapsulating, marked instead with a B.

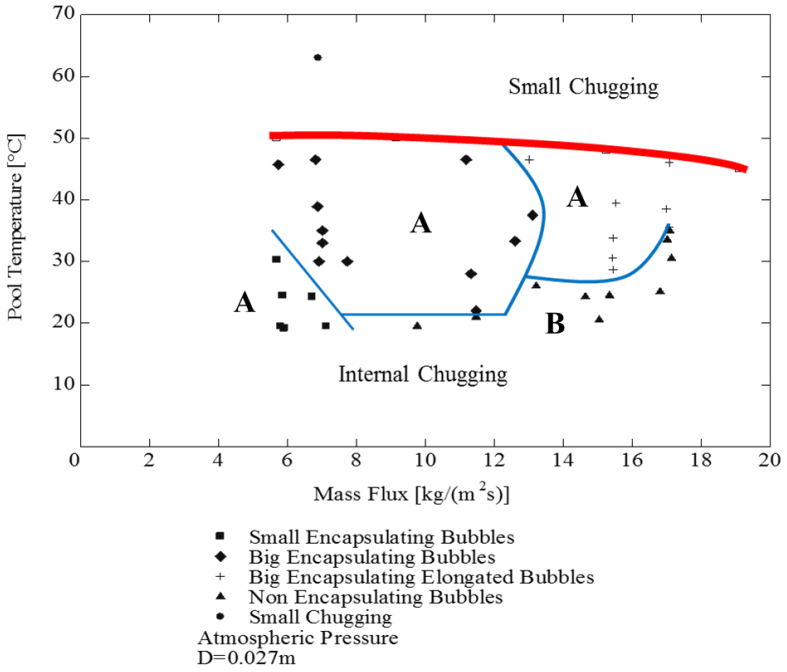

Fig. 4.13 Encapsulating and non encapsulating bubbles in the regime map.

In case of encapsulating bubbles, which correspond to the first three regions of the map, the reason why the collapse occurs is thought to be a rapid increase of the interfacial area due to instabilities at the interface but, in case of non encapsulating bubbles, turbulences and mixing may have a large inference in breaking the hot layer of water surrounding the bubble and increasing rapidly the temperature gradient. This differentiation in the manner of collapsing of encapsulating and non encapsulating bubbles is made as a consequence of the visualization of all the movies recorded and is based on the fact that the time scale (shown in section 4.1.2) and the position where the implosion begins is not similar. This diverse behavior legitimizes another time the need of a map related only to chugging regime.

4.2.1. Encapsulating Bubbles

Fig. 4.14 and Fig. 4.15 show a typical collapse of an encapsulated bubble with syncronous images and pressure transducer signals. A possible explanation of the collapse is an increase of the outer surface.

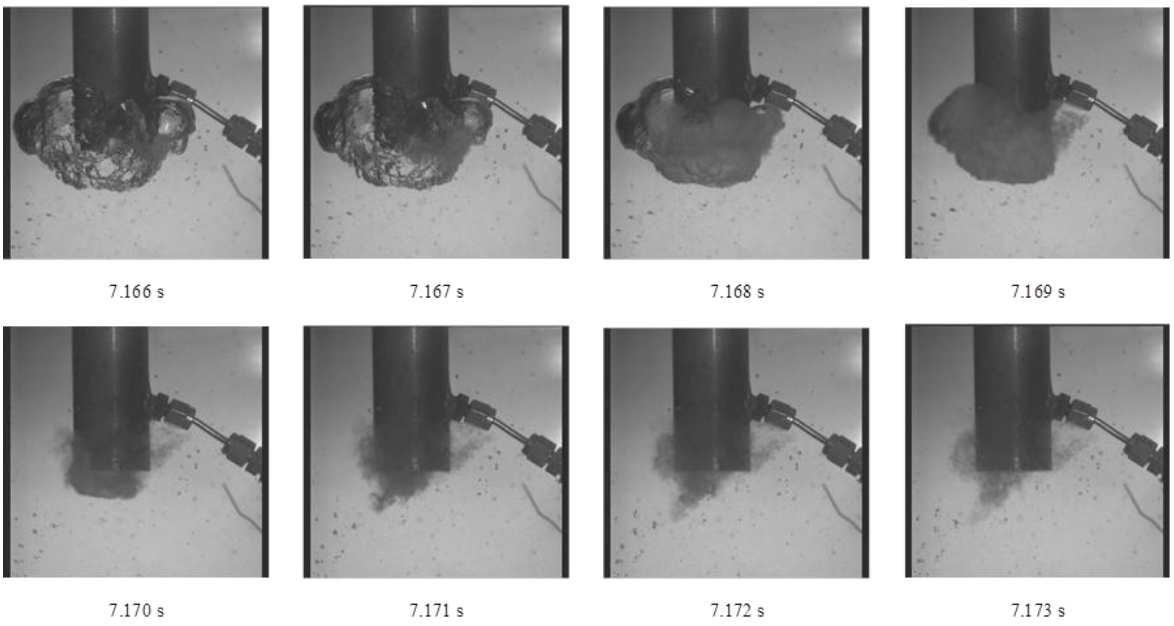

G=15.45 [kg/(m² s)]; Tw=28.7 [°C]; D=0.027 [m]

Fig. 4.14 Pictures of a typical collapse of an encapsulated bubble.

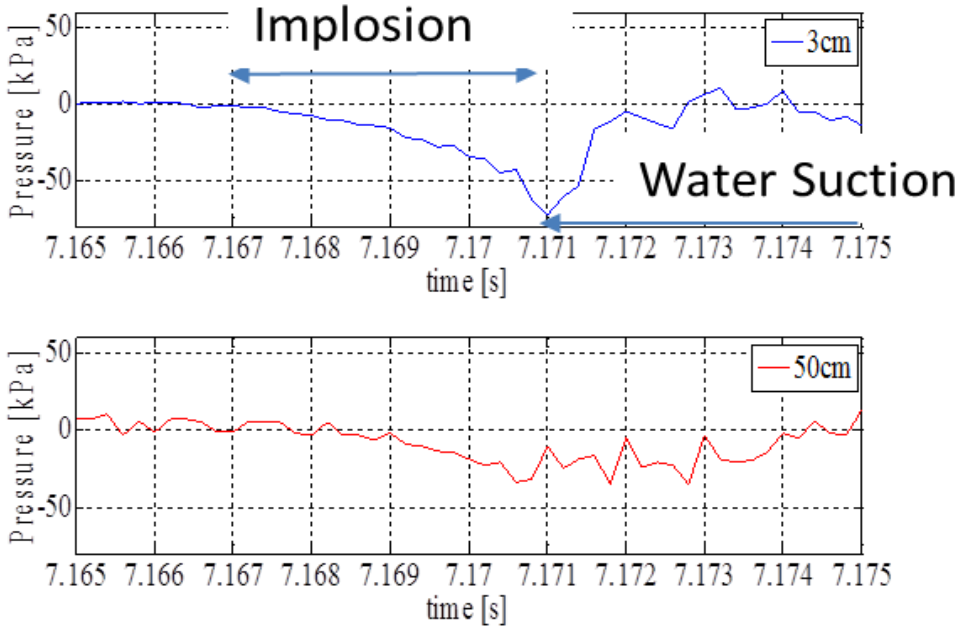

Fig. 4.15 Pressure signals during a typical collapse of an encapsulating bubble.

When the bubble is nearly at its maximum size, ruffles appear on the surface. This surface instabilities cause an increase of the interfacial area and consequently an enhancement of the heat exchange rate and of the condensation rate that produce an abrupt collapse. Initially a small portion of the bubble is involved, as it is possible to see at 7.168 s, but, after a fraction of ms, the collapse is extended to the whole bubble and a reduction of the pressure occurs. This is due to the loss of steam mass and mostly involved the transducer at 3 cm from the outlet. The pressure transducer at 50 cm from the outlet appears to be delayed and damped because of the presence of steam in compressible conditions inside the pipe. This change in pressure causes a suction of water inside the pipe and the third phase of chugging can take place. At 7.171 s, the water reaches the outlet of the pipe and it starts pressurizing locally the steam so that pressure increase. At this point, pressure oscillates after 7.171 as shown in Fig. 4.15, because of two competing factors:

- Condensation of steam in contact with cold water sucked inside the pipe
- Local pressurization of steam caused by water motion in the pipe

Even if high quality images were obtained using the camera, the data processing do not permit to evaluate the supposed increase of the outer surface that causes the collapse or to prove without any doubt that this is the reason for the collapse. The use of already existing analytical or CFD models or the development of new ones, compared with the experimental information provided in this section, can be used to confirm this theory.

4.2.2. Non encapsulating bubbles

A picture of the collapse of these bubbles and the associated pressure signals at 50 cm and 3 cm from the outlet is shown in Fig. 4.16 and Fig. 4.17 respectively. A possible interpretation of non encapsulating bubble implosion is the creation of turbulences which cause mixing of the water. The sudden contact of cold water might lead to a quick increase of the condensation rate and thus the collapse of the bubble. It is possible to notice that, exactly like the growing time, also the bubble collapse of non encapsulating bubbles is faster. This explanation is able to illustrate this different time scale of the collapse relative to non encapsulating bubbles and it is the main reason why it is proposed. However, exactly as it happened for the encapsulating bubbles, the justification of the phenomena should be investigated more in detail from every point of view.

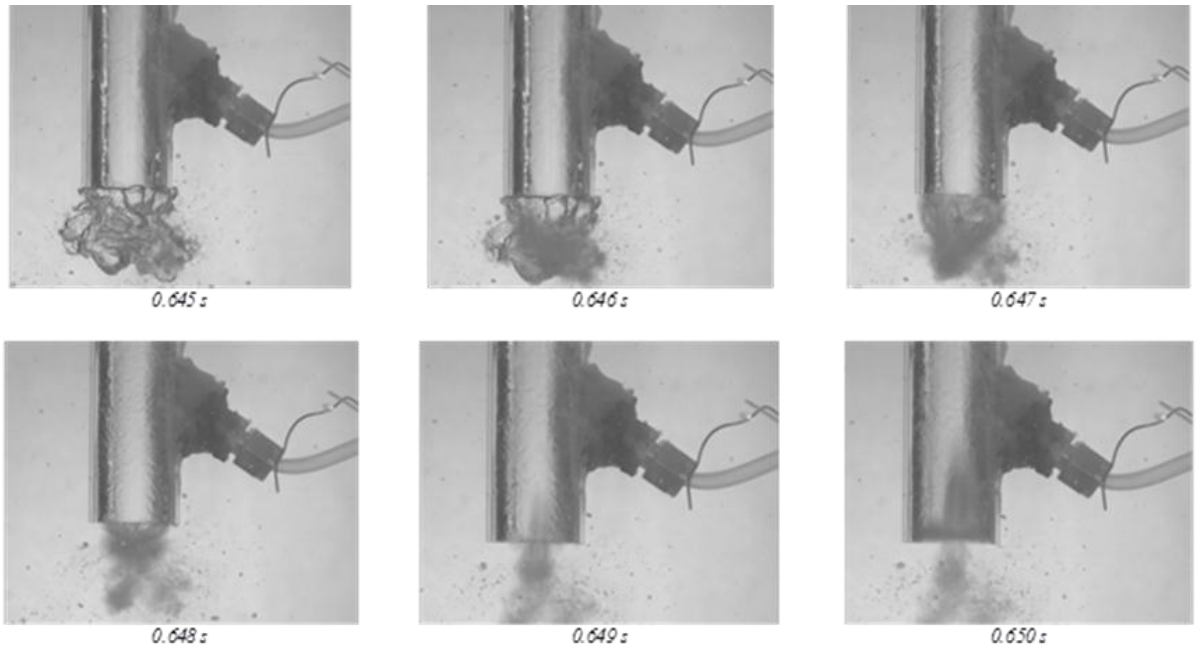

G=9.76 [kg/(m² s)]; Tw=19.5 [°C]; D=0.027 [m]

Fig. 4.16 Pictures of a typical collapse of a non encapsulating bubble.

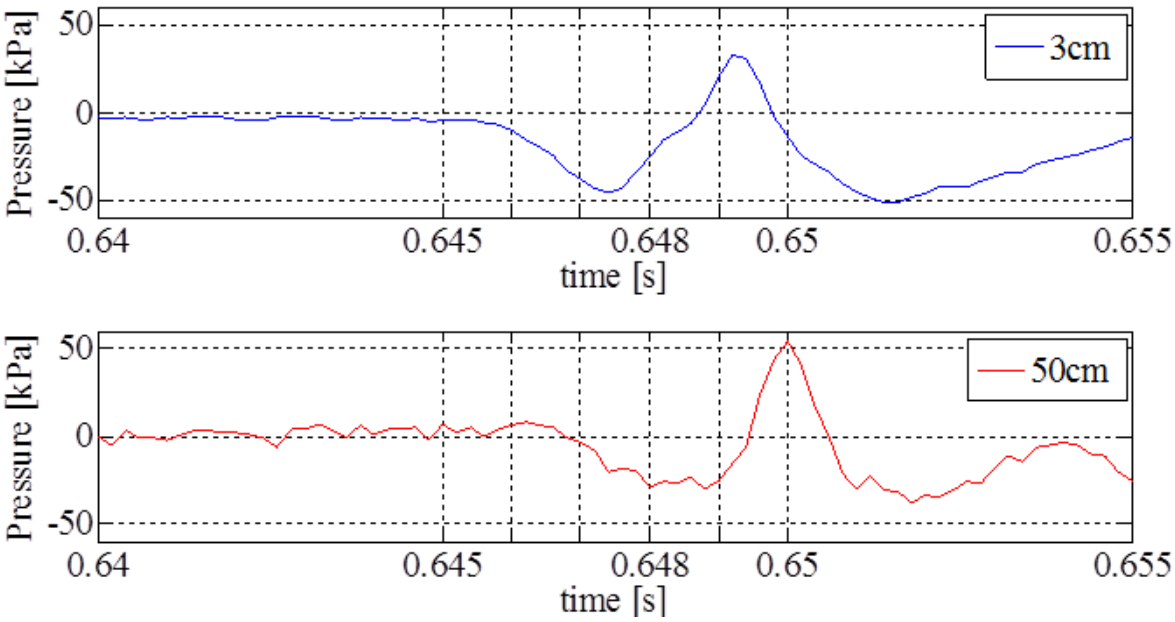

Fig. 4.17 Pressure signals during a typical collapse of a non encapsulating bubble.

Unlike encapsulating bubbles which show a way of collapsing that can be triggered from an instability that may arise from every position of the bubble, non encapsulating bubbles always start the collapse in the region connecting the two parts of the bubble. This region can be seen in Fig. 4.16 Pictures of a typical collapse of a non encapsulating bubble.at 0.646 s because it appears darker than the rest of the bubble. This can be another reason, together with the different time scale, why is not impossible that the implosion is governed by a different parameter than the bubble surface. In the same way as for the encapsulating bubbles, when the collapse takes place there is a reduction of mass and a depressurization around 0.646 s. The reduction of pressure causes the suction of water inside the pipe and again pressure increases around 0.648 s because of the acceleration of the liquid towards the surrounding steam.

In order to better evaluate this theory an array of thermocouples inside the pool is fundamental. Indeed, this might allow to spot the presence of cold water in particular location of the bubble before the implosion. However, it can be difficult to implement from an experimental point of view because bubbles dimensions are not always the same and it must be assured that the presence of the measuring instruments do not affect the bubble behaviour. Another interesting solution can be the application of a PIV technique to this case of study in order to evaluate the velocity field and be able to quantify the turbulences. Furthermore, CFD models can support and validate the explained idea.

4.3. Internal Condensations

This section is mostly focused on what happens when the water is inside the pipe. When the water reaches the outlet of the pipe, independently on what kind of bubble was formed previously, quick violent condensation occurs and water can reach high level inside the pipe. However, this elevation depends strongly on steam mass flux and pool temperature. In the same way, also the pipe size is expected to have an inference on the elevation of water after the bubble implosion at the outlet even if these experiments were all performed with the same diameter equals to 27 mm. In the experimental conditions explained in section 3.4, the highest elevation inside the pipe are related to the small encapsulating bubble shape and are roughly equal to 1 m above the pipe outlet. This is due to the small resistance of the steam coming from the tank and the cold water from the pool that keeps condensing the small amount of steam supplied. Increasing the steam flow rate and/or the pool temperature, the maximum altitude reached by the water decreases until the minimum level equals to roughly the level of submergence of the pipe. After the first quick and sudden condensation and the high elevation of the liquid inside the pipe, other different condensations inside the pipe might occur depending on the steam flow rate and the pool temperature. These condensations inside the pipes are characterized by high pressure peaks because of the confinement of the pipe and the presence of cold water sucked inside the pipe from the bulk of the pool. The intensity of the registered pressure peaks is higher than the ones characteristics of the bubble collapse at the outlet because, in this case, the liquid phase pressure is measured if the interface goes beyond the pressure tap located at 50 cm from the outlet. Due to the average position at which these phenomena occur, the pressure

transducer at 50 cm from the outlet can better reveal the pulses. It is necessary to deeply study why this pressure peaks develop, the intensity of the peaks, and the repetition of every chugging cycle in order to guarantee that the condensation will not be interrupted because of damages to the structure. Indeed, if the venting pipe breaks because of the high intensity and frequency of the loads, steam cannot be discharged anymore in the pool and the suppression pools of the BWRs cannot fulfil the aim they were built for.

4.3.1. Pressure Peaks

In Fig. 4.18 an example of the pressure signal resulting from a condensation inside the pipe is shown. The maximum peak, around 1.2 MPa is more than an order of magnitude higher than the ones related to the bubble implosion phase (around 40 kPa).

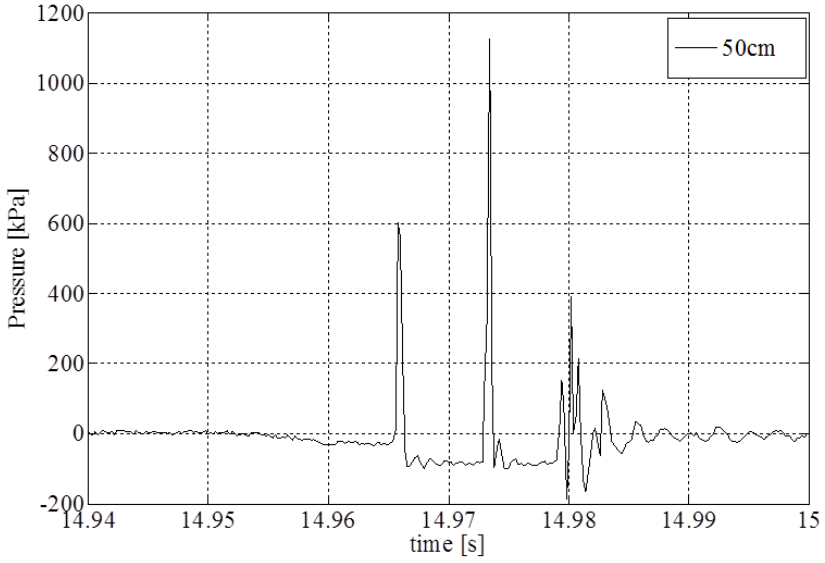

G=6.71 [kg/(m^2 s)]; Tw=24.3 [°C]; D=0.027 [m]

Fig. 4.18 High pressure peak at 50cm from the outlet due to an internal condensation.

The pressure initially is constant but then, around 14.955 s, it slightly decreases because of the condensation. Because of the mixing inside the pipe is possible that small steam bubbles are surrounded by cold water. Condensation reduces the pressure near the interface and the water is accelerated towards the steam. Due to the inertia of the water, the steam is then compressed and collapses. When the bubbles disappear, the empty space is quickly filled by the water that moves towards where there was the centre of the bubble as shown in Fig. 4.19. This fast acceleration of water causes a hit which generates an elastic deformation of the liquid and thus an elastic wave is produced [24]. The elastic wave propagates and it is detected by the pressure transducer at 14.965 s. It must be noticed that in this case, pressure in the liquid phase is measured. The phenomena previously explained is called condensation induced water hammer (CIWH). This kind of high pressure peaks were already detected by Purhonen et al. [9] and Laine et al. [10]. Every pressure peak in the signal is linked to the collapse of different bubbles.

Fig. 4.19 shows a schematic representation of the bubble behaviours during the internal condensation phase.

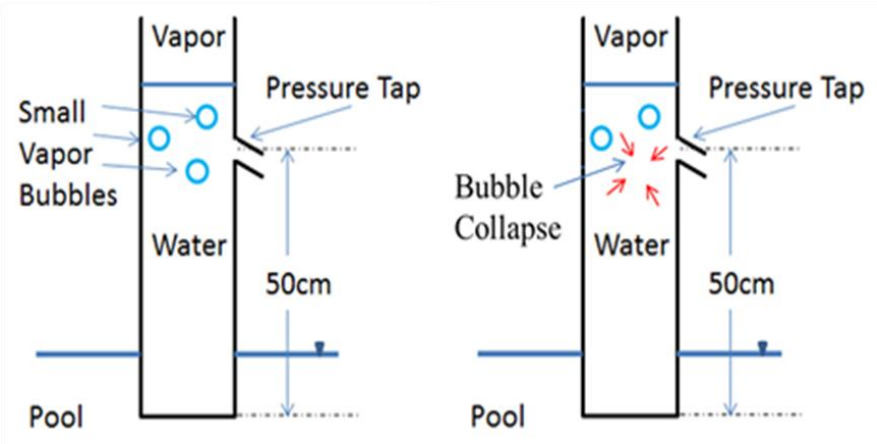

Fig. 4.19 Schematic drawing of the internal condensation.

In order to investigate the pressure peaks due to the small bubble implosion inside the pipe, a series of long experiments at constant flow rate were performed. This kind of experiment was already explained in section 3.5. The pool temperature naturally increased because of the ejection of the steam. This temperature was not measured but only monitored through the thermocouple inserted inside the pool at the same level of the pipe exit in order to avoid the problem of thermal stratification. This was possible because the increase of temperature is linear with time due to the constant flow rate and the higher dimension of the pool compared to the steam flow rate.

Fig. 4.20 shows the pressure signals at 50 cm and 3 cm from the outlet relative to one of the long experiments.

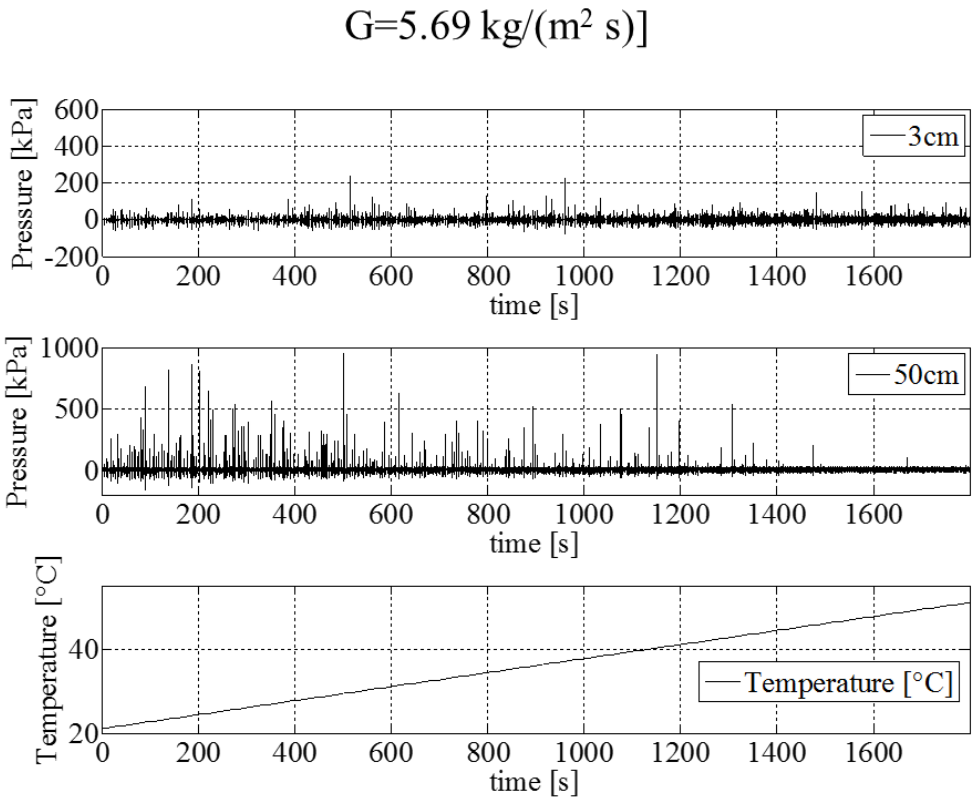

Fig. 4.20 Pressure signals during a long experiment**.**

As it was anticipated before, it is easy to see from Fig. 4.20 that the pressure transducer at 50 cm from the outlet can better reveal the pressure peaks characteristic of the small bubble collapse inside the pipe.

Fig. 4.21 shows the results of the long experiments. Pressure scale is divided into classes. Each class has a range of 100 kPa. Also the pool temperature was divided into classes with a range of 5°C. For every temperature class, the number of pressure peaks were computed and distributed among the correct pressure category. Because of the linearity between time and temperature, every temperature range is associated with an equal time range which allows dividing the number of peaks in each class for the relative time step.

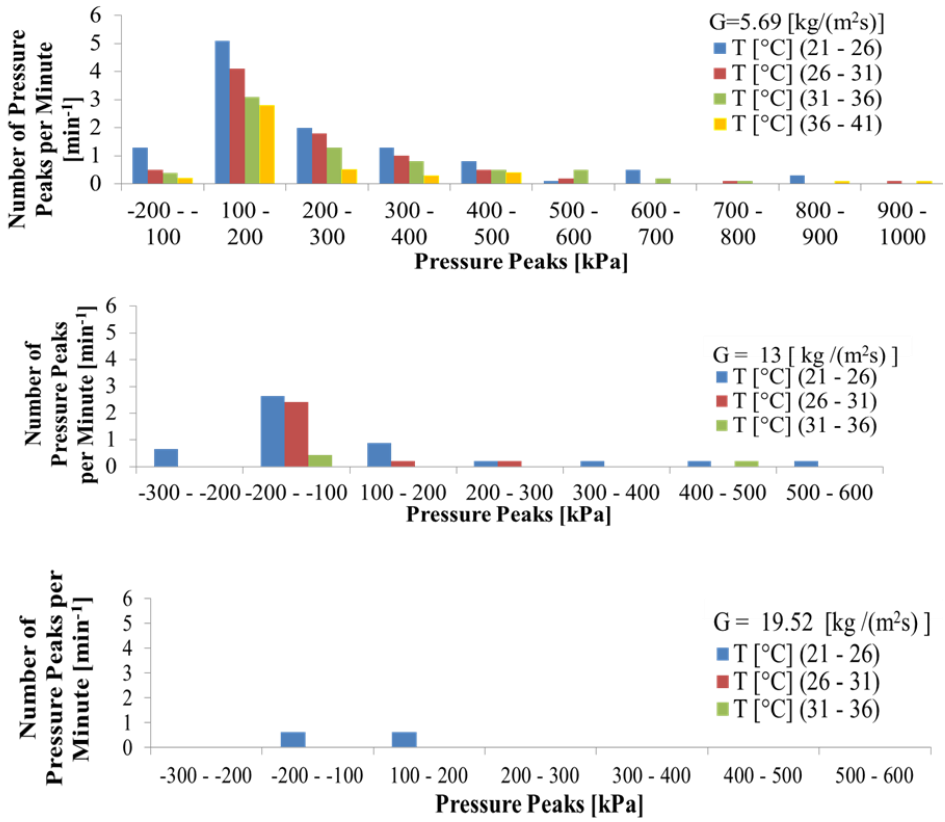

Fig. 4.21 Effect of the mass flux and the pool temperature on the frequency of occurrence of the pressure peaks.

The frequency of occurrence of the pressure peaks depends on both the pool temperature and the mass flux. The conditions for a high frequency of the pressure peaks are:

- Low pool temperature
- Low steam mass flux

Indeed if the pool temperature is low, when the water goes up inside the pipe and encounters isolated steam bubbles can easily cause the collapse. On the other hand, if the flow rate is low, the interface stays inside the pipe for a longer time because it takes more time to decrease the condensation rate and eject again steam out of the pipe.

When the pool temperature becomes high the frequency and intensity of the pressure peaks decrease. In the same way, at the high steam mass flux pressure peaks are not visible anymore due to the small elevation of water inside the pipe.

The two conditions for high frequency of the pressure peaks are relative to the region of the small encapsulating bubbles which means that, when this kind of bubbles are observed at the outlet of the pipe, the possibility of damages because of the pressure peaks is higher. For this reasons, the dimension of the structure should be done considering this part of the map as the most stressed mechanically.

4.3.2. Chugging Frequency

This section focuses on the frequency of repetition of the chugging cycle, which is to say how much time passes between the formations of two bubbles at the outlet of the pipe. Fig. 4.22 shows the effect of the mass flux, keeping the pool temperature constant and equal to 33 °C.

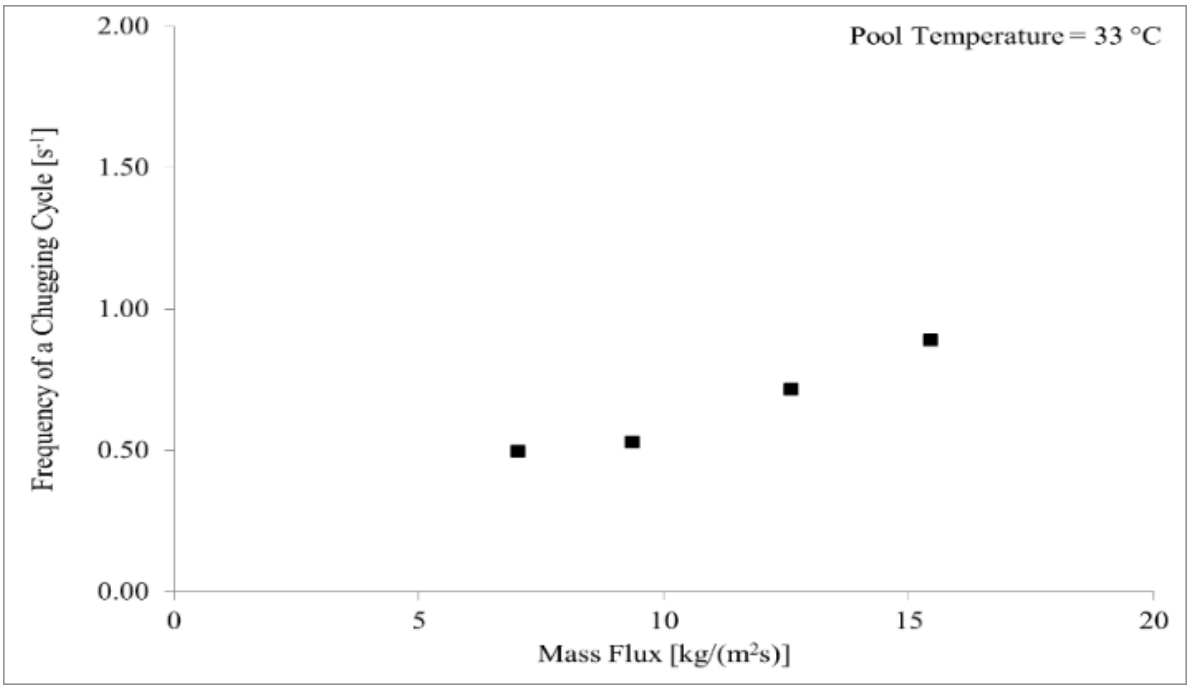

Fig. 4.22 Effect of the mass flux on the frequency of chugging.

When the mass flux is low, chugging phenomena duration is strongly linked to the phase of the internal condensation because the few amount of steam requires more time to heat up the water and finally reduce the condensation rate to values that are lower than the inlet mass flow rate. Moreover, with a low mass flux, the elevation of water inside the pipe is much higher because of the smaller opposition offered by the steam, so that the time required to the interface to descend again along the pipe increases. Increasing the mass flux, the effect of heating up the water faster is dominant because growing time does not change considerably and for this reason the frequency increase and the curve is monotonic.

Fig. 4.23 shows the effect of the pool temperature, keeping the mass flux constant:

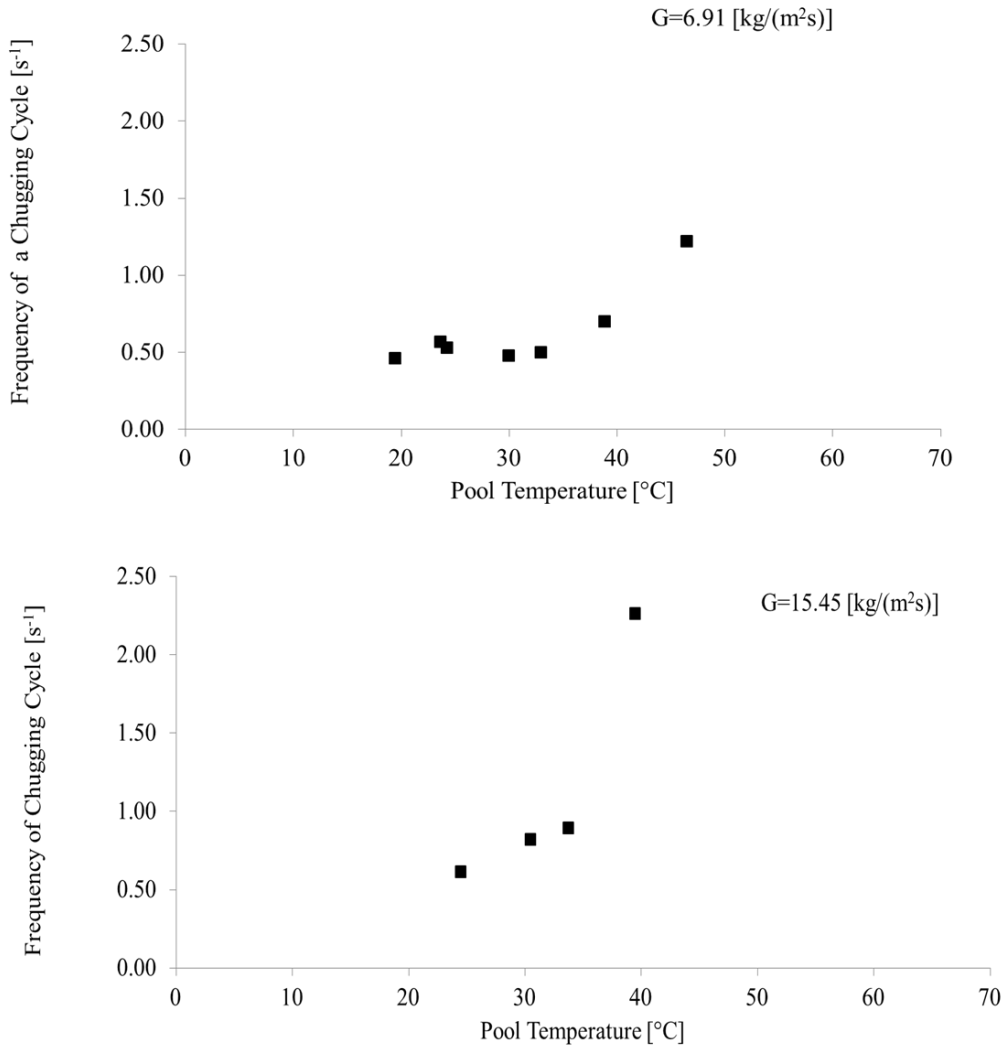

Fig. 4.23 Effect of the pool temperature on the frequency of chugging.

When the pool temperature is low, around 20°C

- At low mass flux bubble formation is rare because of the internal condensations
- At intermediate and high mass flux is not possible to observe encapsulating bubbles so data are not available.

When the pool temperature increases, internal condensation and pressure peaks become less dominant and is easier to form new bubbles so that the frequency of the chugging cycle increases.

Chapter 5

Future Developments

This chapter focuses on the future improvements that might be performed as a second step of chugging phenomena study. Indeed, apart from CFD investigation on chugging theme which are already planned, different ideas might be developed both from the experimental and analytical point of view.

Talking about the experimental part, different variations might be introduced. First of all, a loop for controlling the pool temperature may be added in order to be able to perform long experiments with constant pool temperature. Moreover, this technique will allow a more precise measurement of the pool temperature, which is one of the main limit of the present study. An alternative modification of the current set up of the facility could be the closure of the main loop through injecting the hot water from the pool directly inside the main tank. This will guarantee a reduction of the time that is needed to produce the steam because the feed water will not be anymore at ambient temperature but will be at roughly 50°C. In addition to this advantage, a great reduction of water and electricity waste is achieved.

Considering the measuring equipment, some modification might be applied. First of all, the measurement of the flow rate can be performed in a position closer to the pipe outlet. Furthermore different thermocouples can be installed in different locations inside the pool and inside the venting pipe, using the same method adopted for the pressure transducers. A new volt slider can be introduced to extend the deliverable steam flow rate. This will allow to explore chugging behavior in the region of the mass fluxes higher than those considered in the present study.

In this research, the behavior of the interface in the small chugging region was not of interest. In order to study this part of the condensation regime map, a new tank must be installed. Indeed, the acrylic do not allow to reach temperatures of the pool higher than 70°C. Another idea for a development of a new study is to introduce wire heaters along the outer part of the steam line in order to study the effect of the superheated steam on chugging phenomena. Because the subcooling is still expected to be the fundamental parameter governing the condensation process, the precise temperature of the steam must be evaluated. Another interesting part that might be deepened in a future study is pertinent to the internal condensations phase. In order to visualize the steam pockets and their implosion in the condensation induced water hammer phenomena, a high performing video camera can be placed around 50 cm from the outlet, where is currently located the pressure transducer.

Another field of study that can be investigated more in detail is the analytical work. Among the citied study in section 2.3, Sargis et al [20] paper seems to be the best starting point for developing a new model. Indeed, typical chugging pressure peaks are analytically predicted through the numerical solution of a set of coupled, non linear partial and ordinary equations. However, the amplitude of the spikes due to the condensation induced water hammer revealed in the present study is not well explained.

Steam mass flow rate, m_v, is evaluated through a mass balance, equation 5-1, in which the inlet flow rate, m_{in}, depends on the pressure difference, $(p_D - p_S)$, between the drywell and the downcomer, as shown in equation 5-2.

$$\frac{dM_s}{dt} = m_{in}A_{in} - m_{out}A_{out} - m_{wall}A_{wall} \quad (5\text{-}1)$$

$$m_{in} = C_D\sqrt{|p_D - p_S|}sign(p_D - p_S) \quad (5\text{-}2)$$

The intensity of the condensation is divided into two terms. The first is the interfacial condensation rate, m_{out}, and is obtained from the kinetic theory, equation 5-3; the second is the condensation at the pipe wall, m_{wall}, and depends on the temperature difference between the venting pipe wall and the injected steam, equation 5-4.

$$m_{out} = \frac{\alpha\{p_S - p_{Sat}(T_i)\}}{\sqrt{2\pi R_S T_i}} \quad (5\text{-}3)$$

$$m_{wall} = \frac{\bar{h}(T_S - T_{wall})}{h_{fg}} \quad (5\text{-}4)$$

An energy equation is introduced to evaluate the steam temperature. The motion of the steam-water interface is computed via a hydrodynamic model for the pool. This approach recalls Rayleigh method and leads to the definition of the steam volume and the interfacial area. The effect of the wall friction and end losses are also considered. Pool temperature is estimated using a Lagrangian formulation of the heat conduction equation while tank wall pressure, p_w, is obtained solving Laplace equation.

Fig. 5.1 shows the comparison of the calculated and measured pressure at the bottom of the pool in correspondence to the pipe axis. Results are particularly accurate although, as

explained in the present study, pressure peaks are mostly found inside the pipe at a high position from the outlet.

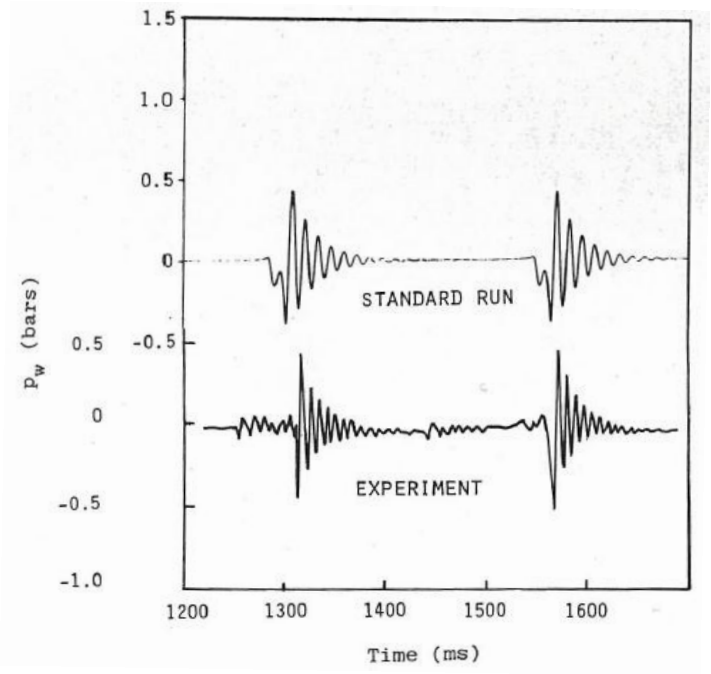

Fig. 5.1 Comparison of calculated and measured pool wall pressure **[20]**.

Sargis himself realised the difficulties in analysing internal condensations due to statistical distribution of frequency, size and temperature of cold water eddies generated when the interface is inside the pipe. Acceptable agreements with experimental results are obtained and this can represent a starting point for a further development despite the fact that the importance of internal condensations was highly underestimated by Sargis. Ali et al. [21] have already tried to improve Sargis work adding the effect of air present in the steam. Moreover they explained step by step the numerical technique, based on the fourth order Runge-Kutta algorithm, used to solve the set of equations constituting the model.

Conclusion

Chugging regime might occur in pressure suppression pool of BWR. The incomplete knowledge of this unstable regime may lead to unpredicted loss of condensation capability which causes high pressure conditions inside the containment building, and the creation of pressure peaks that might raise concern on damages to the venting pipes and to the pool structure. Chugging was studied with the support of a high speed video camera, fast response pressure transducers and transparent polycarbonate or stainless steel pipes with special connectors for the instalment of the pressure measurement equipment.

The present study allowed to:

1. Investigate the mechanisms of every phase of the chugging cycle:
    a. Classify chugging phenomena depending on the bubble shapes.

A regime map was created observing images from a high speed video camera. Two different regimes are evaluated: internal chugging and small chugging. Internal chugging occurs at low pool temperature and is characterized by high elevation of water inside the pipe following the bubble collapse. High pressure peaks are associated to this kind of chugging. Small chugging occurred when the movement of the interface remained close to the pipe outlet. The elevations of the water are much smaller than the previous case.

Four different regions are identified in the internal chugging area, which is the one that was mostly considered in this study: small encapsulating bubbles, big encapsulating bubbles, big encapsulating elongated bubbles, non encapsulating bubbles.

b. Give a qualitative interpretation of bubble collapse phase

Bubble collapse phase was analysed visualizing the images of the high speed camera. Bubbles were divided depending on whether they encapsulate or not the pipe. An abrupt increase of the interfacial area might be the parameter causing the collapse of encapsulating bubbles. On the other hand, the different way of collapsing of non encapsulating bubbles might be due to the break of the layer of hot water due to the turbulences.

c. Inspect the typical pressure peaks occurring during chugging cycle which arise concern on damages to the structure.

High pressure peaks characteristics of chugging phenomena are quantitatively measured with the pressure transducer located 50 cm from the pipe outlet. This pressure spikes are not caused by the bubble implosion (whose peaks are always lower than 100 kPa) but are due to the internal condensations inside the pipe. The highest pressure peak revealed is 1.2 MPa and the conditions of occurrence are with the pool temperature below 25 °C and the mass flux lower than 7 kg/(m^2s). The repetition of these pressure spikes was also inspected. Maximum 10 peaks per minute with an amplitude higher than 100 kPa were measured.

d. Give a simple method for predicting chugging characteristics creating a link between bubble shapes and pressure peaks.

The conditions of low pool temperature and low mass flux highlighted in the conclusion 2b are equivalent to the ones characteristic of small encapsulating bubbles formation. This means that every time small encapsulating bubbles are observed at the pipe outlet, high

frequency of pressure peaks must be expected. This allow to have a simple method to predict the chugging features only looking at the bubble shape at the outlet. This possibility is particularly important while doing small scale tests, especially if it is considered that stainless steel pipe are mostly adopted and visualization of what is happening inside the pipe is impossible.

e. Illustrate time scale of chugging phases and its variation as a function of DCC parameters.

Bubble growing time was investigated as a function of the pool temperature and the mass flux. The values ranged from 30 to 100 ms for encapsulating bubbles while 30 ms was the maximum registered growing time for non encapsulating bubbles. This differences in the growing time are due to the different ways of collapse of these two categories of bubbles.
In addition to this, chugging frequency was shown to increase with the increase of the mass flux and with the increase of the pool temperature. This is mainly explained with a reduction of the internal condensation phase. The maximum chugging frequency is around 2.5 Hz.

2. Provide experimental results for the validation and development of CFD approaches.

High quality video images and synchronous pressure transducer signal at 50 cm and 3 cm from the outlet might be used for validating CFD codes. Moreover, the adoption of transparent polycarbonate pipe and a transparent pool allow to visualize the interface while it is inside the pipe and better check the accuracy of the computer models.

References

[1] I. Aya and H. Nariai, "Boundaries between regimes of pressure oscillationinduced by steam condensation in pressure suppression containment," *Nuclear Engineering and Design*, vol. 99, pp. 31-40, 1987.

[2] C. K. Chan and C. K. Lee, "A regime map for direct contact condensation," *International Journal of Multiphase Flow*, vol. 8, no. 1, pp. 11-20, 1982.

[3] S. Cho, C. H. Song, C. K. Prak and S. K. Yang, "Experimental Study on Dynamic Pressure Pulse in Direct Contact Condensation of Steam Jets Discharging into Subcooled Water," in *NTHAS 98: First Korean-Japan Symposium on Nuclear Thermal Hydraulics and Safety*, Pusan, Korea, October, 21-24, 1998.

[4] R. T. Lahey and F. J. Moody, The Thermal-hydaulics of a Boiling Water Nuclear Reactor, Second Edition, La Grange Park, Illinois USA: American Nuclear Society.

[5] A. Petrovic de With, R. K. Calay and G. de With, "Three-dimensional condensation regime diagram for direct contact condensation of steam injected into water," *International Journal of Heat and Mass Transfer*, vol. 50, pp. 1762-1770, 2007.

[6] D. H. Youn, K. B. Ko, Y. Y. Lee and M. H. Kim, "The Direct Contact Condensation of Steam in a Pool at Low Mass Flux," *Journal of Nuclear Science and Technoloy*, vol. 40, no. 10, pp. 881-885, 2003.

[7] J. S. Marks and G. B. Andeen, "Chugging And Condensation Oscillation," in *18 h National Heat Transfer Conference*, San Diego, California, 1979.

[8] H. Nariai and I. Aya, “Fluid and pressure oscillations occuring at direct contact condensation of steam flow with cold water,” *Nuclear Engineering and Design,* vol. 95, pp. 35-45, 1986.

[9] H. Purhonen, M. Puustinen, J. Laine, A. Rasanen, R. Kyrki-Rajamaki and J. Vihavainen, “Steam Blowdown Experiments with the Condensation Pool Test Rig,” in *Nuclear Energy for New Europe 2005*, Bled, Slovenia, Spetember 5-8, 2005.

[10] J. Laine and M. Puustinen, “Condensation Pool Experiment with Steam Using DN200 Blowdown Pipe,” Lappeenranta University of Technology, Finland, August 2005.

[11] G. Class, S. Raff and R. Meyder, “The mechanism of violent condensation shocks,” *International Journal of Multiphase FLow,* vol. 13, no. 1, pp. 33-46, 1987.

[12] K. S. Liang and P. Griffith, “Experimental and analytical study of direct contact condensation of steam in water,” *Nuclear Engineering and Design,* vol. 147, pp. 425-435, 1994.

[13] M. Solom and K. Vierow, “Experimental Investigation of BWR Suppression Pool Stratification during RCIC System Operation,” in *Japan-US seminar on two phase flow*, Purdue University, May 10-15, 2015.

[14] D. Song, N. Erkan, B. Jo and K. Okamoto, “Dimensional analysis of thermal stratification in a suppression pool,” *International Journal of Multiphase Flow,* vol. 66, pp. 92-100, 2014.

[15] L. Araneo, H. Ninokata, M. Ricotti, M. Pellegrini and M. Naitoh, “Suppression pool testing at SIET labs (2) - Steam chugging investigation under the presence of non-

condensable gas in a vertical opened pipe," in *10th International Topical Meeting on Nuclear Thermal-Hydraulics, Operation and Safety (NUTHOS-10)*, Okinawa, Japan 日本, December 14-18, 2014.

[16] I. Ueno, J. Ando, Y. Koiwa, T. Saiki and T. Kaneko, "Interfacial instability of a condensing vapor bubble in a subcooled liquid," *The European Physical Journal*, vol. 224, pp. 415-424, 2015.

[17] J. H. Pitts, "Steam Chugging in a Boiling Water Reactor Pressure-suppression System," *International Journal of Multiphase Flow*, vol. 6, pp. 329-344, 1980.

[18] S. G. Bankoff, "Some condensation studies pertinent to LWR safety," *International Journal of Multiphase Flow*, vol. 6, pp. 51-67, 1980.

[19] J. A. Block, "Condensation driven fluid motion," *International Journal of Multiphase Flow*, vol. 6, pp. 113-129, 1980.

[20] D. A. Sargis, J. H. Stuhmiller and S. S. Wang, "A fundamental thermalhydraulic model to predict steam chugging phenomena," in *ASME 1978 Winter Meeting. Topics in Two-Phase Heat Transfer and Flow*, Del Mar, California, 1978.

[21] S. M. Ali, V. Verma and A. K. Ghosh, "Analytical thermal hydraulic model for oscillatory condensation of steam in presence of air," *Nuclear Engineering and Design*, vol. 237, pp. 2025-2039, 2007.

[22] J. P. Sursock and R. B. Duffey, "Condensation of steam bubbles in a subcooled pool," in *ASME 1978 Winter Meeting. Topics in Two-Phase Heat Transfer and Flow*, Del Mar, California, 1978.

[23] M. Pellegrini, M. Naitoh, C. Josey and E. Baglietto, "Modeling of Rayleigh-Taylor Instability for Steam Direct Contact Condensation," in *Proceedings of the 16th International Topical Meeting on Nuclear Reactor Thermalhydraulics (NURETH-16),* Chicago, USA, August 30 - September 4, 2015.

[24] C. Urban and M. Schluter, "Investigations on the stochastic nature of condensation induced water hammer," *International Journal of Multiphase Flow,* vol. 67, pp. 1-9, 2014.

[25] "Energy, Electricity and Nuclear Power Estimates for the Period up to 2050," 2013. [Online]. Available: http://www-pub.iaea.org/MTCD/Publications/PDF/RDS-1-33_web.pdf.

[26] "Nuclear Power Reactors in the World," 2014. [Online]. Available: http://www-pub.iaea.org/MTCD/Publications/PDF/rds-2-34_web.pdf.

[27] Cameco, [Online]. Available: www.cameco.com.

[28] "Nuclear Regulatory Commission, Boiling Water Reactor Systems," [Online]. Available: http://www.nrc.gov/reading-rm/basic-ref/teachers/03.pdf.

[29] "IAEA," [Online]. Available: https://www.iaea.org/PRIS/WorldStatistics/OperationalReactorsByType.aspx. [Accessed 06 2015].

[30] "General Electric," [Online]. Available: http://files.gereports.com/wp-content/uploads/2011/10/NEI-Mark-1-White-Paper.pdf.

[31] "Information Portal for the Fukushima Daiichi Accident Analysis and

Decommissioning Activities," [Online]. Available: https://fdada.info/docdata/accident_analysis/Unit3_RCIC-quencher.pdf.

[32] "Information Portal for the Fukushima Daiichi Accident Analysis and Decommissioning Activities," [Online]. Available: https://fdada.info/docdata/accident_analysis/Unit3_T-quencher.pdf.

[33] Y. Kukita and K. Namatame, "The Vent-to-Vent Desynchronization Effects on LOCA Steam Condensation Loads in BWR Pressure Suppression Pool," *Nuclear Energy and Design*, vol. 85, pp. 141-150, 1985.

[34] IAEA-TECDOC-1677, "Natural Circulation Phenomena and Modelling for Advanced Water Cooled Reactors," Vienna 2012. [Online]. Available: http://www-pub.iaea.org/MTCD/Publications/PDF/TE-1677_web.pdf.

[35] C. H. Song, S. Cho and H. S. Kang, "Steam jet condensation in a pool: from fundamental understanding to engineering scale analysis," *Journal of Heat Transfer*, vol. 134, March 2012.

[36] T. L. Norman, S. T. Rankar, M. Ishii and J. M. Kelly, "Steam-air mixture condensation in a sucooled water pool - final report," Purdue University, West Lafayette, US, December 2006.

Appendix

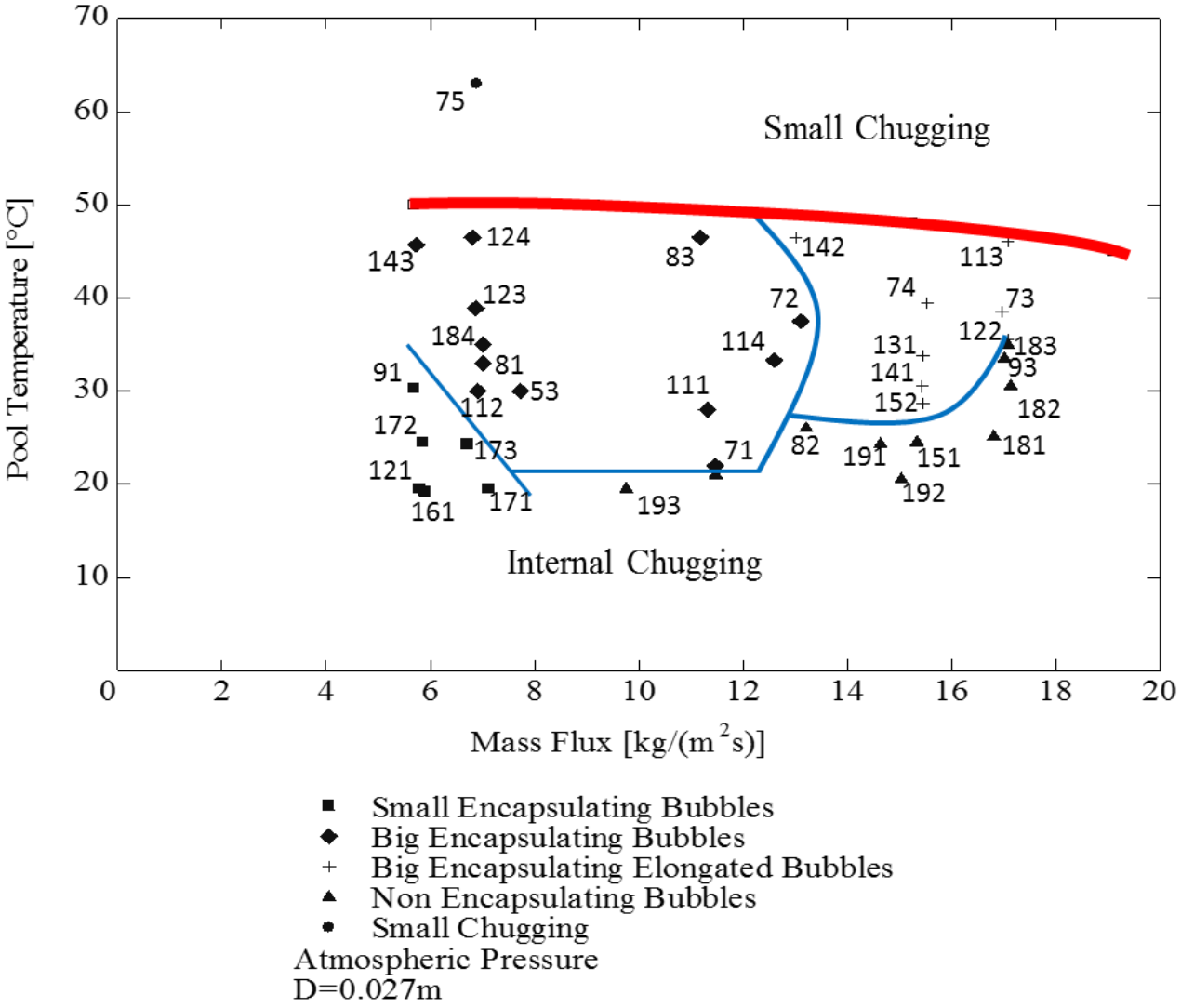

Figure 1 Condensation regime map with experiment name labels.

Table 1 Experimental results summary.

Experiment name	Mass Flux [kg/(m^{2}s)]	Pool Temperature [°C]	Bubble Shape	Pipe Material	Notes
161	5.9	19.2	Small Encapsulating	SS	2000 fps
121	5.8	19.5	Small Encapsulating	P	No synchronization, damping
172	5.9	24.5	Small Encapsulating	SS	No synchronization, damping
91	5.7	30.3	Small Encapsulating	P	Pressure tap only at 50cm, no synchronization, damping
171	7.1	19.5	Small Encapsulating	SS	No synchronization, damping
173	6.7	24.3	Small Encapsulating	SS	
112	6.9	30	Big Encapsulating	P	No synchronization, damping
53	7.7	30	Big Encapsulating	P	No synchronization, damping 2000 fps
81	7.0	33	Big Encapsulating	P	Pressure tap only at 50cm
184	7.0	35	Big Encapsulating	P	Pressure tap only at 50cm
123	6.9	38.9	Big Encapsulating	P	No synchronization, damping
143	5.7	45.7	Big Encapsulating	P	No synchronization, damping
124	6.8	46.5	Big Encapsulating	P	No synchronization, damping
71	13.1	22	Big Encapsulating	SS	Transition region observed during experiment
111	11.3	28	Big Encapsulating	P	No synchronization, damping
114	12.6	33.3	Big Encapsulating	P	No synchronization, damping
72	13.1	37.5	Big Encapsulating	SS	
83	11.2	46.5	Big Encapsulating	P	Pressure tap only at 50cm

Experiment name	Mass Flux [kg/(m^{2}s)]	Pool Temperature [°C]	Bubble Shape	Pipe Material	Notes
152	15.4	28.7	Big Encapsulating Elongated	SS	5000 fps
141	15.4	30.5	Big Encapsulating Elongated	SS	
131	15.4	33.8	Big Encapsulating Elongated	SS	
74	15.5	39.5	Big Encapsulating Elongated	SS	No synchronization, damping
142	13	46.5	Big Encapsulating Elongated	P	
122	17.1	35.5	Big Encapsulating Elongated	P	No synchronization, damping
73	17	38.5	Big Encapsulating Elongated	SS	Offset in the pressure signal
113	17.1	46	Big Encapsulating Elongated	P	No synchronization, damping
193	9.7	19.5	Non Encapsulating	P	
82	13.2	26	Non Encapsulating	P	Pressure tap only at 50cm
191	14.6	24.3	Non Encapsulating	P	No synchronization, damping in the transducer at 3 cm
192	15	20.5	Non Encapsulating	P	Offset in the pressure signal
151	15.3	24.5	Non Encapsulating	SS	No synchronization, damping
181	16.8	25.1	Non Encapsulating	P	No synchronization, damping in the transducer at 3 cm
182	17.1	30.5	Non Encapsulating	P	No synchronization, damping in the transducer at 3 cm
93	17	33.5	Non Encapsulating	P	
183	17.1	35	Non Encapsulating	P	No synchronization, damping in the transducer at 3 cm

Experiment name	Mass Flux [kg/(m^{2}s)]	Pool Temperature [°C]	Bubble Shape	Pipe Material	Notes
41	6.8	23.7		P	Wide image
42	9.3	32.5		P	Wide image
43	17.9	38.9		P	Wide image, 3000 fps

P = polycarbonate; S = stainless steel; fps= frame per second.